



H2020-INFRAIA-2019-1

Europlanet 2024 RI has received funding from the
European Union's Horizon 2020 Research and Innovation Programme under

Grant agreement no: 871149

Deliverable D8.3

Deliverable Title: Mapping training material: Basic geological maps
Due date of deliverable: 31st August, 2021
Nature¹: R
Dissemination level²: PU
Work package: WP8
Lead beneficiary: UNIPD
Contributing beneficiaries: UDA, UNICH, WWU, CBK-PAN, JacobsUni
Document status: Final

Start date of project: 01 February 2020
Project Duration: 48 months
Co-ordinator: Prof Nigel Mason, UNIKENT

1. **Nature:** R = Report, P = Prototype, D = Demonstrator, O = Other

2. **Dissemination level:**

PU

Public
Restricted to other programme
participants (including the
Commission Service)

PP

RE

Restricted to a group specified by
the consortium (including the
Commission Services)

CO

Confidential, only for members of
the consortium (excluding the
Commission Services)

Executive Summary / Abstract:

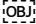
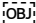
The approach of geoscientific mapping is introduced. This document describes best practice in geoscientific mapping, including the different types of mapping. The role of geologic processes in specific mapping practices is described, Case studies from published geologic and geomorphic maps over several Solar System bodies are used to exemplify best practice in mapping. Specific mapping types, such as those aimed at resource evaluation are included.

Acronyms and abbreviations

Acronym	Description
CaSSIS	<u>Colour and Stereo Surface Imaging System</u>
CSFD	<u>Crater size-frequency distribution</u>
CRS	<u>Cartographic Reference Systems</u>
CTX	ConTeXt camera
DEM	Digital Elevation Model
DTM	Digital Terrain Model
EDL	Entry Descent and Landing
ESA	European Space Agency
GCP	<u>Ground Control Points</u>
GIS	Geographic Information System
HiRISE	High Resolution Imaging Experiment
HRSC	<u>High Resolution Stereo Camera</u>
IAU	<u>International Astronomical Union</u>
ISIS	Integrated Suite for Imagers and Spectrometers
ISRU	In Situ Resource Utilisation
ISS	International Space Station
LRO	Lunar Reconnaissance Orbiter
MOC	<u>Mars Observer Camera</u>
PLANMAP	<u>PLANetary MAPping project</u>
PLD	Polar Layered Deposits
SSSB	Small Solar System body
TRN	Terrain Relative Navigation
TC	<u>Terrain Camera</u>
USGS	<u>U.S. Geological Survey</u>
WAC	Wide Angle Camera

Table of Contents

1. Categorisation of Geoscientific Maps	4
a. Approaches in Geoscientific Cartography	4
b. Cartography: scale vs approach	5

c.	The concept of ‘stratotype’ in planetary mapping: ‘reference area’	6
d.	Focus on stratigraphic relations	7
2.	Feature-based mapping	8
		
3.	Process-based ‘interpretative’: Geomorphological/Morphostratigraphic Map	11
a.	Planets with an atmosphere: Mars as a paradigm	11
i.	Mars Volcanic Processes	12
1.	Science rationale	12
ii.	Mars Sedimentary Processes	13
Outflow channels		14
Fluvio-lacustrine deposition		16
Ice-related deposition		21
Aeolian deposition		24
b.	Airless bodies: Moon as a paradigm	28
i.	Science rationale	28
ii.	Approaches	28
c.	Small Bodies	30
Map projections and small bodies		30
Mapping on small bodies		31
Gravity		32
Regions Definitions		33
Geological Mapping Terminology for Small Bodies		33
d.	Icy Bodies	36
iii.	Science rationale	36
iv.	Approaches	36
		
	Limitations	40
4.	Process-based ‘objective’: Geological Map	47
5.	Chronostratigraphic Maps	51
a.	Science rationale	51
b.	Approaches	54
6.	Landing site characterization	56
a.	Science and engineering rationale	56
b.	Approaches	56
7.	Resource maps for ISRU	60
a.	Science, exploration, and commercial rationale	60

b. Approaches	60
References	62

1. Categorisation of Geoscientific Maps

Planetary geological mapping is a very broad and continuously evolving discipline. Accordingly, the maps that are produced for scientific purposes are often based on different methods to distinguish and categorize the geological units. Contextual (\approx standardised) maps, published and planned by standard surveys, are rigid in their approach (both in scale and basemaps, which include a low response to data curve), because they are aimed at providing the basis for further geological investigations, regardless of the specific target (Skinner et al., 2019). Instead, topical maps are flexible in approach (which include a high response to data curve) and are mostly focused on scientific investigation, often published in scientific journals (Skinner et al., 2019; PLANMAP, 2020a).

The aim of this document is to find, organise, and rationalise some best practices in order to make the language of geological maps as uniform as possible, specifically when dealing with topical maps. Moreover, in this ongoing and very dynamic context with new data constantly added, we think that scientists should be free and encouraged to test new mapping approaches and/or unit classification. Accordingly, we focus on providing broad guidelines to improve the possibility to share information effectively rather than constraining the work into rigid standardisation.

a. Approaches in Geoscientific Cartography

Different science or technical aims drive different mapping approaches that result in different cartographic products.

Feature-based maps are used to address the distribution of a specific landform (or set of landforms), structure (or set of structures), or composition (or set of compositions). Geomorphologic maps focus on the recognition of landforms and landscapes and their genetic interpretation. Genetic processes can show substantial differences and/or peculiarities depending on which planetary body they exist in, but they can be roughly classified into four major groups: planets with an atmosphere, airless bodies, small bodies, and icy satellites.

Geological mapping aims at the realisation of an ‘as objective as possible’ cartographic product. On Earth, it makes use of the rock lithology as the base to distinguish the units. Accordingly, the meaning of geological mapping of other solar system bodies should be partially redefined in order to be applicable to planetary settings. Traditionally standard geological maps of other planetary bodies are based on a morphostratigraphic approach where units are distinguished on the bases or their morphological/genetic character and ordered according to relative ages constrained by cross-cutting and overlapping relationship as well as crater density.

In this way geologic maps of planetary bodies can be considered as morphostratigraphic or chronostratigraphic maps which represent the basic cartography to

distinguish the units on the base of their relative depositional age, tied where possible to absolute model ages.

Recently this approach has been however coupled with spectral or compositional information that in some instances can contribute to the definition of different geological units. In this case the maps have been alternatively defined as geostratigraphic or spectromorphic maps (PLANMAP, 2020a; Semenzato et al. 2020).

In addition, like on Earth, maps can be produced focusing on some specific geological aspects such as the distribution of structural elements (i.e. which define the structural maps), volcanic complexes, glacial/periglacial morphologies, fluvial networks etc.

Landing site maps serve a variety of purposes including geological context for mission operations, as well as terrain and hazard characterisation for landing and surface operations. Such map products allow scientific goals and engineering constraints to be balanced to optimize mission outcomes.

Resource mapping is aimed at understanding the surface and subsurface distribution of potential resources (e.g. minerals, elements, volatiles) in order to estimate the feasibility of extraction and perform a cost-benefit analysis.

b. Cartography: scale vs approach

The scientific and/or technical outcomes of the different cartographic products are maximised for specific scales of mapping (Table 1).

Table 1: Relation between the cartographic approach (row) and the scale of mapping (column)

	Feature-based maps	Geomorphologic maps	Geostratigraphic maps	Chronostratigraphic Maps	Landing site maps	Resource mapping
GLOBAL	X			X		
REGIONAL	X	X	X	X		
LOCAL		X	X	X		
DETAIL			X	X	X	X

Some exceptions can certainly be possible, depending on specific needs or available datasets, but this framework is still a general expression of the relations between mapping approaches and scales. Global maps refer to the entire planetary globe (possibly but not necessarily including the polar regions). Regional maps cover a wide range of possible extensions because they do not refer simply to a ‘large’ area (where large takes different meanings depending on different planetary bodies) but to an area crossing through different geological contexts (i.e. different geological evolution). Local maps refer to the representation of areas sharing the same geological history, bounded by geologically significant boundaries (e.g. a volcanic province with associate deposits/morphologies). Detail maps aim at providing the most detailed information in a geographically limited area with a very specific purpose.

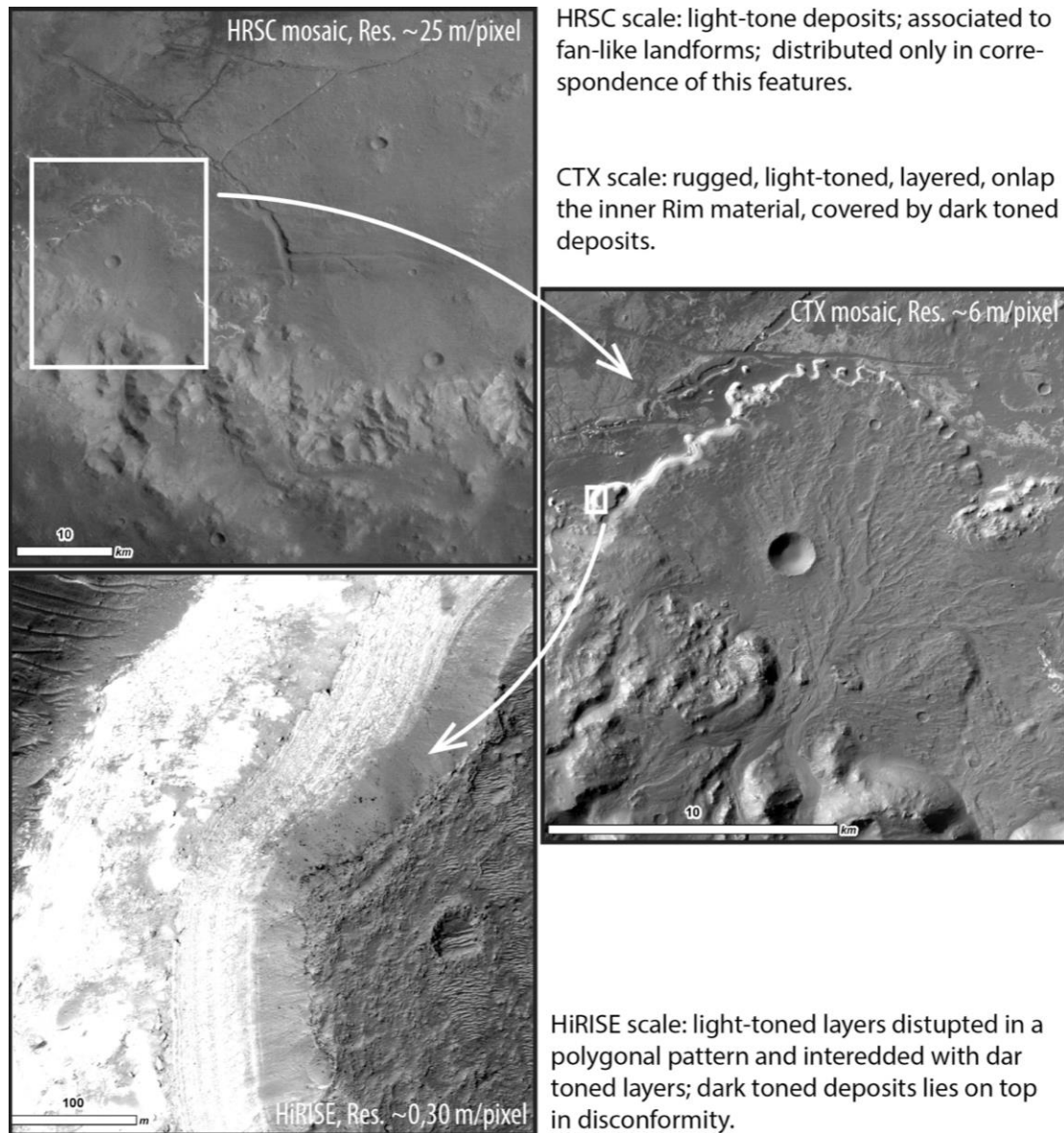
c. The concept of ‘stratotype’ in planetary mapping: ‘reference area’

Regardless of the mapping approach and/or stratigraphic units under consideration, the definition of a physical place that can serve as a reference is of essential importance. On Earth, the concept of stratotype is defined as ‘the designated exposure of a named layered stratigraphic unit or of a stratigraphic boundary that serves as the standard of reference’ (ISSC, 1999). The baseline is to have a reference that allows to standardize the definition of the units, so as to allow reproducibility of the observations first within the study area, but then also outside and potentially worldwide. Although such a concept cannot be simply mutated to planetary settings, clearly defining the units making use of their best occurrence in order to always have a reference is a good practice generally already used for example in the description section of scientific papers. Here we propose some procedures to maximize the effectiveness of such practice, introducing the concept of ‘reference area’, without constraining its definition with a formal procedure.

The ‘reference area’ should correspond, regardless of the kind of unit, to the place where this unit is best exposed, visible, and data covered. If the unit or its boundaries are not fully represented in one single location, more reference areas may be envisaged. When the unit displays a complexity that cannot be represented in a single area, one or more ‘complementary reference areas’ should be introduced.

Both in the reference and in the complementary reference areas, the unit should be represented with all (or all of the pertinent) available datasets, and described accordingly at the different necessary scales. As an example, the light-toned deposits of Holden crater (Mars) are represented at HRSC (High Resolution Stereo Camera; Neukum et al., 2004), CTX (Context Camera; Malin et al., 2007), and HiRISE (High Resolution Imaging Science Experiment; McEwen et al., 2007) scale (Figure 1.1). The unit should be described at all the different scales allowed by the different datasets.

Figure 1.1: Representation of the same unit (light-toned deposits, Holden crater, Mars) at HRSC, CTX, and HiRISE scale. Different data allows different observations.



d. Focus on stratigraphic relations

With the notable exception of feature-based maps, stratigraphic relations are conceptual frameworks of any kind of geoscientific cartography. The definition of the vertical and lateral relations between the different units must accompany the unit distribution information provided in the map. Relative stratigraphy among the different units should always be documented and properly represented. In stratigraphic sequences attention should be paid to recognize and document unconformable boundaries, in order to emphasize the presence of hiatus in the depositional record, as well as cross cutting relationships should be taken into account in intrusive magmatic and volcanic environments.

Such relations can be conveyed with stratigraphic sketch, stratigraphic columns and/or geological sections (Figure 1.2) in order to focus on the geometrical relations between

the units but also in space-time diagrams to convey the age of the units and the missing time. These schemes are specifically effective when the age of some units is tied by crater count absolute dating (Figure 1.3). As on Earth geological maps, stratigraphic columns and sketches might even report the eventual different erodibility of the geological units.

Figure 1.2: Example of geological section from Firsoff crater (Pondrelli et al., 2015)

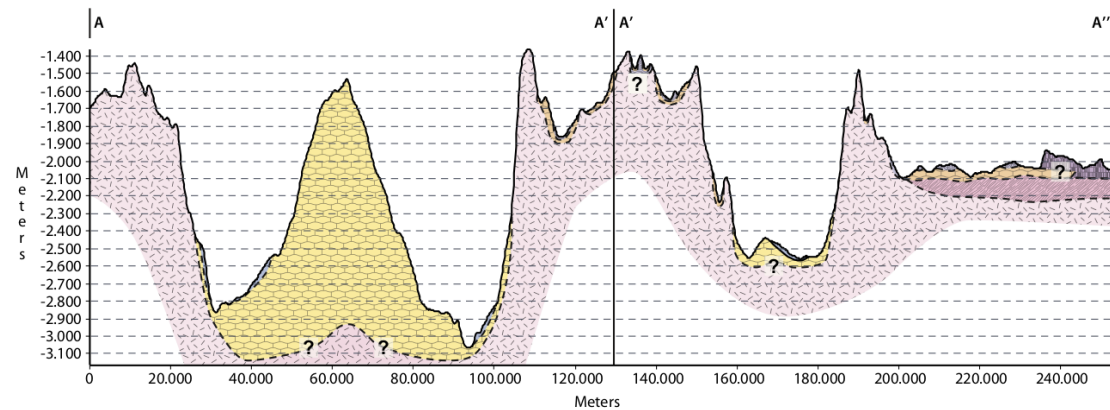


Figure 1.3: Example of correlation diagram from the Navua Valles (Hargitai et al., 2016)

CORRELATION OF MAP UNITS

PERIOD	BOCH (Pichard 2013)	IMPACT* AND CRUSTAL UNITS		BASIN SLOPES AND RIM UNITS		CHANNEL AND VALLEY UNITS		BASIN UNITS		CHANNEL UNITS	
AMAZONIAN	Late	c, cl cp, cg		b	fc fl	Navua A	Navua B	c, cl cp, cg		fc fl	db
	Middle	1.23				cm	cm	AcH75 Acg1089			cm
	Early	1.17		AHp				AcP1579 AcP	AHp2 AHpb		cm
HESPERIAN	Late	Hcl35 HclM	HNms	Hpd	e f					Hmib Hml	f
	Early	3.71	Hcl124		NH126			Hcl346			
			Ncl126 c, cl, cr cp, cg								
NOACHIAN	Late	3.83	HNcl431	Nmi				c, cl cp, cg			
	Middle										
	Early	3.94	Nm								

*Numbers in impact unit designations refer to the crater ID in the crater catalog in Robbins, S. J., Hynes, B.M., 2012. doi: 10.1029/2011JE003966.

2. Feature-based mapping

The cartography of one (or few) specific landform(s), structure(s), and/or mineral(s) address the distribution of such elements over the whole planetary body (or a large portion of it). Typical examples consist of crater catalogues (e.g. Salamunićar et al., 2012) (Figure 2.1), valley networks and putative shorelines distribution on Mars (e.g. Baker et al., 2015) (Figure 2.2), or dune database on Mars (Hayward et al., 2007) (Figure 2.3), faults on diverse planetary bodies (e.g. Byrne et al., 2014), major volcanic provinces on Moon, Mars, Venus (Platz et al., 2015).

Figure 2.1: Examples of feature-based mapping: crater distribution on the Moon and on Mars (Salamunićar et al., 2012)

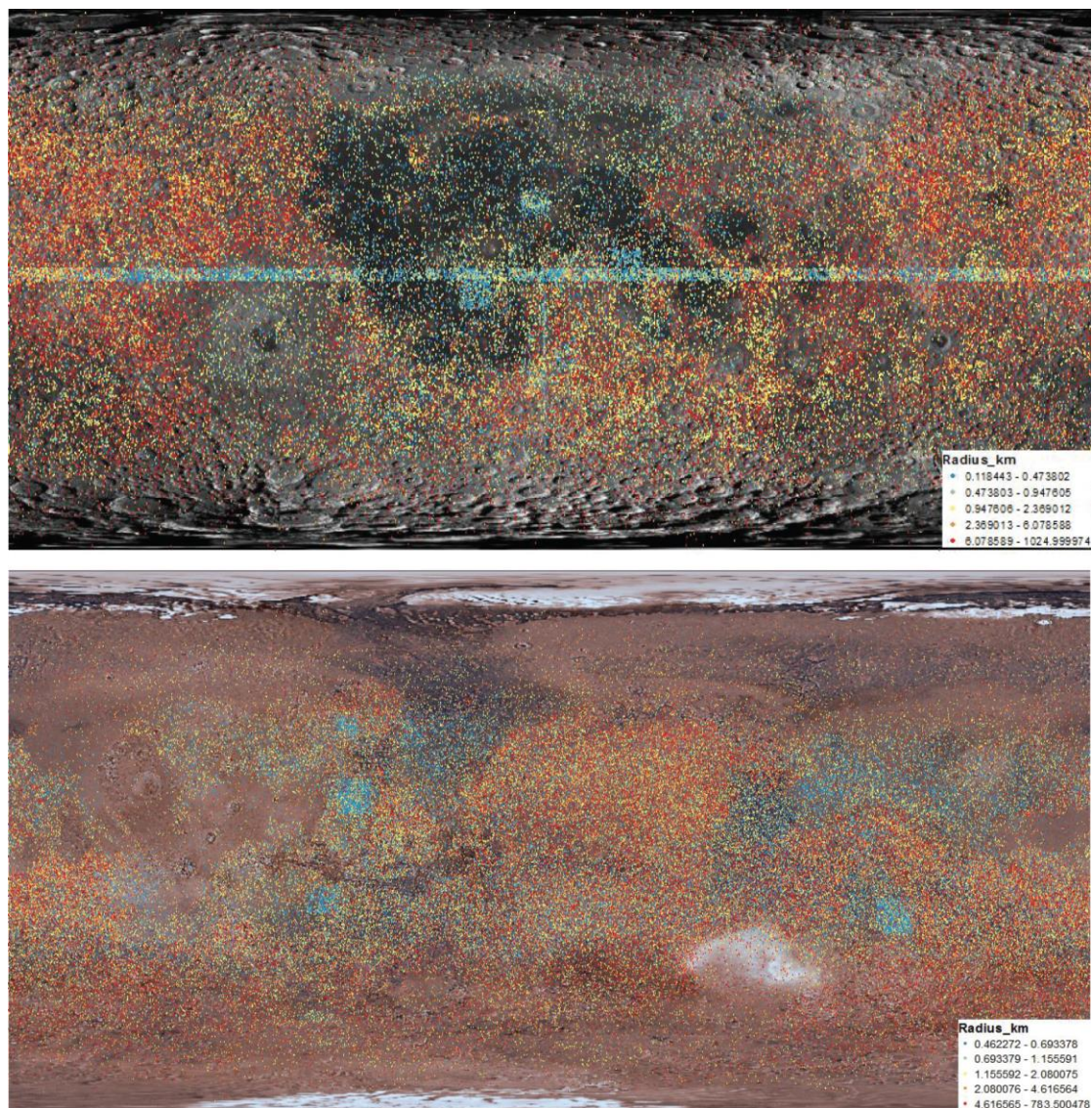


Figure 2.2: Example of feature-based mapping: valley network and shorelines on Mars (Baker et al., 2015)

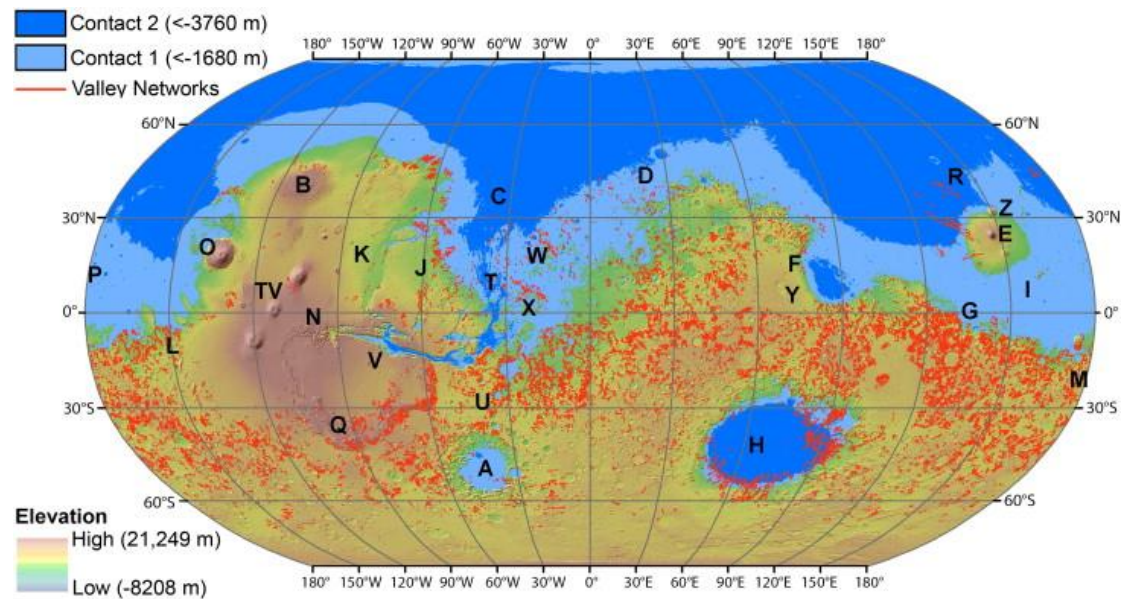
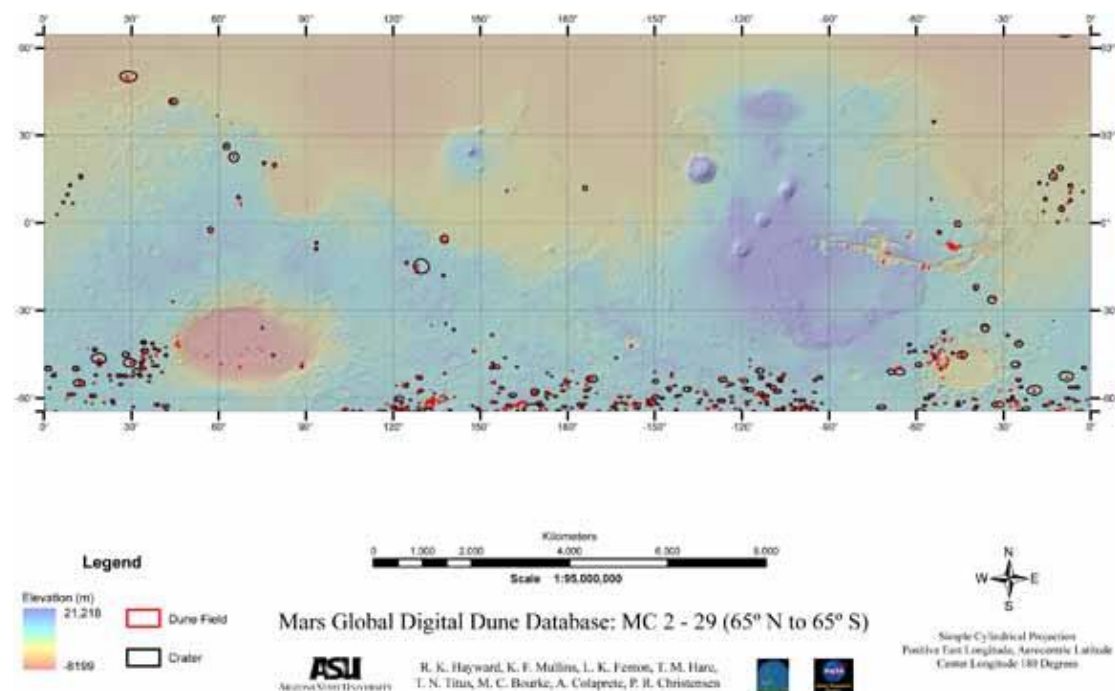


Figure 2.3: Examples of feature-based mapping: Mars dune database (Hayward et al., 2007)



Such cartography serves as a base for wide reconstructions both in terms of scale and genetic processes. Accordingly, unit definitions should be broad, avoiding unnecessary details that might defocus from the aim. For these reasons, fields of the attribute tables assigned to the units should be broad as well, making use of definitions able to convey general concepts. Still, geometric and geographic characteristics should be included (e.g. Figure 2.4).

Figure 2.4: Attribute table from the catalogue of Martian craters (Salamunićar et al., 2012)

	Lon_E	Lat	p	Name	Radius_deg	Radius_km
1	2,363280	73,593748	1,000000	S000001B00371R11256C00269T75557Y2005S (144,-4;20,-4;128,-184)	0,151909	8,988000
2	-170,335936	60,656246	1,000000	S000002B00603R10024K20241T75303Y2005S (84,-8;-4,0;108,-284)	0,145563	8,612526
3	-108,886714	60,167967	1,000000	S000003B01099R06820K20279T75084Y2005S (84,0;12,-4;108,-284)	0,183144	10,836081
4	-37,417967	56,761718	1,000000	S000004B01803R05240C00134K20533T74496Y2005S (0,0;4,8;120,-308)	0,225853	13,363044
5	37,992187	58,617187	1,000000	S000005B02753R13896K20444T74775Y2005S (0,0;4,-4;104,-292)	0,10686	6,322586
6	112,425777	58,675777	1,000000	S000006B04456R19225C00762K20395T74879Y2005S (0,0;0,0;108,-296)	0,07321	4,331616
7	-178,480467	27,593748	1,000000	S000007B05742R15282C00513K23109T60916Y2005S (0,0;12,0;100,-276)	0,101329	5,995333
8	-142,742184	34,015620	1,000000	S000008B00700R09967T61918Y2005S (0,0;4,0;112,-308)	0,136975	8,104400
9	-106,992187	24,382812	1,000000	S000009B06120R12987T63269Y2005S (0,0;12,12;104,-272)	0,120404	7,123943
10	-72,957029	31,027342	1,000000	S000010B01311R08872K22792T65176Y2005S (0,0;20,0;104,-304)	0,162883	9,637298
11	-38,640623	26,460937	1,000000	S000011B07886R03253C00080K23201T69396Y2005S (0,0;12,4;100,-276)	0,291313	17,236116
12	0,660155	32,835937	1,000000	S000012B03926R03014T46708Y2005S (0,0;12,0;108,-316)	0,308203	18,235447
13	37,472652	26,156248	1,000000	S000013B09386R02385C00045T49287Y2005S (0,0;-8,4;100,-276)	0,343768	20,339721
14	71,660155	32,753905	1,000000	S000014B04762R12194T52608Y2005S (0,0;12,0;104,-304)	0,119199	7,052647
15	107,964842	30,343748	1,000000	S000015B04638R15305C00623K22911T55419Y2005S (0,0;4,0;104,-296)	0,087985	5,205808
16	143,429687	30,710937	1,000000	S000016B05179R07375K22856T58525Y2005S (0,0;8,-8;104,-304)	0,179027	10,592491

3. Process-based ‘interpretative’: Geomorphological/Morphostratigraphic Map

Geomorphological maps are based on the qualitative-quantitative representation and genetic interpretation of landforms. On Earth, such study is generally possible only in the most recent deposits (\approx Quaternary), while many planetary settings are characterized by a limited degree of weathering and erosion that favour good preservation of morphologies also in the deep geological time. Since detailed outcrop or laboratory analyses are only rarely possible in planetary settings, geomorphological/Morphostratigraphic maps represent the basic tool to infer the geological evolution of planetary bodies. Accordingly, geomorphological maps are topical maps mostly oriented to science investigations.

Different geological settings characterize different planetary bodies, and each planet/satellite displays its own peculiarities, but some generalizations within broad groups are nevertheless possible. We distinguish bodies with atmosphere, focusing on Mars as a paradigm, airless bodies, with the Moon as a paradigm, small bodies, and icy satellites.

a. Planets with an atmosphere: Mars as a paradigm

Here we classify the main different geological processes that can be found on Mars. Needless to say, more of those can be found somewhat associated together within the same map. Moreover, all the described systems will be affected by the interaction with two processes which are ubiquitous on Mars: cratering and mass wasting.

Craters can be mapped with different detail and down to smaller dimensions depending on the chosen scale of work. In a map finalized to the reconstruction of the depositional systems and of their stratigraphy at the regional scale, only bigger craters (e.g. exceeding 1 km in diameter) should be mapped and without need of internal distinction,

even if bigger craters (i.e. diameter exceeding tens of kilometers) can be subdivided in crater rim, crater floor, and crater ejecta.

In a detailed map at the local scale, even smaller craters (down to diameters of 100 meters or even less in case of very detailed maps) can be mapped and their internal distinction reported.

Craters should be categorized depending on their dimensions and morphology:

- simple craters
- complex crater
- peak ring basins

Their degree of preservation should also be reported in another descriptive field:

- pristine crater
- eroded crater
- partly covered crater
- ghost crater
- pedestal crater
- rampart crater

Similarly, mass wasting processes can be mapped as unique features in a regional map, while at a local scale different landslides can be listed following Crosta et al. (2018) classification. This classification is very detailed and specifically designated to a dedicated process study. For a non-specifically aimed mapping project, the classification of the type of landslide can be sketched as follows:

- rock avalanche
- slump
- slump/rock avalanche
- debris flow
- rock avalanche/ejecta
- spreading/sagging/deep-seated gravitational slope deformations

i. Mars Volcanic Processes

1. Science rationale

Topical Map. Aim: science (interpretative). Define the scale(s) of work.

Volcanic processes were widespread throughout the geological history of Mars and greatly shaped its surface. The volcanic province of Tharsis covers 25% of the Martian surface and contains the giant shield volcanoes of Olympus Mons and Tharsis Montes. The formation of these giant shield volcanoes (up to 21 km high for Olympus Mons) results from the accumulation of low viscosity lava combined with the lack of plate tectonics (i.e. the edifice always remains above the source of magma). Volcanic shields display major caldera collapses as well as volcano-tectonic features. Global and regional maps should focus on main volcanic complexes and their associated units. The units should be classified according to their ages (Garry et al. 2018).

A wide variety of features of different smaller scale features are associated to volcanic events on Mars. Various lava flows are covering the flanks of the edifices as well as the plains surrounding them. These lava flows should be the focus of higher-resolution maps and can be represented individually, if possible, or as different lava fields. Symbology of the map can indicate stratigraphical relationships as well as typology (lava sheets, inflated lava flows, ridged lava flows, lava channels, lahars etc.). Mapping of lava flows allows chronostratigraphic reconstruction of volcanic episodes and provides valuable information on Mars' internal processes. Relative stratigraphy can be completed by impact crater retention age in order to further reconstruct the eruptive history.

Alongside lava flows, other smaller-scale elements are also suited for local maps such as scoria cones, tuff rings, secondary vents, potential dykes, pit chain craters, smaller calderas and jameos underlying development of subsurface lava tunnels. Crosscutting relationships between these features and lava flows can help to estimate the when they formed during the eruptive timeline. Moreover, features like lava tubes can be linked to emplaced lava flows downstream and could indicate flow inflation. Such information is important as flow inflation can affect the apparent thickness of the lava flow and provide misleading information on lava flow viscosity during emplacement.

The map scale could be both global/regional and local. In the first case major units of the different volcanic complexes are highlighted according to their ages, in the second single lava flows should be mapped trying to distinguish their typology (lava sheets, inflated lava flows, ridged lava flows, lava channels, lahars etc.) and overlapping relationships. The regional maps are particularly suited also to represent volcanotectonic structures and major caldera collapses, whereas high resolution maps can report also smaller features such as pit chains, calderas, jameos underlying the development of subsurface lava tunnels, scoria cones, tuff rings, secondary vents and potential dikes.

ii. Mars Sedimentary Processes

Mars displays a large variability of sedimentary deposits/morphologies/successions/basins, reflecting air, water, ice, and gravity-driven transport/deposition. These materials show that at least Early Mars had an active sedimentary cycle, but they are present in some form during most of Mars' geological time so that Mars displays sedimentary rock successions with close similarities, and some considerable differences, with the Earth.

Sedimentary materials are specifically important because they can provide information on the climatic evolution of the planet, and on potential habitable conditions and environments. Moreover, the dynamics/evolution of the sedimentary records can be an insight into the comprehension of the same processes and environments present on Earth in the fossil record but not actualistic.

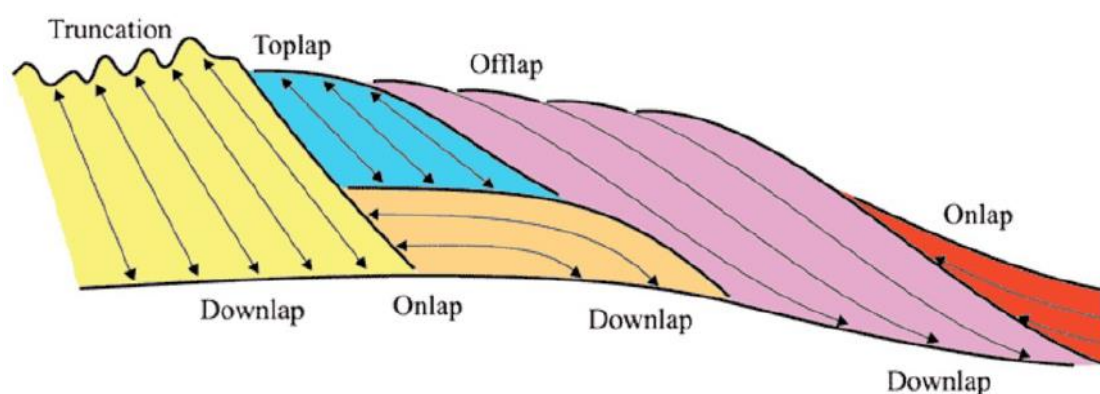
The study of such systems on Mars is somewhat flawed by the lack of information at the outcrop and hand specimen scale (with the notable exception of the landing sites investigations), which obviously limit the detail of any kind of reconstruction. On the other hand, their understanding is helped by the low weathering degree that preserves

morphologies even billions of years old. The problem of Convergence (Equifinality) that is intrinsic to the interpretation of morphologies by remote sensing means, implies the necessity to strengthen the interpretations by laterally and vertically relating different landforms. This is at the base of the importance of geomorphological mapping, but at the same time emphasize the importance of constraining the interpretation as much as possible. Correlating different landforms is indeed essential because it allows moving from the interpretation of a single landform to the interpretation of associated landforms (i.e. a landscape), providing much more constraints and solidity to genetic interpretations.

Following these issues, geomorphological mapping of sedimentary systems needs a good degree of detail, ranging from the regional to the local (= basin) scale, depending on the kind of sedimentary system and data availability. More detailed analyses can be possible, but the lack of coeval correlated landforms might hamper the genetic interpretation.

The relative stratigraphic distribution among the different mapped morphological elements should be presented in a stratigraphic sketch that, together with the legend, constitute the key to 'read' the geomorphological/morphostratic map (e.g Pondrelli et al., 2008; Hargitai et al., 2018). The realization of stratigraphic sketch is particularly important in sedimentary settings, especially when layers are visible. In this case the use of the term bedset instead of layers is encouraged, in order to take into account the limits associated to the available resolution which hamper the identification of thin beds. Bedset represents a number of superposed, similar beds. This definition appears more appropriate in all the settings affected by resolution-related limits. The identification of bedsets termination is particularly important to infer the relations between sedimentary input and available accommodation space within the basin (Figure 3.1).

Figure 3.1: Geometry of bedsets termination (Catuneanu, 2006)



Outflow channels

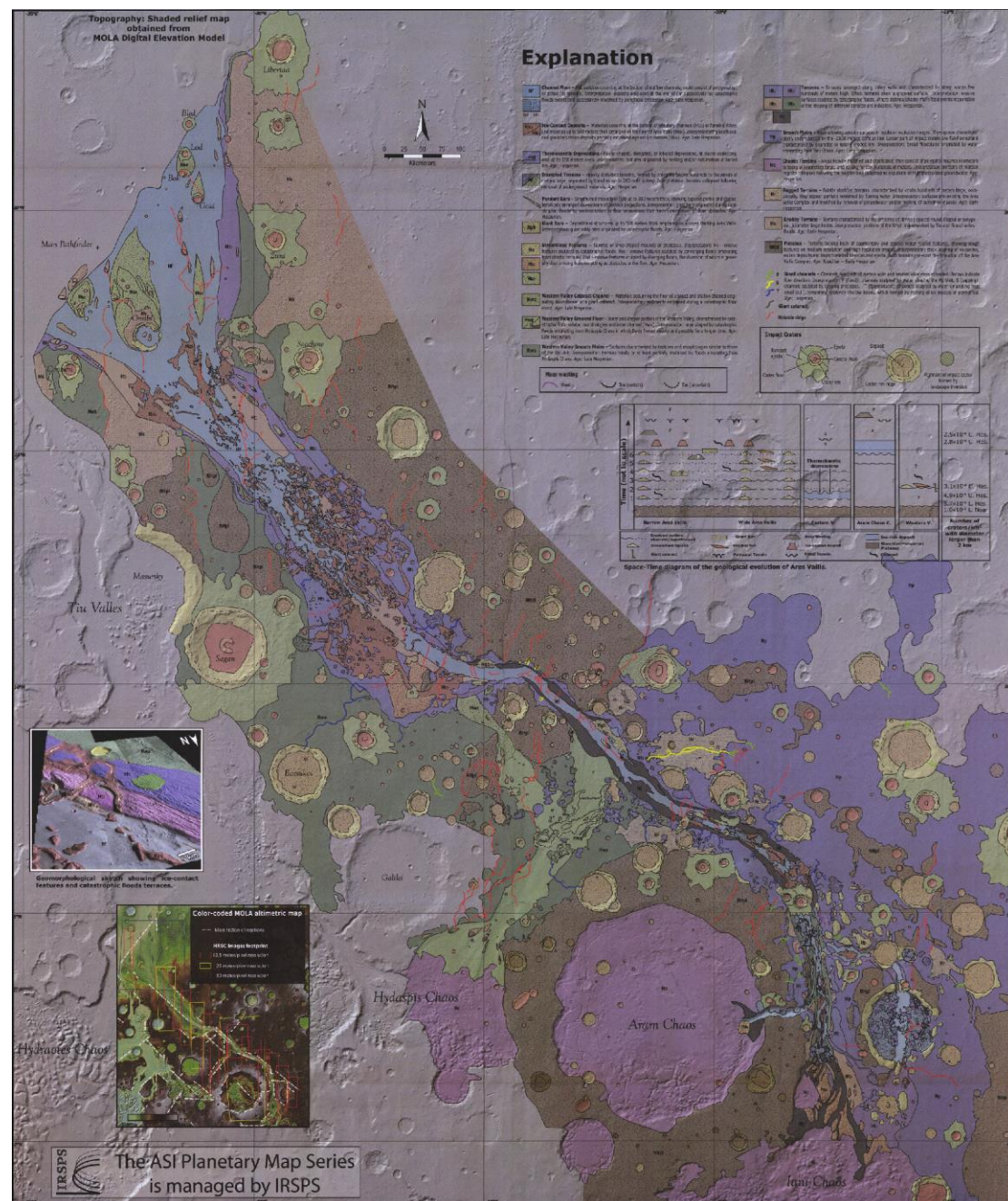
Outflow channels on Mars have particular importance, because they had been the first deposits suggesting the presence of water-related processes to be identified but also because their relatively pristine morphology was functional to a better understanding of the same morphological assemblages on Earth. They have been described extensively in many papers (e.g., Baker et al., 1983, 1992; Carr, 1996; Wilson et al.,

2004; Rodriguez et al., 2015). They represent mostly erosional very large structures that can be up to thousands of kilometers long and tens of kilometers large, carved by catastrophic flooding generated by rapid groundwater evacuation.

Provided the scale of these morphologies, even a detailed map should be developed at the regional scale to include and correlate elements that form the system.

Examples of geomorphological maps describing outflow channels systems can be found for example in Pacifici (2008), Chapman et al. (2010), Glamoclija et al. 2011, Erkeling et al. (2011), and Kukkonen et al. (2018) (Fig. 3.2).

Figure 3.2: Geomorphological Map of Ares Vallis (Mars) (Pacifici, 2008)



The morphological elements associated with such a process are:

- Chaotic Terrains/Remnant Terrains - polygonal mounds and knobs
- Smooth Plains - smooth-textured surface
- Terraces - sometimes showing grooved surfaces
- Grooved floor - valleys or portions of valleys sculpted by grooves
- Cataract channel - material deposited downstream of a cataract
- Streamlined features - tapered and/or drop-shaped mounds or plateaus
- Giant bars - features paralleling the flow direction
- Pendant bars - streamlined, tapered mounds or hills, which parallel the flow direction downstream to a bedrock projection
- Channel floor - flat surfaces occurring at the base of the channels
- Small channels

Such a list is general and intended to serve as a reference rather than to be an all-encompassing framework. Other units can be present depending on specific local conditions and on the interaction with other geological settings and/or processes (e.g. glacial, volcanic).

Some features need to be mapped using a polygonal shapefile (e.g. Smooth Plains, Channel floor), other with a linear shapefile (e.g. Grooved floor, Channel floor), in other cases, the choice can be arbitrary (e.g. Streamlined features, bars). Specifically for the linear shapefile, alongside the unit definition, a field describing the degree of preservation of the features is envisaged.

The following qualitative classification is a possible reference but can be adapted to the specific need of the specific mapped area.

- Poorly preserved
- Eroded
- Partially buried
- Subdued
- Well preserved
- Pristine

In the polygonal shapefile, a good practice is to include a field with the unit extensive name alongside one with the unit acronym which might be later visualized in the map.

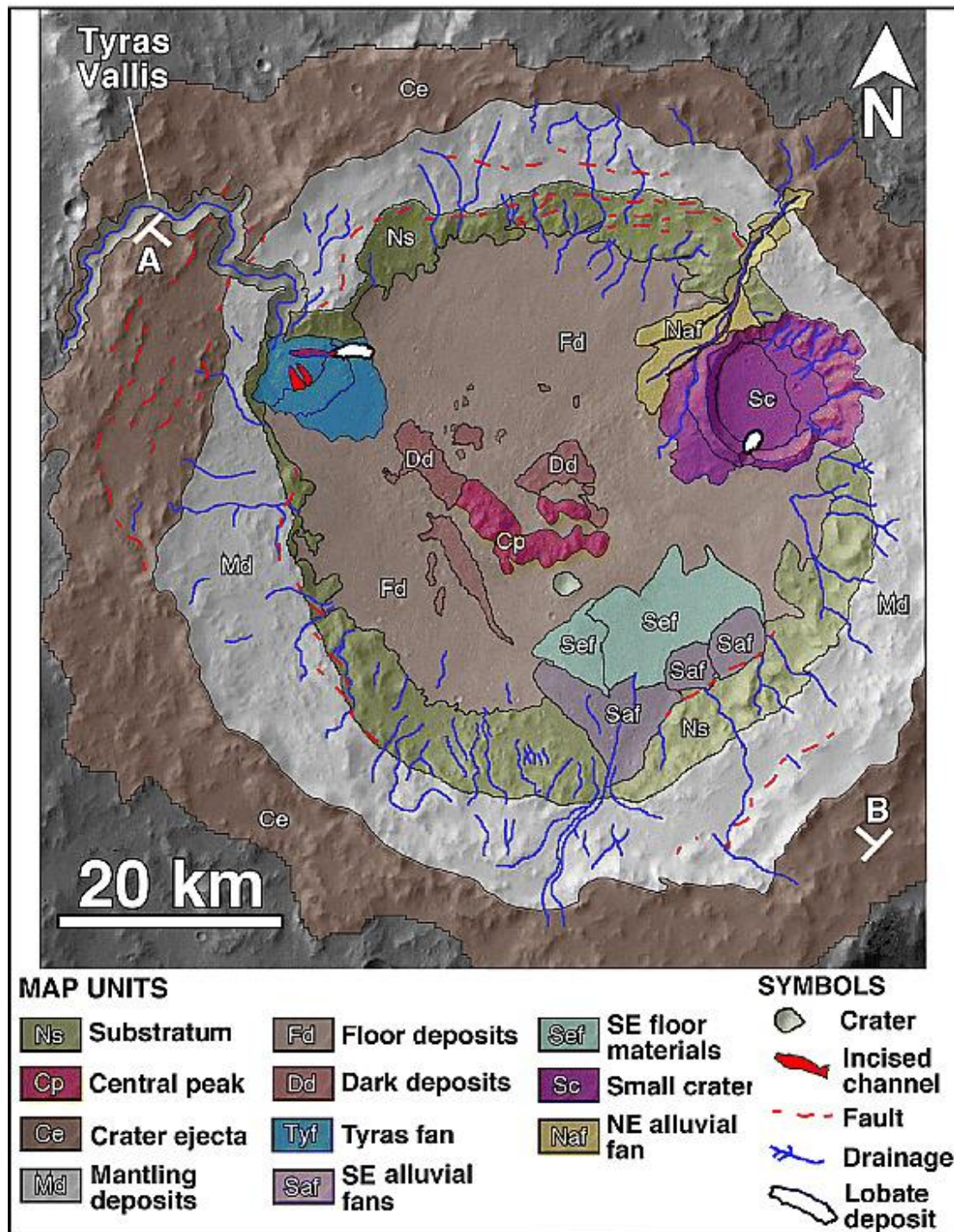
Fluvio-lacustrine deposition

Fluvio-lacustrine depositional environments are among the most important deposits and morphologies on Mars because they do not only prove the presence of water to shape the Martian landscape but they suggest that water was stable on the planet surface for a geologically significant amount of time. This has pivotal implications in the climate evolution and habitability potential analyses of Mars. Fluvio-lacustrine systems were described in many papers (e.g. Craddock and Howard, (2002); Malin and Edgett (2003); Moore and Howard, 2005; Baker et al., 2015). Although, geomorphological evidence to constrain the existence of an ancient ocean such as paleo-shorelines in the northern lowlands (e.g. (Parker et al., 1989, Baker et al., 1991; Parker et al., 1993; Clifford and Parker, 2001; Carr and Head, 2003; Tanaka et al., 2003, Tanaka et al., 2005) are more difficult to find, because easily subjected to erosion, on the other hand bedrock as well as alluvial rivers and fan-shaped deposits (alluvial fans and deltas) leave enduring traces

on the planet surface, allowing water-related depositional environments to be recognized and mapped (e.g. Malin and Edgett, 2003).

Fluvio-lacustrine structures can be mapped at different scales and with different degrees of detail, depending on science interests and data availability and resolution. From the regional scale (i.e. a scale exceeding the extension of a single drainage basin) to the basin scale, depositional sub-environments can be recognized (e.g., Di Achille et al. 2006; Hargitai et al., 2018), without entering into the details of the depositional elements (Fig. 3.3).

Figure 3.3: Geomorphological Map of Tyras crater (Mars) (Di Achille et al., 2006)



These depositional sub-environments are:

- Channels
- Alluvial fans
- (Fan)deltas
- Terraces (shorelines)
- Basin floor

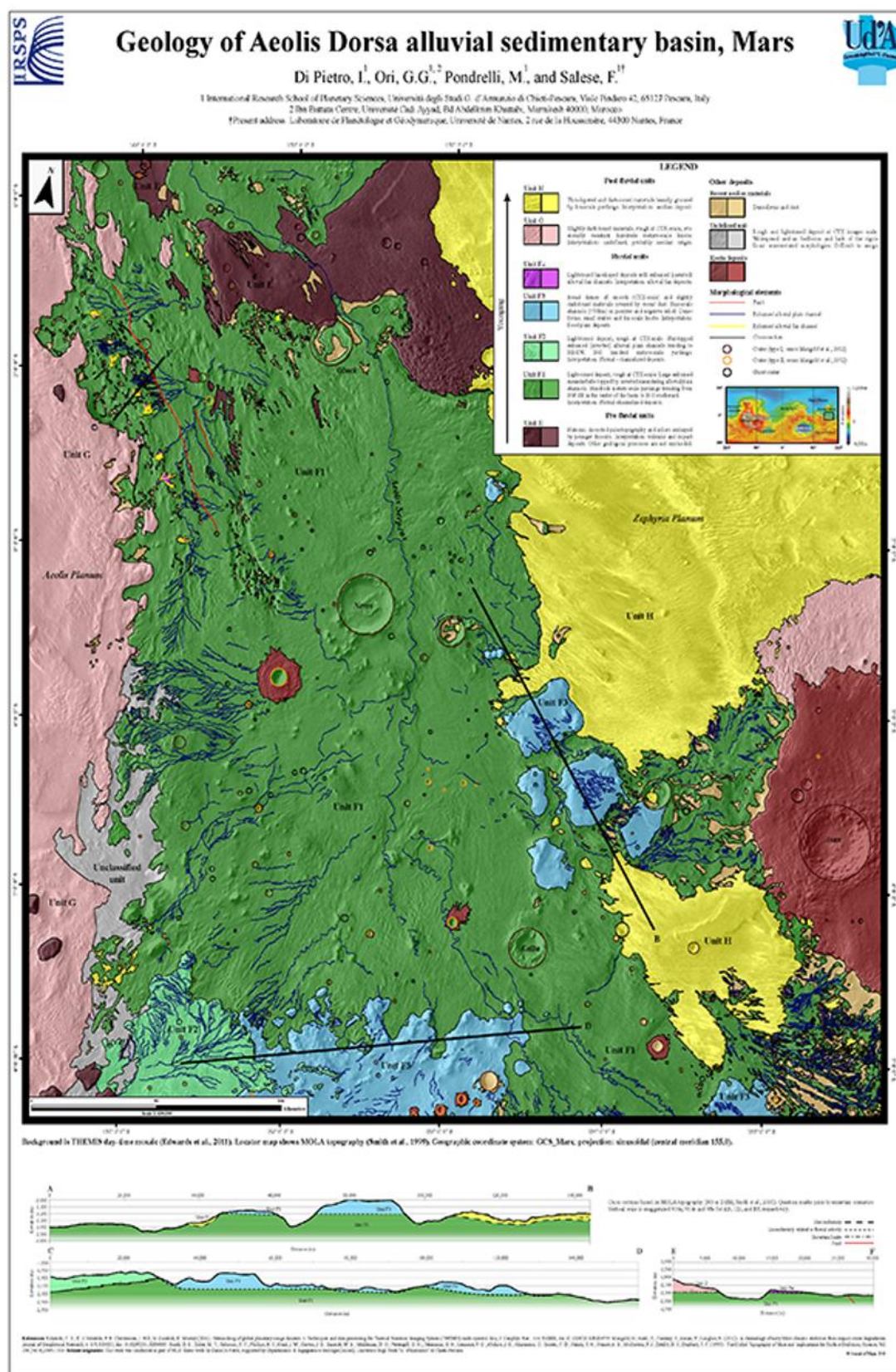
In order to distinguish between clastic-dominated and evaporite-dominated systems it can be important to include mineralogical hints derived from hyperspectral data. These data can integrate the morphological assemblage to constrain the interpretation. Clay-bearing deposits associated with surface runoff, deltas and shorelines are strong indications of clastic-dominated lacustrine systems (e.g. Thomas et al., 2017); sulfate-bearing basin floor materials possibly associated with fluid expulsion morphologies (e.g. Pondrelli et al., 2019).

Other units related for example to glacial, mass wasting, fluid expulsion phenomena can be associated to the fluvio-lacustrine ones depending on specific local conditions and on the interaction with other geological settings).

At the basin scale (Figure 3.4), when high-resolution data are available (i.e. HiRISE and or MOC NA images), even the discrimination of the following depositional elements is possible (Pondrelli et al., 2008; Di Pietro et al., 2018).

- Source area: Bedrock rivers
 - Runoff
 - Sapping valleys
- Alluvial fans:
 - alluvial channels
 - interdistributary areas
- Alluvial plain
 - alluvial channels
 - braided channels
 - rectilinear channels
 - meandering channels
 - anabranching channels
 - floodplain
 - crevasse splays
- (Fan)deltas
 - Delta plain
 - channels
 - braided channels
 - rectilinear channels
 - meandering channels
 - interdistributary areas
 - crevasse splays
 - interdistributary bay
 - Delta front
 - input-dominated
 - wave-dominated
 - Prodelta
- Fluid-expulsion
- Basin
 - Shorelines
 - basin floor
- Playa

Figure 3.4: Geomorphological Map of Aeolis Dorsa (Mars) (Di Pietro et al., 2018)



Not all these depositional elements are necessarily present or recognizable in the study area; moreover, these features might be associated with other structures related to erosional (e.g. mesas and cuevas) and/or other depositional bodies (e.g. sedimentary volcanoes, detrital cones), either coeval and/or genetically connected with fluvio-lacustrine deposition.

Available mineralogical hints derived from hyperspectral data should be integrated in order to constrain the genetic interpretation. The difference of resolution between spectral and imagery data is always an issue to be carefully considered, but specific attention must be given to such detailed reconstructions. The reconstruction of the Stratigraphic relationships is the base for a proper association of the mineralogical hints to the related morphological assemblage.

Some features should be mapped using a polygonal shapefile (e.g. floodplains, basin floor), others with a linear shapefile (e.g., all the types of channels). Alongside the unit definition, the shapefiles should be associated also to a field describing the degree of preservation of the features. This list might serve as a reference, even if other definitions, related to local specific conditions, can be used:

- Poorly preserved
- Eroded
- Partially buried
- Subdued
- Well preserved
- Pristine

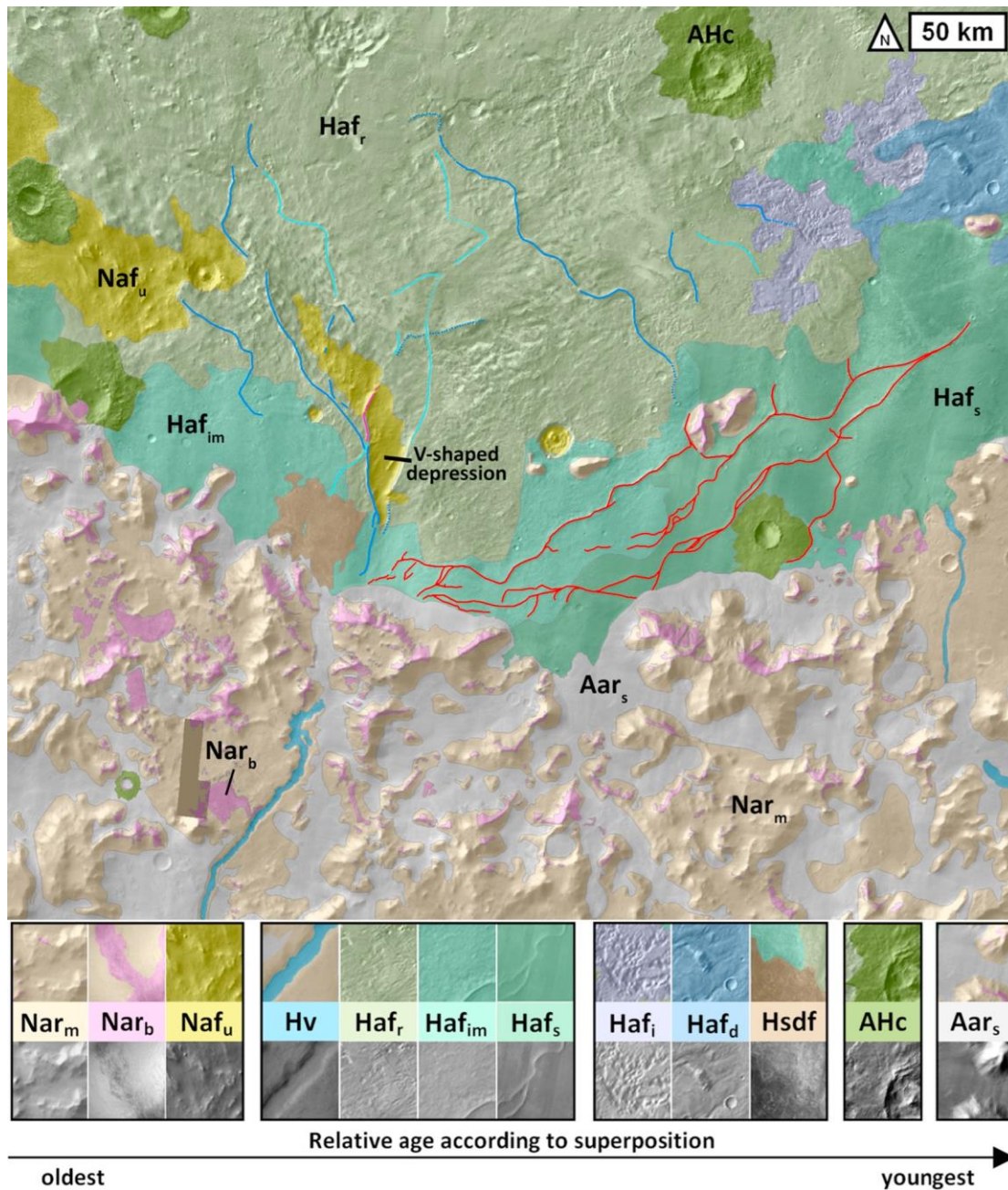
With such a detailed representation, stratigraphic relations but also the internal depositional geometry of the units can be well represented. Geological sections and stratigraphic sketches need to accompany the legend as a key to understanding the map (e.g. Pondrelli et al., 2008; Ansan et al., 2011; Di Pietro et al., 2018).

Ice-related deposition

Ice represents a very important exogenic factor in the geological history of Mars (e.g. Head and Marchant, 2003; Head et al., 2005, van Gasselt et al., 2007). Glacial processes occur directly in contact with the glaciers while periglacial features are related to cold climate, typically near glaciated areas.

Glacial landforms and processes occur even today in ice sheets in correspondence of the polar regions where the Polar Layered Deposits (PLDs, made of mostly water ice and dust) occur (e.g. Smith et al., 2016). Also, valley glaciers (e.g. Dickinson et al., 2008; Head et al., 2010) have been proposed to be active in the recent geological past of Mars. Specifically, wet based glaciers have been proposed and mapped (e.g. Bernhardt et al., 2013; Gallagher and Balme, 2015; Tsibulskaya et al., 2020; Butcher et al., 2021) (Figure 3.5). These systems are associated with fluvial systems developing in subglacial (eskers) and supraglacial settings, and at the glacier terminus (Figure 3.5), and as a consequence they have very effective erosional capabilities.

Figure 3.5: Geomorphological Map of southern Argyre Planitia (Mars) (Bernhardt et al., 2013)

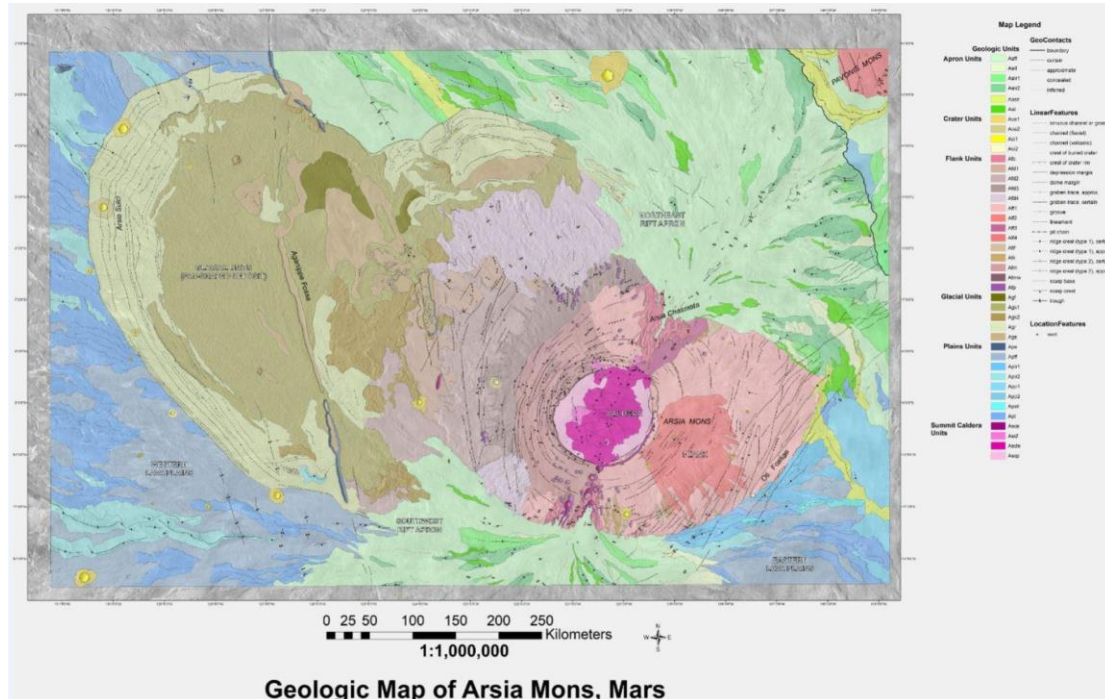


Such systems can be mapped at the regional scale as complete systems while at the local scale, the different sub-environments can be distinguished. An exemplary list is provided:

- terrains modified by glacial and/or fluvial action
- lobate debris apron
- lineated valley fill
- terminal lobes
- sublimation till (knobby)
- drop moraines (ridged)
- eskers
- fluvio-related environments

Cold-based glaciers have been documented and mapped in several locations (i.e. Head et al., 2003; Hernández and Carrillo, 2012; Garry et al., 2018) (Figure 3.6).

Figure 3.6: Geomorphological Map of Arsia Mons (Mars) (Garry et al., 2018)



Because of the lack of interaction with water, such glaciers are less effective in shaping the landscape and also more difficult to recognize, still very large examples have been documented along the slopes of Tharsis volcanoes.

Such systems can be mapped at the regional scale as complete systems while at the local scale, the different sub-environments can be distinguished. An exemplary list is provided:

- terrains modified by glacial action
- lobate debris apron
- lineated valley fill
- sublimation till (knobby)
- drop moraines (ridged)

Periglacial environments are considered to be very extensive and active in the very recent geological history of Mars (e.g. Rossi et al., 2011; van Gasselt et al., 2011; Barrett et al., 2018). Ground ice related features are part of several maps, including Soare et al. (2018), Ramsdale et al. (2019). Some of the features that can be mapped at the local scale are represented by:

- surface polygonization
- clastic patterned ground
- pitted cones
- Lineated crater/depression-fill materials
- lobate hill slope features
- scalloped depressions
- protalus lobes and ramparts

Aeolian deposition

Aeolian erosional and depositional processes represent probably the most effective ones to shape Mars surface in the last few million years. Accordingly, their understanding is critical in order to infer present wind circulation and geologically recent high-frequency climate changes. Such relatively recent deposits and processes have been broadly described in the literature, including Hayward et al. (2007), Hobbs et al. (2010), Silvestro et al. (2013, 2021), Ayoub et al. (2014), Bridges et al. (2017), Lapotre et al. (2018). Examples of maps related to such processes are reported for example in Silvestro et al. (2010), Cardinale et al. (2012), and Vaz and Silvestro (2014).

In the fossil record, different deposits involving aeolian processes, or with a contribution of aeolian processes, have been suggested to have formed on Mars. Thick successions (up to several hundred meters) of cross bedded sandstones have been interpreted as formed by aeolian dunes, interbedded with lacustrine or playa deposits (Grotzinger et al., 2005; Banham et al., 2018; Rapin et al., 2021). Airfall, probably related to volcanic/pyroclastic flows, have been suggested to have an important role in the deposition of several sulfate-bearing deposits (i.e. Zimbelmann and Griffin, 2010).

‘Recent’ aeolian deposits can be mapped at different scales: they can be represented as areas where uniform morphologies occur (e.g. fields of dunes of different typologies) or each single morphology can be distinguished as an area (mapping the entire distribution of the landform) and/or as line (e.g. dune crestline).

Mapping areas where uniform morphologies (or morphological assemblages) occur is recommended for regional or supra-regional studies, the extreme case becoming a feature-based map. Distinguishing single different morphologies using their areal extent is extremely useful from the regional to the local scale, for describing landform distribution, performing source to sink analyses, and as a context for further studies focusing on depositional processes and/or wind regime reconstruction (Figures 3.7, 3.8).

Figure 3.7: Location and geomorphological Map of aeolian deposits in the East Thaumasia region (Mars) (Silvestro et al., 2010)

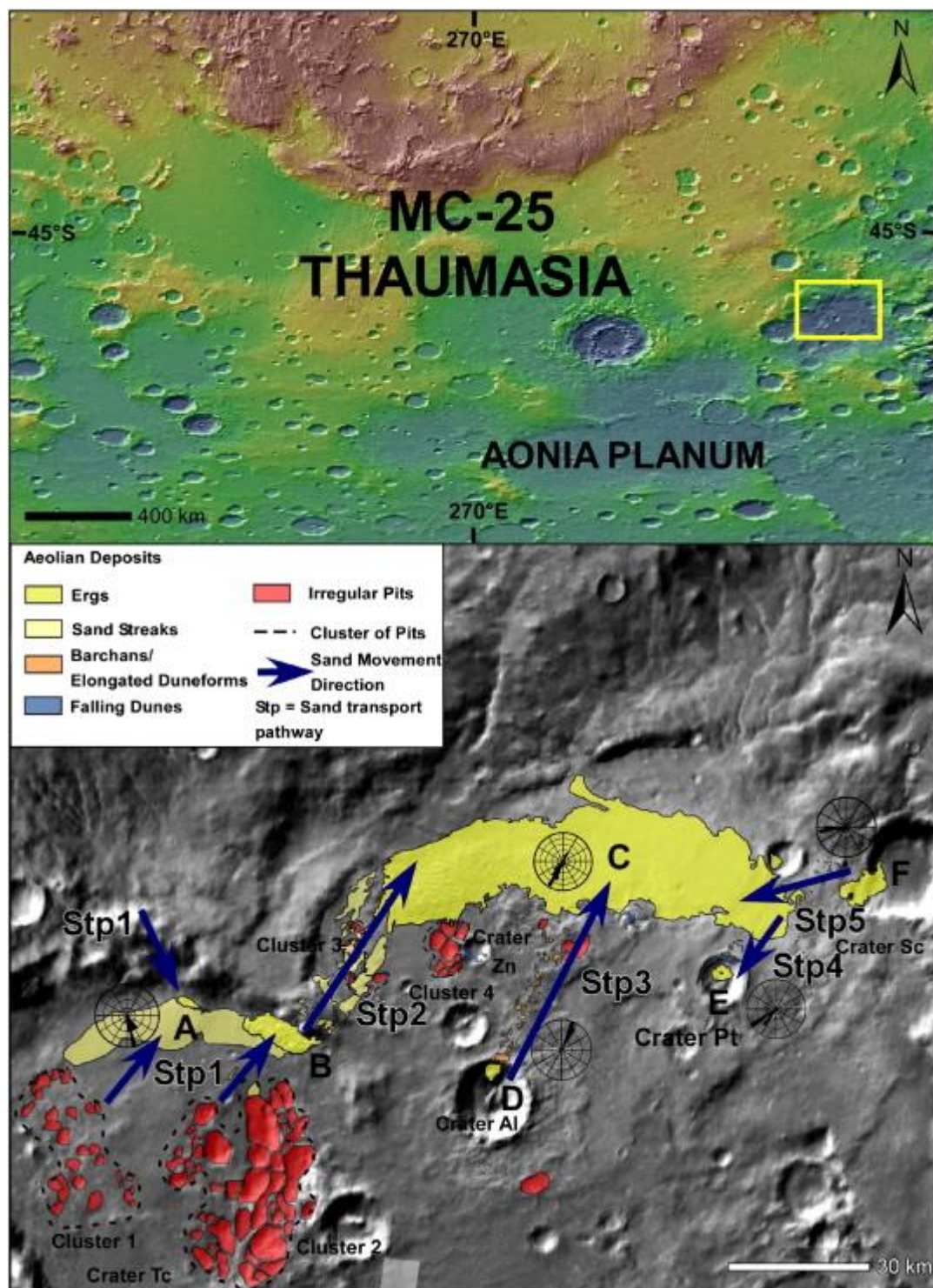
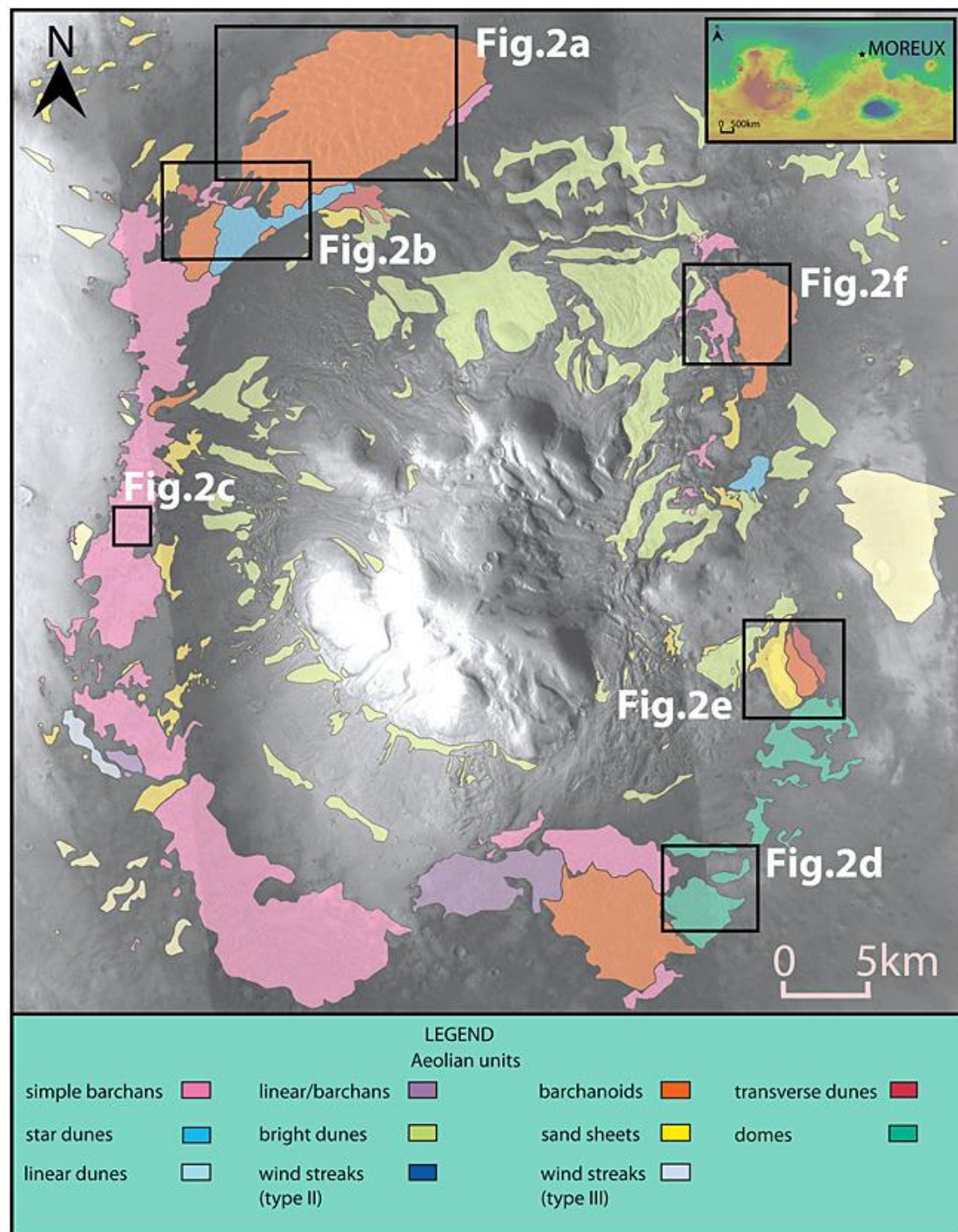


Figure 3.8: Geomorphological map of the Moreux Crater showing aeolian features overlain over a hill shade Mars Orbiter Laser Altimeter (MOLA) dataset and a Thermal Emission Imaging System (THEMIS) infrared daytime mosaic. The inset at the top represents a MOLA map showing the location of the Moreux Crater. (Cardinale et al., 2012)



In such maps, an indicative list of the sedimentary bodies to be mapped is:

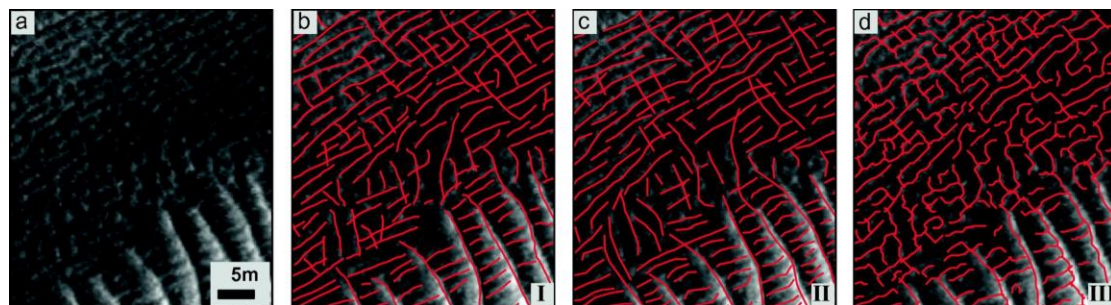
- erg
- barchan dunes
- barchanoid dunes
- transverse dunes
- domes
- linear dunes

- sand sheets
- tars (Transverse Aeolian Ridges)

Mineralogical hints provided by hyperspectral data can improve the landform characterization and distinction, providing tools for source area evaluation and stratigraphic reconstructions.

At a local (or even detail) scale, when high resolution data are available (i.e., MOC and/or HiRISE), more detailed investigations can be possible in order to infer wind directions even from small scale structures such as megaripples (Silvestro et al., 2013; Ayoub et al., 2014) or better understand the process dynamics (Lapotre et al., 2018; Silvestro et al., 2021) (Figure 3.9).

Figure 3.9: Three mapped ripple patterns in Gale crater (Mars) (Vaz and Silvestro, 2014)



In such detailed maps, the sedimentary bodies listed for the regional maps can be potentially used as polygonal shapefiles. In addition, the following is a rough list of features either depositional and erosional that can be found and mapped using a linear shapefile:

- dunes crestline (including wind direction)
- megaripple creastline (including, where visible, wind direction)
- ripple creastline (including, where visible, wind direction)
- wind streaks
- yardangs
- dust devils

In such detailed studies, a qualitative evaluation of the degree of preservation of the features is envisaged, also in the framework of a potential stratigraphic reconstruction. Accordingly, a list like the following one can be used in the attributes list. Other definitions can be better suited to the local specific conditions:

- Poorly preserved
- Eroded
- Partially buried
- Subdued
- Well preserved
- Pristine

‘Fossil’ aeolian deposits, or deposits formed with a contribution of aeolian processes (e.g. volcanoclastics) can be roughly divided in deposits dominated by tractive processes in subcritical flows (i.e. formed by ripples, megaripples, and dunes), suggestive of formation in arid or semi-arid conditions, tractive processes in supercritical flows (i.e.

pyroclastic surge), suggestive of formation due to volcanoclastic processes associated to slopes, and dominated by settling from a suspension (i.e. dust, ashfalls), suggestive of fine-grained clastic deposition from a suspension either related to volcanoclastic processes or simply dust transport and deposition. The term ‘loess’ is often used in planetary settings to refer to settling of fine-grained-sized materials but on Earth this term possesses a specific meaning implying a source from glacial environments. Such formation might have occurred episodically on Mars but it is very difficult to constrain, so the use of a more generic term (e.g. dust deposition) is envisaged.

The distinction among the different aeolian depositional processes can be difficult, especially in the absence of high-resolution imagery (i.e., MOC and/or HiRISE) which can allow to document meter-scale sedimentary structures (i.e. cross-bedding) or textures (i.e. boulders). Still, even in the presence of high-resolution imagery, such depositional environments need to be constrained by observing the geometric patterns of distribution and the relation with other environments and landforms.

b. Airless bodies: Moon as a paradigm

i. Science rationale

Airless bodies provide globally exposed outcrops holding the scars of endogenic and exogenic processes that characterize the evolution of these planetary bodies. Impact cratering and space weathering are the main processes shaping their surfaces today, while volcanic and tectonic processes mainly acted in their early history, along with major basin-forming impact events. Because airless bodies do not have atmospheric or water-related processes, the characteristics of volcanic, tectonic, and impact processes are more clearly preserved compared to bodies with atmospheres. This means that airless bodies often preserve information about the early evolution of the Solar System. Hence, mapping the morphological diversity of an airless body helps to reveal its global stratigraphy and evolution, as reflected by the assessment of Trask and Guest (1975): “[On Mercury], *surface morphology reflects the age, composition, lithology, and mode of formation of the underlying rock unit*”. Indeed, their observation can be applied to any airless body. The same principles were applied by Shoemaker in the first, yet unpublished, planetary geological map ever, in the Copernicus crater area of the Moon in 1961. The “Copernicus LPC 58 Prototype Chart” helped define the chronostratigraphy of the Moon, which is still in use today, meaning that the geological history of the Moon was already understood by means of photo-interpretation, before the first crew landed on our satellite. Therefore, studying the Moon case can serve as a paradigm for any other airless body.

ii. Approaches

Photo-interpretation of lunar units highly depends on the chosen mapping scale.

Global to regional scale

At a global scale, morphology and albedo help identifying four main units:

Mare Units: dark albedo, smooth infilling of large basins;

Terra Units: high albedo, rough, heavily cratered highland terrains;

Crater Units: materials linked to the formation of impact craters; **Basin Units:** materials linked to the formation of large impact basins.

At the regional scale further information is provided by crater degradation stages. Our current knowledge of the Moon permits us to distinguish at least six crater classes pertaining to specific chronostratigraphic systems (Figure 3.10).

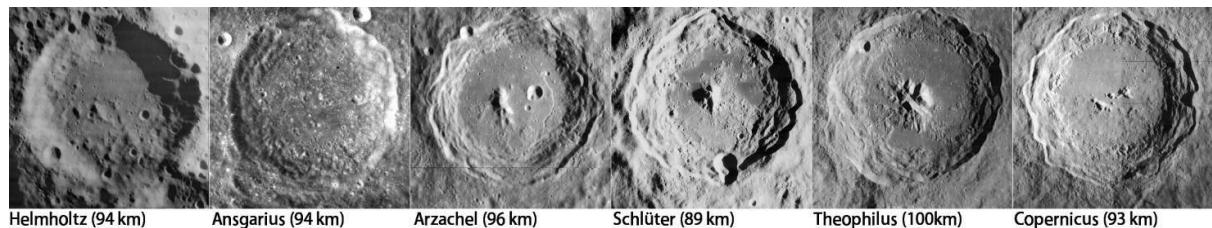


Figure 3.10. Six example craters of similar sizes showing different degradation stages and pertaining, from left to right, to the Pre-Nectarian, Nectarian, Lower Imbrian, Upper Imbrian, Erathostenian, Copernican Systems (image by M. Packer, see also Wilhelms and Byrne, 2009, <http://www.imageagain.com/Strata/StratigraphyCraters.2.0.htm>).

Depending on the chosen mapping scale, craters larger than a certain size threshold are *divided* into different units, otherwise the whole impact structure can be mapped as *undivided*.

For *divided craters* we usually distinguish:

Crater Floor

Crater Central Peak/Peak Ring (when complex)

Crater Proximal Ejecta

Crater Distal Ejecta

Ejecta units and central complex structures are usually coloured with a shade of the same colour pertaining to the degradation-class system of the crater.

Crater floors may be distinguished into further units based on their morphology:

Crater Smooth Floor

Crater Hummocky Floor

Larger basins floors may present *smooth infillings* covering the original floor, which is the case of *maria* at a global scale.

Local scale

Local and Detailed maps are instead focussed on a better understanding of single processes such as the distribution of different impact related deposits, post impact modification gravitational collapses, fracturing at craters' floors, emplacement of pyroclastic materials within craters, distribution of volcanic vents and deposits,

differentiation of maria units and lava emplacements etc. On the Moon many detailed maps have been specifically produced for landing site characterization (see dedicated section 6). In the case of Mercury particular attention has been paid on sublimation features called hollows for which several high-resolution maps have been produced (e.g. Pajola et al. 2021).

c. Small Bodies

A Small Solar System body (SSSB) is an object in the Solar System that is neither a planet, a dwarf planet, nor a natural satellite. The term was first defined in 2006 by the International Astronomical Union (IAU) as follows: "All other objects, except satellites, orbiting the Sun shall be referred to collectively as 'Small Solar System Bodies' ". SSSBs are: the comets; the classical asteroids, with the exception of the dwarf planet Ceres; the trojans; and the centaurs and trans-Neptunian objects.

Map projections and small bodies

Due to the size and the irregular shape of small bodies, standard mapping reference systems often cannot be consistently employed. An overview of this topic can be found in (Stooke & Pajola, 2019). Depending on observational constraints, the imagery often covers a large portion of the whole body, making it difficult or impossible to orthorectify the imagery in a sensible way (avoiding extreme distortions of the original images), even when detailed shape models are available. This issue poses limitations on consistently using small-bodies datasets into generic GISs for data processing (e.g. measuring distances and areas), mapping, and visualization.

As an example consider 67P: it has a bilobate shape, which seems to be a recurrent feature also for other Jupyter-family comets (see e.g. 19P/Borelly, 103P/Hartley 2, 1P/Halley). Large portions of the comet's body thus have a convex shape which causes two major drawbacks: a) the shape does not allow to consistently define a latitude/longitude coordinate system on the body (the same latitude and longitude coordinates are duplicated in some places); b) the classical assumption of a bi-axial ellipsoidal approximation for projective cartographic reference systems (CRS) tend to produce extreme distortions on most of the body.

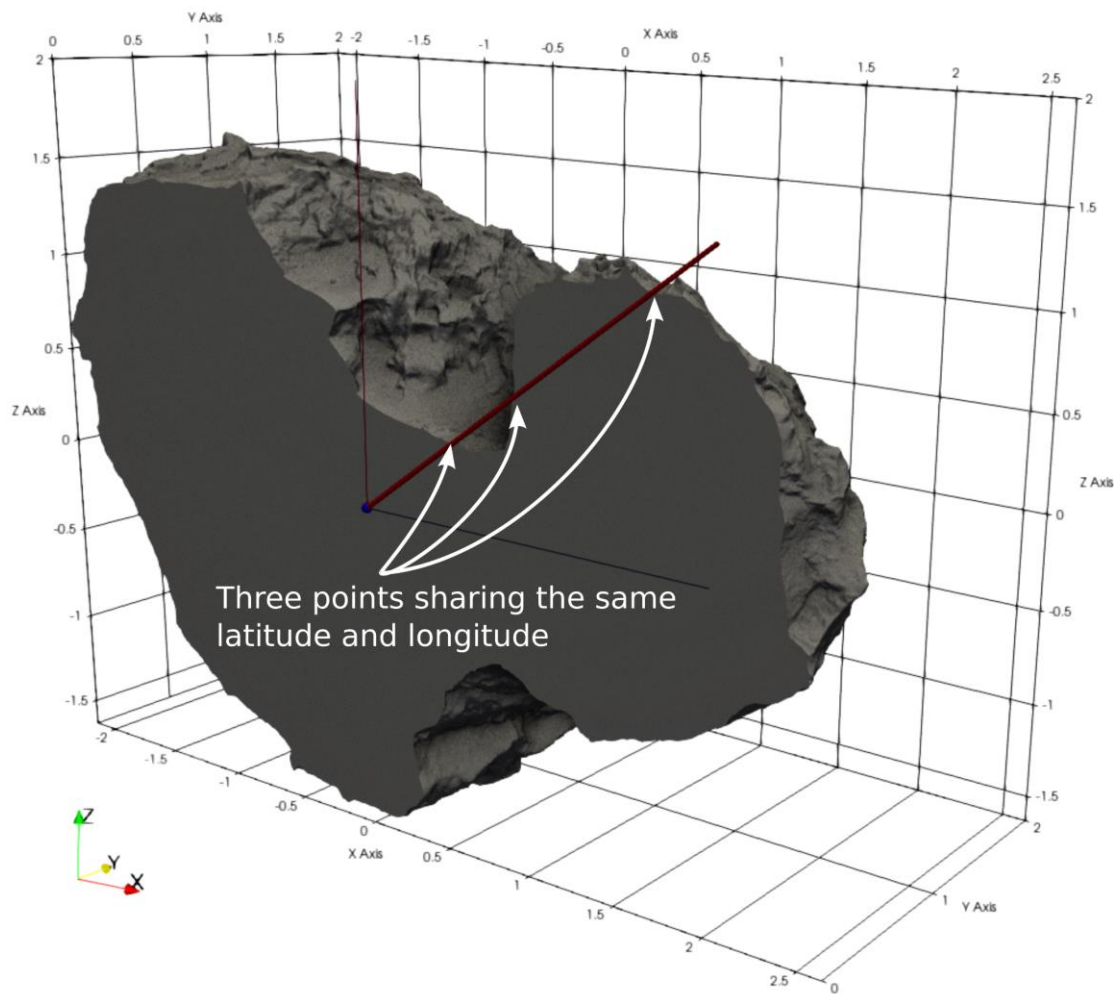


Figure 3.11: an example of the impossibility of defining a unique latitude-longitude grid on an irregular body featuring extended convexities, as the neck region of 67P comet, here portrayed as a cross-section passing for the center of the Cheops Reference System.

In the case of comet 67P these problems were never consistently solved. For mapping purposes it was suggested that several different mapping projection systems could be used: a global one for the whole body (with extreme distortions) and three local ones for the two lobes and the neck region of the comet (Preusker et al., 2015). Using multiple reference systems for one body was often impractical, especially for such a small body where global maps would have been preferred in many cases.

Tentative solutions based on non-ellipsoidal reference surfaces were also proposed (Grieger & Vincent, 2018), but require ad-hoc processing and would not be easily implemented in standard GIS software. See also (Clark & Clark, 2020) on a constant-scale projective system for 67P.

Mapping on small bodies

As detailed above, no standard cartographic tools and CRSs can be always used on bodies with convex shapes or with small sizes in respect of the available imagery used for mapping. We will not detail here the cases in which "standard" cartographic

methods can be employed, but we will limit the discussion to the cases in which a different approach might be preferable for mapping, by listing some possible suggestions to evaluate depending on the specific case.

Ideally, mapping should be done directly on the three-dimensional shape model on which the imagery would be reprojected on the fly. This is often impractical, due to dataset limitations (e.g. at the very beginning of a mission imagery might be available but no shape model) or software limitations (dedicated software with fully 3D GIS capabilities, adequate for mapping, is still in development).

When reprojection of the imagery in a GIS-compliant format is difficult, it might be better to use the imagery "as it is", possibly starting from optically undistorted images and keeping in mind that the distortion introduced due to the perspective geometry of the camera might be highly deceptive. The state of the imagery in terms of optical distortion should be always reported in the metadata of the final mapping product, possibly together with a literature reference pointing to the camera's calibration parameters.

The imagery can be imported in any GIS software without specifying a CRS and mapped in image (pixel) coordinates. Refer to your GIS user manual to identify the right settings to use for this case. It might be better also to not apply any scaling (setting pixel size) to the imagery because such information might be deceptive, and valid only for portions of the image. If a pixel size shall be provided, it should be provided in the metadata (e.g. "approximated_pixel_size" or "central_pixel_size"). Adding the scale information directly to the imagery e.g. with a tiff/jpg world file has an additional drawback: further operations of reprojection on the body of the vector data will require additional removal of the applied transform to restore the data to the original pixel-based reference frame.

Additionally, consider that depending on GIS software used for mapping the (0,0) pixel coordinate can be placed either in the centre of the top left corner or on the edges of that pixel. This information should be reported in the metadata.

For easier future data processing it would be good practice to also provide, together with the metadata, the projective matrix for the image in a given reference frame (e.g. for Rosetta-67P the Cheops R.F), which should be also listed in the metadata. Providing the best available identifier for the used image is also important. It can be done by providing detailed information on the camera system, timing and image naming.

Whenever a position on an irregular body should be communicated, try to avoid using purely latitude-longitude couplets, but prefer, whenever practical, to use latitude, longitude plus radius or euclidean x,y,z coordinates. This is especially important when dealing with shapes having extreme convexities.

Gravity

Gravity on a small body can be in most cases derived by using the shape model and assuming fixed density (Werner, 1994). Some morphological terms are related to the local gravity: e.g. terraces/mass wasting deposits etc. This should be taken into account

during mapping, especially on bodies with complex shapes: the direction and the magnitude of the gravity vector might not always be obvious.

Regions Definitions

Regions are often defined for the practical purpose of providing a generic subdivision for different portions of the body. Often, the regions are defined very early in the mission with the available imagery, when 3D shape models are possibly not yet available (e.g. for comet 67P see Thomas et al., 2018).

Geological Mapping Terminology for Small Bodies

The main geological process recorded on most of the asteroids is impact cratering, but landslides, boulder fields and fractures are also common (e.g. Buczkowski et al. 2008; Massironi et al. 2012; Simioni et al. 2015). The major impact events can be ordered in stratigraphic sequences and dated through crater counting (Massironi et al. 2012). So that the main features that can be mapped on an asteroid are as follows: polygonal units encompassing craters rims and floors, polygonal units encompassing ejecta blankets, polygonal units including landslides deposits of different natures, linear features indicating fracture, faults and scarps.

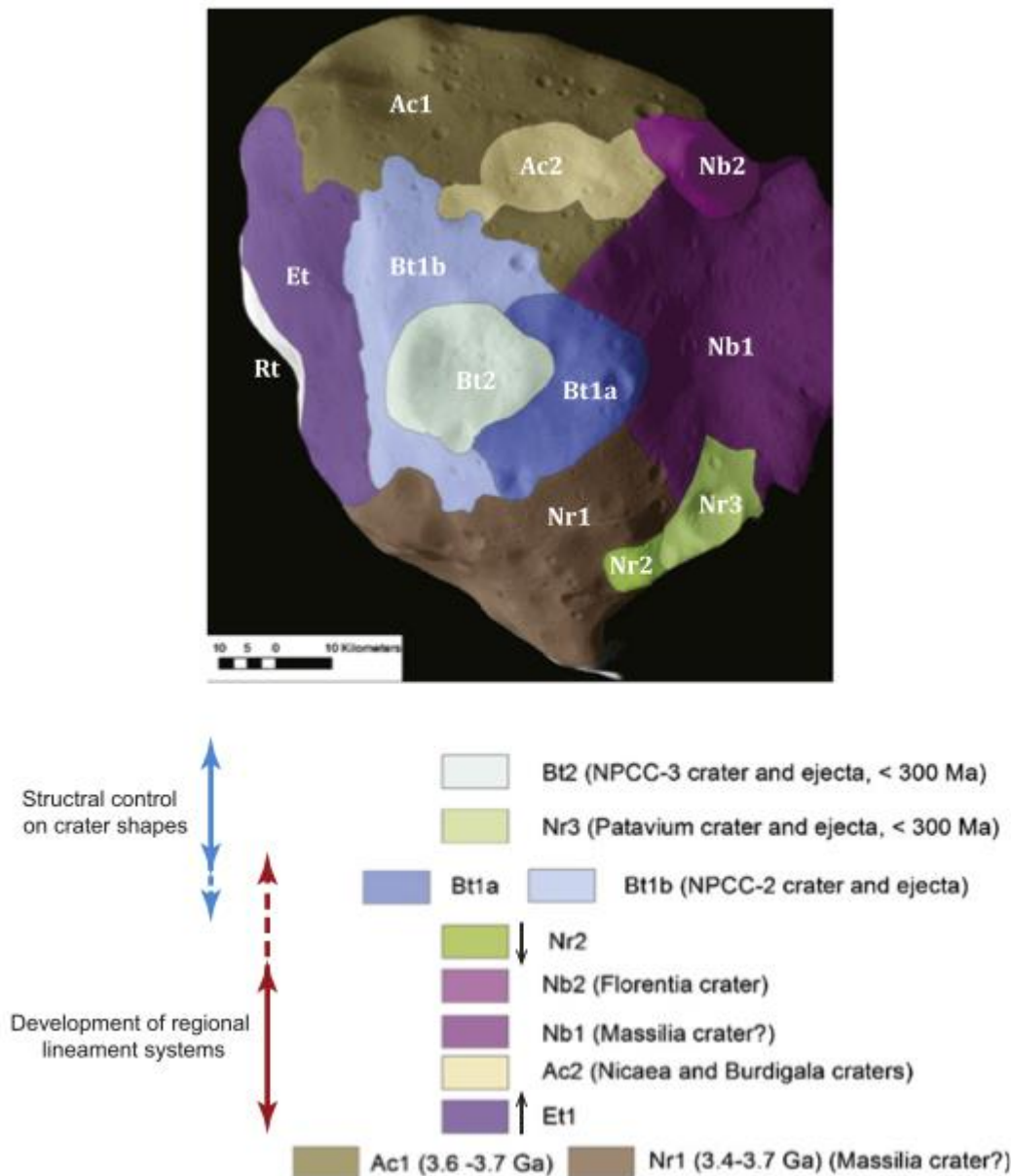


Figure 3.12: Example of geological map indicating different cratering events on Lutetia surface (Massironi et al. 2012)

A prominent exception is Vesta given its considerable dimension and the presence of magmatic rocks whose fragments are considered to have reached the Earth as diogenite and eucrites meteorites. In this case the units are more variable recalling the airless body ones (e.g. Williams et al. 2014).

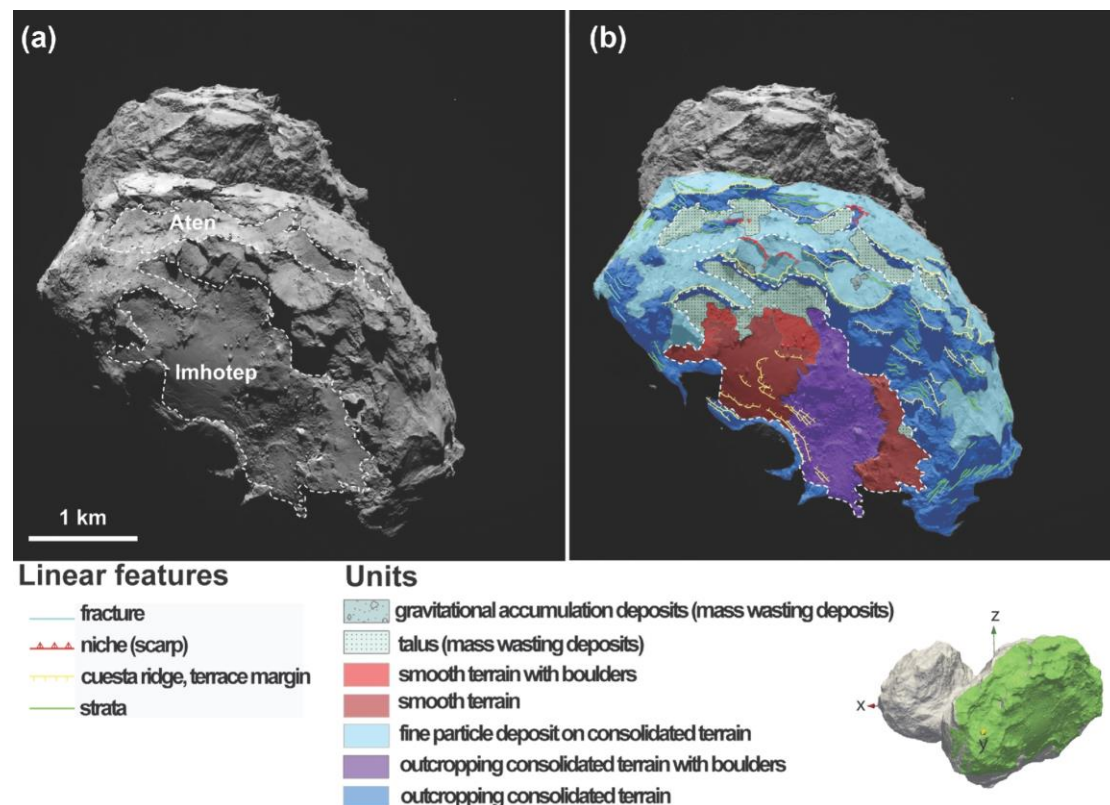
Geological processes on cometary bodies are still quite poorly understood, hence some morphological features might be of difficult attribution in terms of the specific shaping process. In such a case the terminology employed for mapping should preferably avoid using naming that imply specific formational processes (e.g. using "crater" for a circular feature of unclear origin). Preferring purely morphological terminology over

formational terminology might be a better choice whenever a feature is of difficult attribution (e.g. "circular depression" for a crater-like feature of unclear origin).

Examples of geological mapping on 67P can be found in Giacomini et al. (2016) (Figure 3.13), Lee et al. (2016). We report here a list of the features known to have been mapped on small bodies (some would require a terminological unification):

- boulders or blocks,
- linear features of various kind: fractures, strata heads (layering-related linear features),
- thermal cracks and polygons,
- crater-like depressions (circular features of unclear origin),
- other negative-relief features as pits on cometary bodies,
- niches,
- cliffs,
- deposits of various kind: mass wasting deposits, talus, diamicton, fine particles deposits, smooth terrains, consolidated terrains outcropping and variation,
- landslides (with related niches and deposits),
- layering related morphologies: terraces, mesas and similar features (possibly hogbacks/razorbacks etc depending on local gravity),
- unknown features (existing descriptive terminology should be used for those),
- dunes on fine deposits and similar wind-like features.

Figure 3.13: Example of geological Map of Comet 67P/Churyumov–Gerasimenko's Northern hemisphere (Giacomini et al., 2016)



d. Icy Bodies

Icy satellites, and more in general icy bodies are located in the outer Solar System from the asteroid belt outwards. Differently from dry planetary objects with a relatively small water fraction ($<0.1\%$), in these bodies ice constitutes a very large portion of the solid material ($>20\%$) preserving also a liquid phase (Monteux et al., 2018).

They typically present an icy crust (or an ensemble of polymorphs of water ice), a fluid portion underneath, usually oceans and a rocky core.

The most notable icy bodies in the Solar System are the Galilean satellites Europa, Ganymede and Callisto, the Saturnian moon Enceladus and Titan, as well as the recently observed Pluto and Charon, and a number of objects such as Mimas and Triton. Note that some of these fall into the definition given above of SSSB (Small Solar System Body).

Ceres is a peculiar case since it is located in the asteroid belt and cannot be classified as a satellite and formally falls into the SSSB definition, although it shares most of the characteristics with the previously mentioned objects.

The same concept applies for Pluto and Charon, as they formally are dwarf planets but present an icy crust overlying a subsurface ocean and most likely rocky core.

iii. Science rationale

Topical Maps aims

Characterization of the surface of icy bodies and their geologic mapping has a number of high-priority implications both for upcoming missions target locations planning for observations with both optical and active probing systems (e.g. ground penetrating radars and alike) as well as improving our knowledge in i) understanding the tectonic and resurfacing history of the brittle icy shells II) detect and distinguish cryovolcanic landforms and associated products III) help constraining cryomagma formation mechanisms IV) help constraining the internal structure of icy bodies both at global scale and, where possible thanks to sufficient image coverage and resolution, at local scale V) astrobiological implications related to the previous points.

iv. Approaches

Mapping techniques on icy bodies/satellites do not differ in any way from the standard GIS-based mapping techniques commonly used. There are only two major issues to be taken into account: the mapping scale and the features list/nomenclature.

Overall, the scale of work is, by necessity on these bodies more than on others, tied to the availability of enough image coverage of sufficient quality/resolution.

In general, global mapping is always possible apart from those bodies whose data belong uniquely to flybys which imaged just a portion of the entire body (e.g. Pluto and Charon).

Relative age relationships are based on mutual crosscutting relations on different terrains/materials (Collins et al., 2013) and, due to the peculiar nature of icy bodies, thematic maps such as structural maps or grid-based maps can also be produced (see Rossi et al., 2020).

All the icy bodies present basically four main categories of features that can be mapped: terrains (defined by relative albedo, roughness, degree of tectonization) impact craters, tectonic elements, cryovolcanic features/morphologies.

The features known to have been mapped on icy bodies (some would require a terminological unification) can be listed as follows. This is a comprehensive list as several of the features can be common between different icy bodies:

- *Terrains* as major geologic units for stratigraphy, distinguished for their tectonization and their relative albedo
 - Bright terrains (usually correspond to “*sulci*”, highly tectonized elongated regions in bright terrains)
 - Dark terrains (Ganymede)
 - chaos material (Europa)
 - ridge material (Europa)
 - ridge complex material (Europa)
 - smooth/lineated/ridged band material (Europa)
 - palimpsest material (Ganymede: moderate to high albedo forming flat, circular structures, result of ancient impacts)
 - Lakes (Titan)
 - Labyrinth (Titan; incised and dissected plateaus, possibly structurally controlled)
 - Hummocky (Titan)
 - Dunes (Titan)
 - Cellular terrain (Pluto: high-frequency pitted terrain)
- *Impact craters*
 - simple craters: bowl shaped or paraboloid-shaped
 - complex craters
 - pitted impact craters (typical on Ganymede)
 - bulged impact craters (typical on Ganymede)
 - ringed basins (Ganymede, Callisto, Europa)
- *Structural features*
 - furrows (associated to ancient planetary-wide impacts)
 - grooves (Ganymede, associated to tectonics)
 - ridges (Europa)
 - double ridges (Europa)
 - cycloidal structures (Europa, see Groenleer & Katternhorn, 2008)
 - grabens (all, see especially Charon)
 - normal faults/fault scarps (all)
 - strike-slip faults(all)
 - open fractures (clearly visible on Enceladus Martin et al., 2017; and Europa, Schenk et al., 2020)

- pit chains due to dilational faulting (visible on Enceladus, Martin et al 2017)
- *Cryovolcanic features*
 - maculae (chaotic regions of dark material on Europa, probably due to cryovolcanic material expulsion, see Fagents 2003 and references therein)
 - dark halos/maculae (typical on Europa, see Fagents, 2000)
 - sublimation pits, single or clustered (typical on Pluto/Charon, see Howard et al., 2017, White et al., 2019)
 - low albedo moats, lenticulae, spots (typical on Europa, see Fagents, 2003, related to cryovolcanism/cryovolcanic effusions)

Even though some features, morphologies and nomenclatures are common across the different analyzed icy bodies, for a more detailed and thorough description of geologic units, typical morphologies, and relative stratigraphy, specific nomenclature and mapping examples refer to:

- Ganymede: Patterson et al., (2010); Collins et al., (2013)
- Europa: Figueredo and Greeley, (2004)
- Callisto: Greeley et al., (2001); Schenk, (1995)
- Pluto: Stern et al., (2015); White et al., (2013)
- Charon: Robbins et al., (2019); Stern et al., (2015)
- Titan: Lopes et al., (2019)
- Enceladus: Crow-Willard & Pappalardo (2015); Yin and Pappalardo (2015)

Triton: Martin et al., (2018). *Feature-based mapping*, mostly related to tectonic elements are in Rossi et al., 2020 for Ganymede, Yin et al., 2015 and Crow-Willard and Pappalardo, 2015 for Enceladus. Instead, *process-based interpretative mapping* are in the maps of the Pluto/Charon system by White et al., (2017) and Robbins et al., (2019) which are mostly related to impact cratering and cryovolcanism.

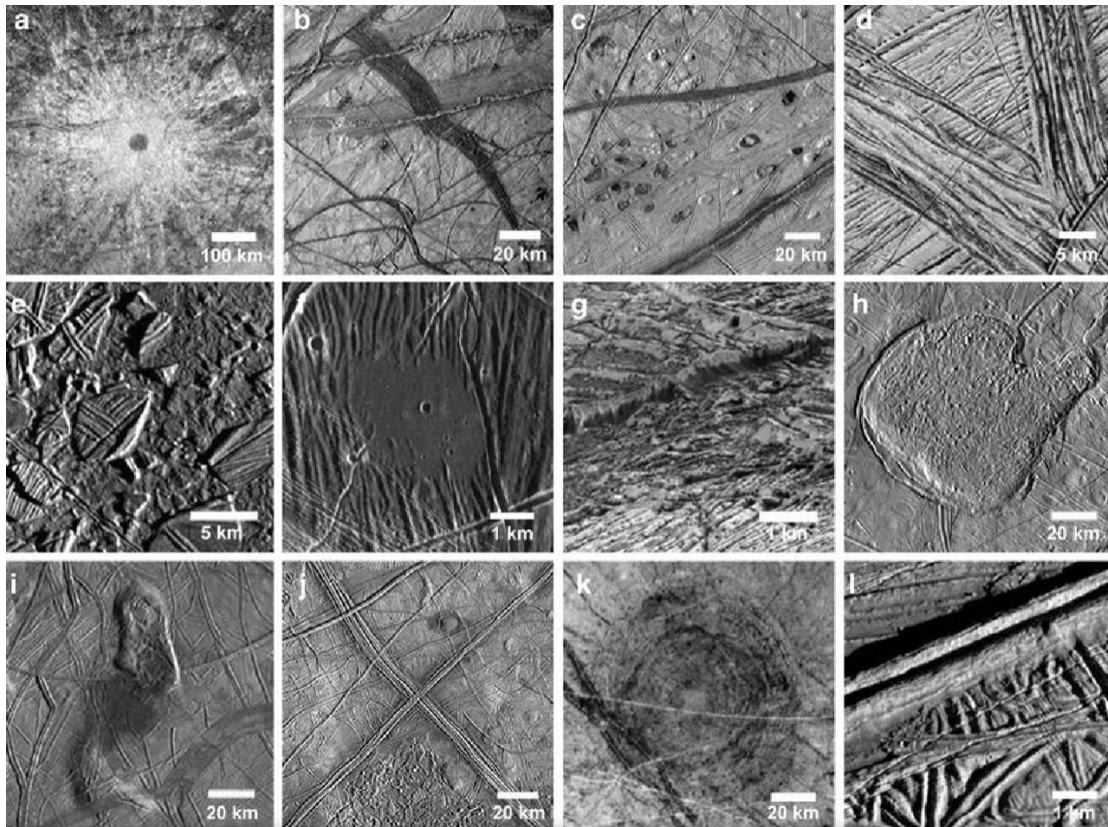


Figure 3.14: example of surface features on Europa, with a) recent impact crater, b) bands, c) lenticulae, d) ridges e) chaos terrain f) dark smooth material g) cliff/scarp h) Murias chaos (“mitten” feature), i) dark macula south of a moat/dome j) intersecting ridges k) multiple ringed impact l) double ridge (image and caption modified from Pappalardo et al., 2013)

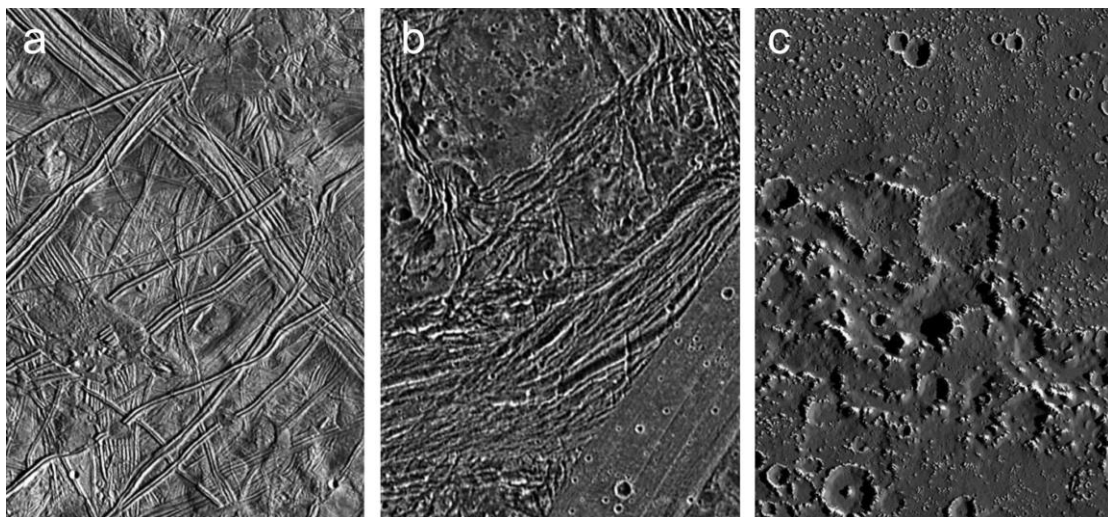


Figure 3.15: the surfaces of a) Europa, b) Ganymede and c) Callisto in comparison. The different degree of tectonization is clearly visible at a common resolution of 150 m/pixel. Images taken from Galileo SSI instrument. Source NASA/JPL/DLR.

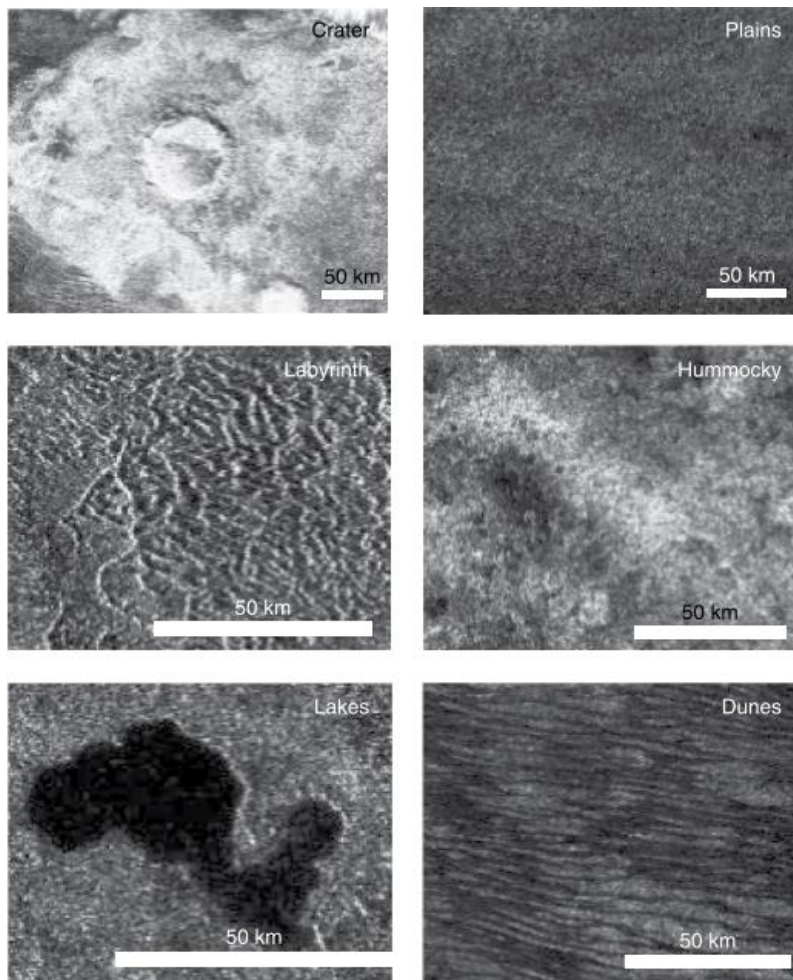


Figure 3.16: features corresponding to geomorphological units on Titan (Lopes et al., 2019)

Limitations

In several cases, such as the Jupiter Icy moons of Europa and Ganymede, the global image coverage is in the order of hundreds of meters per pixel, but at targeted places the resolution can improve dramatically up to one/two orders of magnitude. This discrepancy in the high resolution of very small targeted areas and the global resolution of the body-wide mosaics, makes high resolution local-scale mapping very difficult in terms of contextualizing features and processes to the surrounding areas making the mapping process and the homogenization of geologic contacts and features particularly difficult.

Such a problem is present also on bodies such as Enceladus where the global basemap derived from a mosaic of Cassini ISS images resolution ranges from 50 to 500 meters/pixel (see Bland et al., 2018).

Since most of the observation of such bodies (apart from Ceres globally imaged by the Dawn mission) derive from flybys or from the merge of datasets from different epochs and instruments (e.g. Voyager and Galileo for the Galilean satellites), the illumination conditions can also differ dramatically and, coupled with the limited dynamic range of

20+ years old images can partially affect the possibility to perform highly detailed mapping.

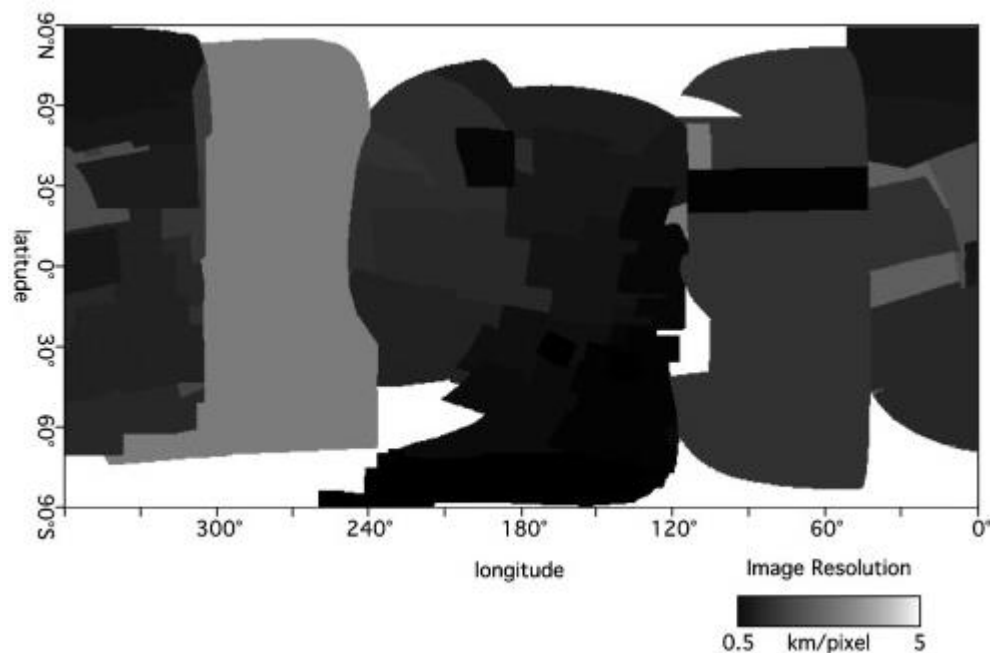


Figure 3.17: example of the heterogeneity of resolutions in the Ganymede global mosaic. From Patterson et al., (2010). Such limitations apply also for Europa, Callisto and Enceladus in the case of global mosaics, whereas Pluto and Charon rely only on partial observation acquired during the New Horizons flyby (Stern et al., 2015).

Topography is available for the New Horizons flybys of Pluto and Charon through stereo images (Stern et al., 2015) through the usgs astrogeology website as well as for the global mosaic and DEM of Ceres (Roatsch et al., 2016).

In the particular case of the Jupiter icy satellites and for Enceladus as well, the stereo coverage is somehow limited to the closest approach of the satellites during the flybys, where high-resolution images were taken. In particular for the case of Ganymede and Europa, such high-resolution frames are only partially overlapping as they were used to be mosaicked in slightly larger areas, and the goodness of the stereo reconstruction is highly dependent on the amount of overlap, illumination conditions and dynamic range. Large-scale topography is still possible to obtain through photoclinometric techniques (see Schenk et al., 2004 and Zubarev et al., 2017 and references therein for more details), and a dedicated software from USGS (not maintained anymore) is available and called *pc2d* (Kirk et al., 2003) and usable through an ISIS2 installation.

Overall, topography is not well constrained in such cases, also due to the fact that topographic expressions and variations on such icy bodies, especially the most tectonized ones, are very subtle. It is however possible to enhance the mapping by, for example, coupling this information where available, with images and also with the UV channels of Galileo (where available) for the icy moons of Jupiter to provide a more comprehensive mapping.

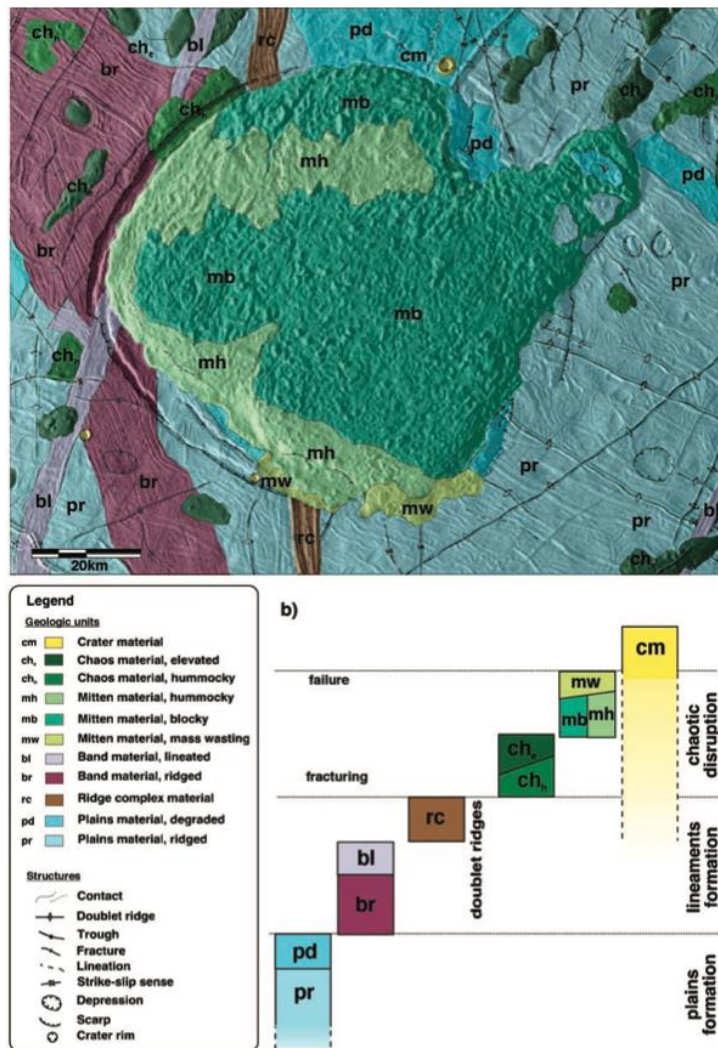


Figure 3.18: Example of a local-scale geological map of the Mitten feature area on Europa from Figueredo et al., (2002). The stratigraphic column and geologic units are a heritage of Figueredo and Greeley (2000) then expanded in the Figueredo and Greeley (2004)

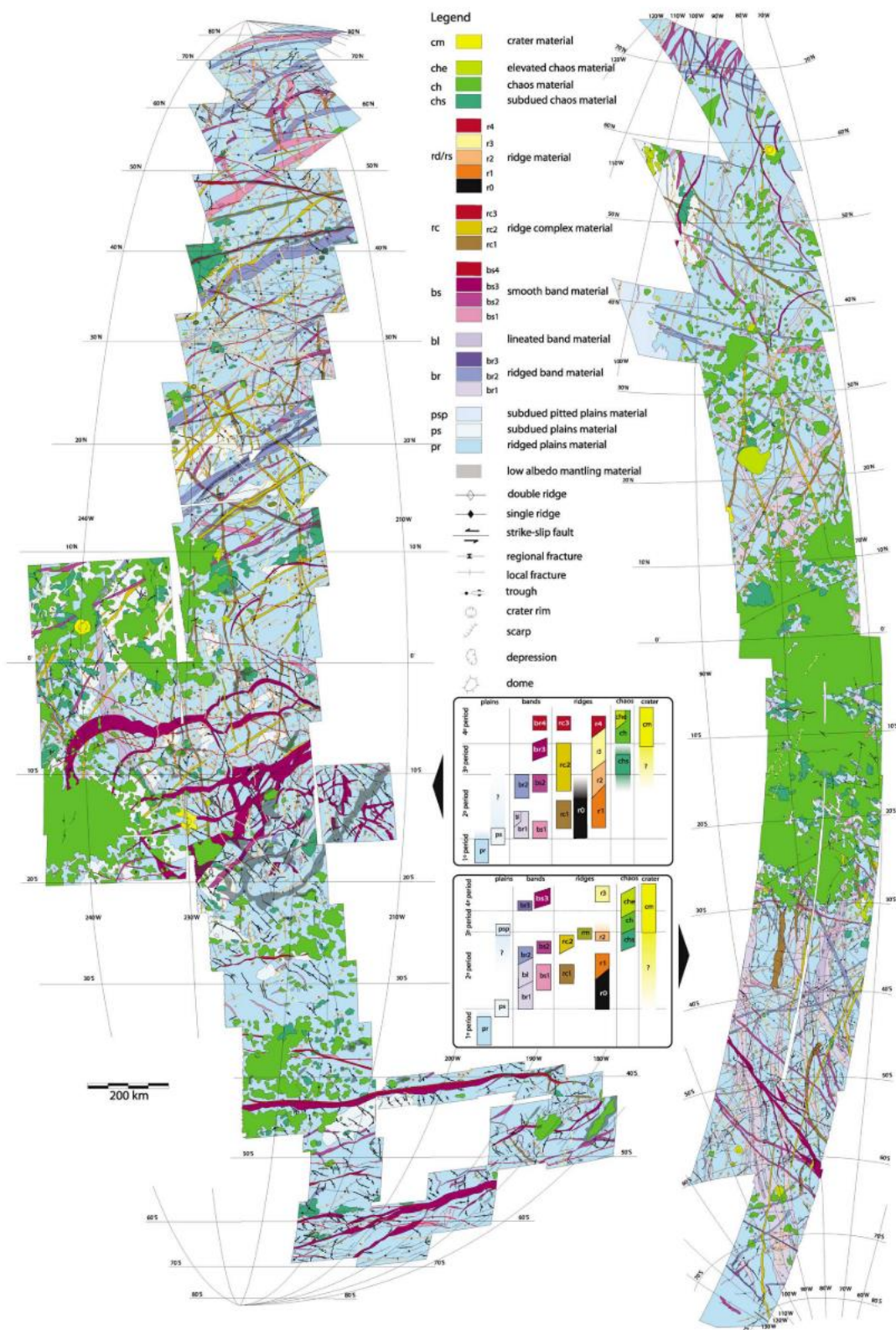


Figure 3.19: Example of a satellite-scale geologic mapping of the trailing and leading hemispheres of Europa based on the flybys of Galileo mission (Figueredo and Greeley 2004).

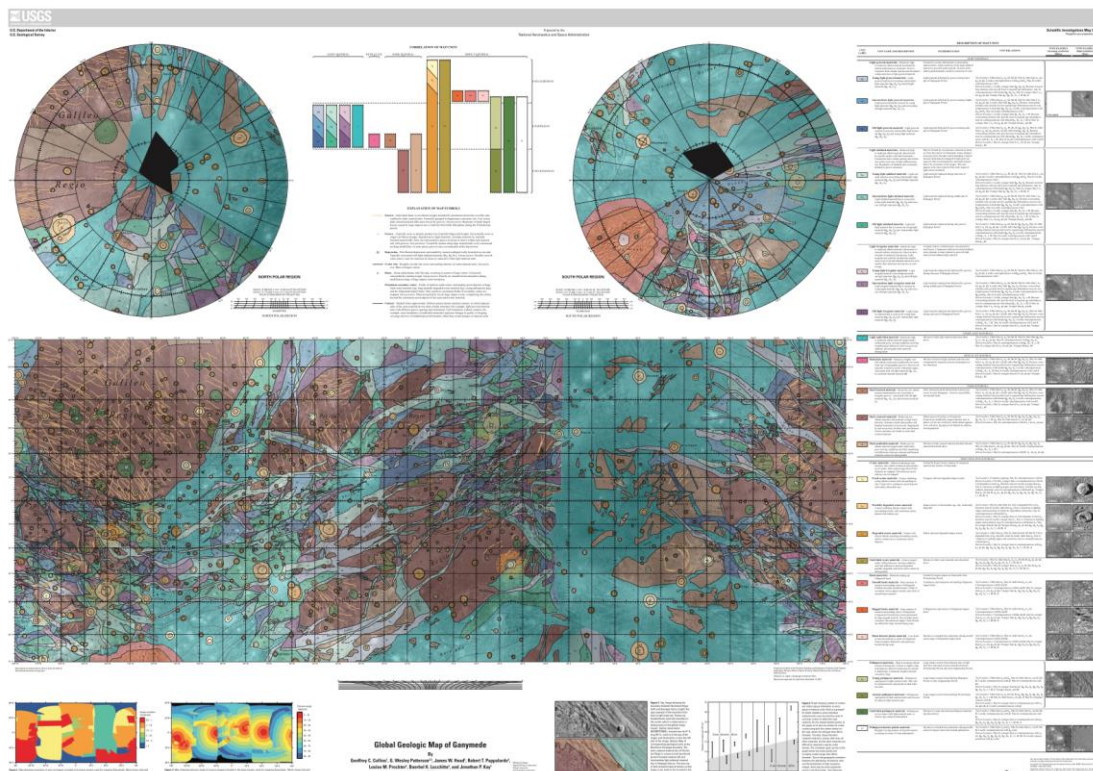


Figure 3.20: global geological map of Ganymede by Collins et al., (2013).

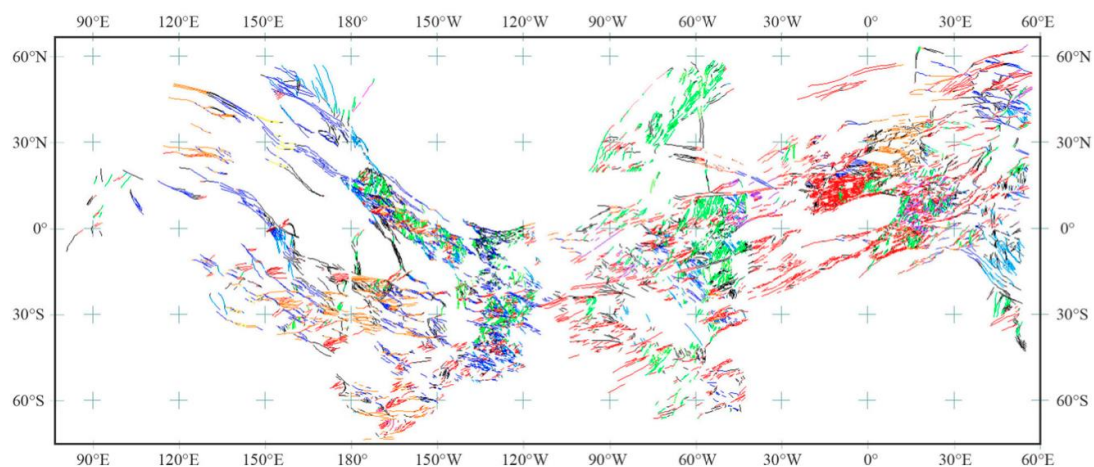


Figure 3.21: example of a global structural map of Ganymede by Rossi et al., (2020) with different families of structural features colour coded according to kinematics/orientation.

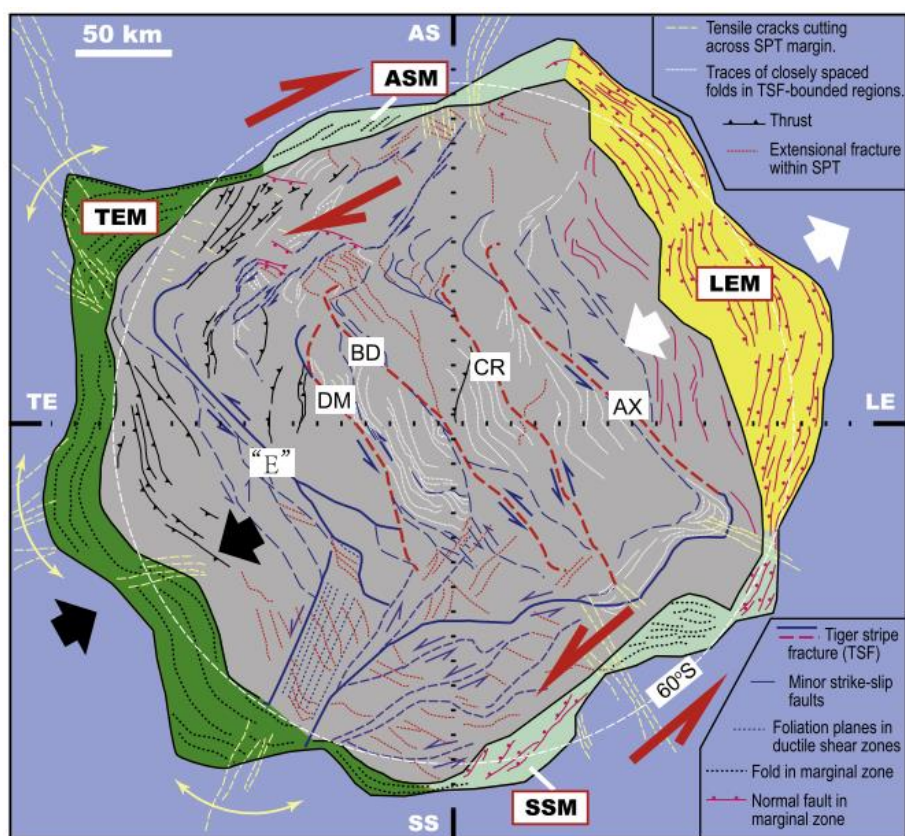


Figure 3.22 Example of structural interpreted map on the Tiger Stripes region at the south pole of Enceladus (Yin et al., 2015)

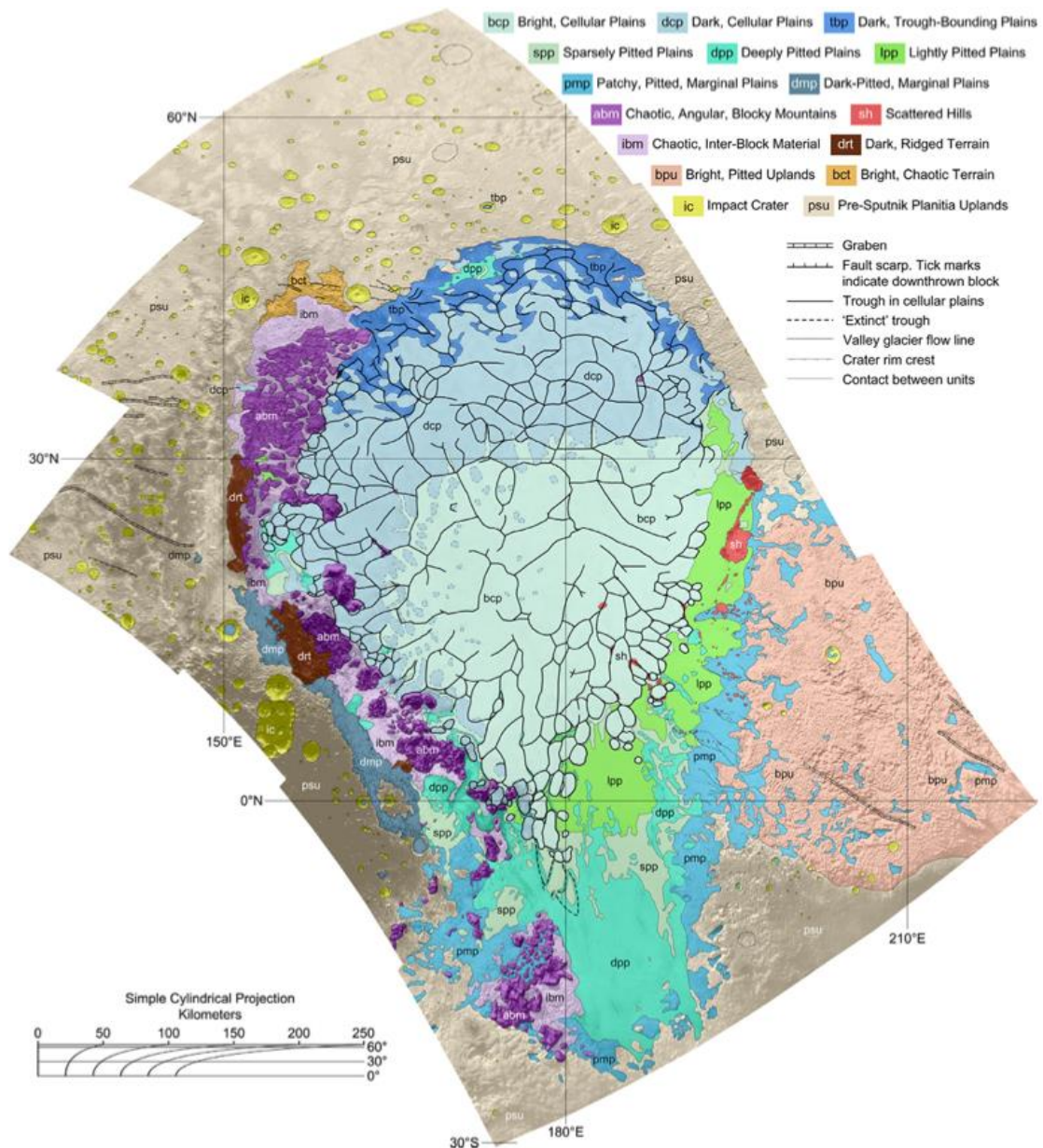


Figure 3.23: local scale map of Sputnik planitia on Pluto (White et al., 2017).

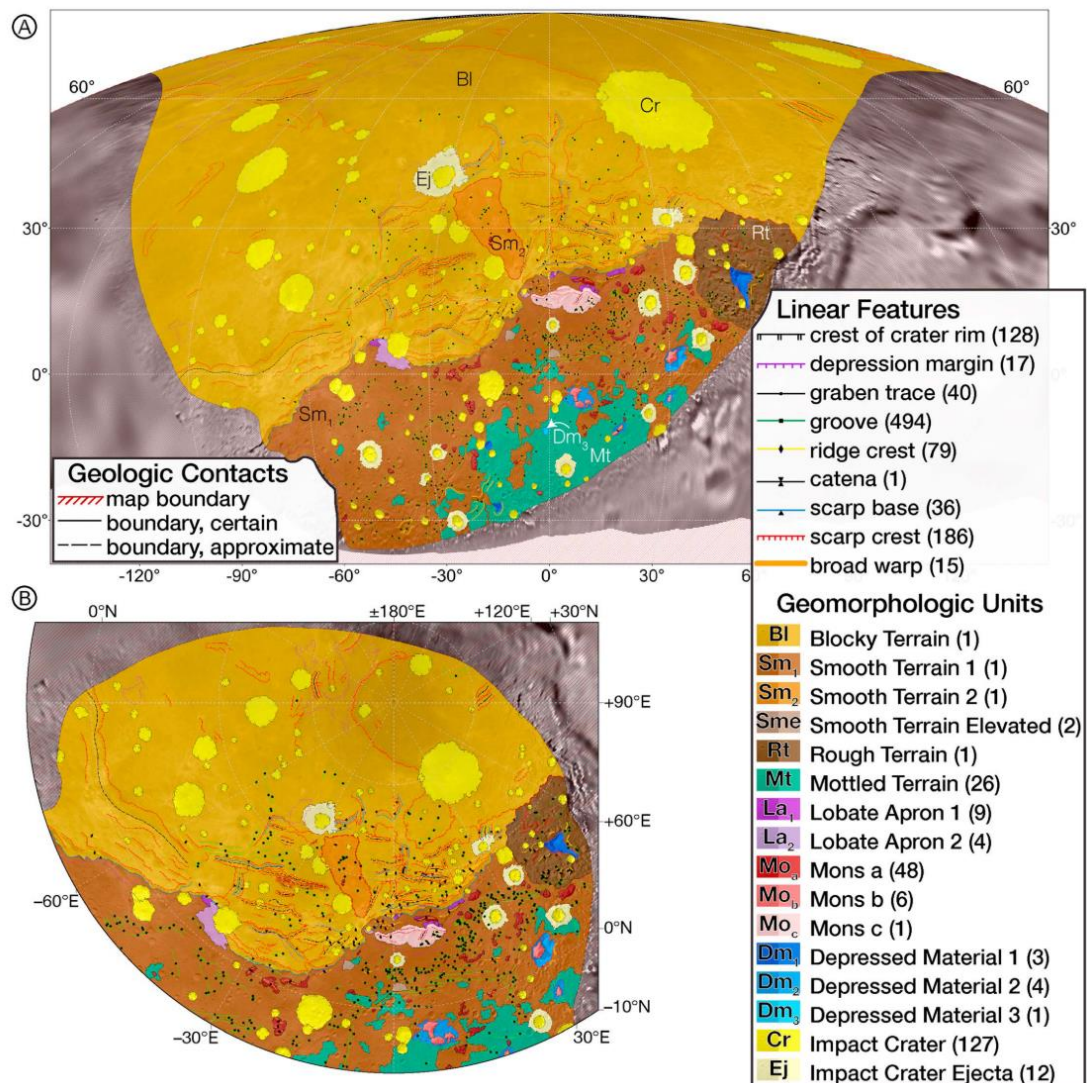


Figure 3.25 hemispheric map of Charon with a) cropped Mollweide and b) polar stereographic projections, taken from Robbins et al., (2019).

4. Process-based 'objective': Geological Map

Geological maps on Earth represent the first and basic geological knowledge of a specific territory, providing the most possible 'objective' framework of that area, based on lithological characteristics and changes. According to such a definition, strictly speaking, geological maps cannot be defined in planetary settings with no or very limited ground-truth (i.e. without lithological characterization). Still, sometimes there is a need for a relatively more 'objective' cartography product, for example when genetic interpretations are ambiguous or when correlation between different areas is envisaged, and to focus on the identification and meaning of unconformable boundaries. Since, unlike on Earth, on many planetary surfaces, morphologies are preserved in the deep geological time, sometimes major unconformities might occur even within a single landform.

Geological maps aim at distinguishing observations from interpretation (i.e. deposits from landforms) and at emphasizing the importance and hierarchy of the different kinds

of unconformities. The production of such maps, needing detailed analyses, is possible only when high-resolution data are available, allowing a study at the regional down to local scale.

The ‘technical’ rationale is that if the observations, interpretations and stratigraphic boundaries must be included in a single cartographic product, but must remain clearly distinguishable, three shapefiles are necessary: contact (linear shapefile), geological unit (polygonal shapefile); geomorphology/tectonics interpretation (linear shapefile).

A linear shapefile must focus on the stratigraphic relations, so a field defining the ‘contact’ must be included, together with the validation of the observation:

- Continuous, certain
- Continuous, inferred
- Disconformity, certain
- Disconformity, inferred
- Nonconformity, certain
- Nonconformity, inferred

A polygonal shapefile must focus on the as objective as possible description of the ‘geological units’. Geological units are considered as deposits formed by a succession of landforms formed through time. Units should be defined on the base of their characteristics, specifically colour, texture, association with non-genetic morphologies (geometries without interpretation, e.g. mound, peak), and in the case of sedimentary deposits, presence/absence of layering and sedimentary structures.

Mineralogical hints, when available, represent an additional very important characteristic to be included in the unit definition. Still, such operations must be done very carefully in order to take into account the different resolutions of hyperspectral and imagery data that might not allow an unambiguous association between deposits and mineralogical hints. Image sharpening processes might help in integrating the multi or hyperspectral colour information of lower resolution spectrometers with high resolution data sets from cameras. When the association is possible, it represents a very powerful tool for a further constrained genetic interpretation.

In addition, the position within the stratigraphic succession is a criterion for distinguishing units.

Because of the importance of an ‘objective’ description, also in the framework of correlation and comparison between distant areas, the importance of defining the units using a ‘reference area’ is especially important. In correspondence of such an area, the unit description (as well as the description of the stratigraphic boundaries) must be done with all the available dataset.

In the shapefile field, beside the name of the unit, an acronym to be reported on the map is envisaged.

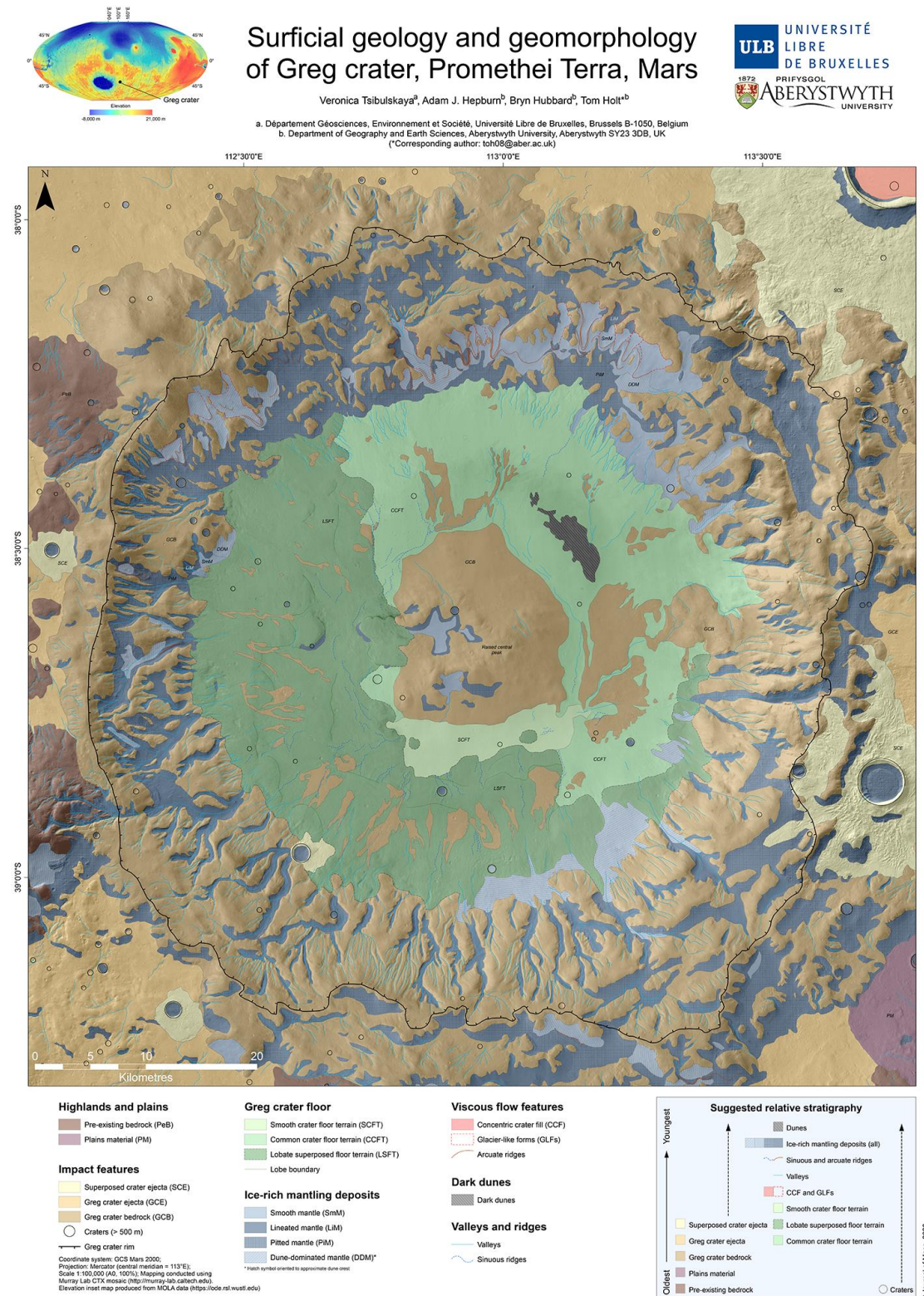
Another linear shapefile, ‘geomorphology/tectonics’, conveys the information on the genetic interpretation of morphological as well as tectonic features. A field should refer to the genetic interpretation (following the same rough checklist provided in the geomorphological map section, adapted depending on the local specific characteristics). Another field should refer to the degree of preservation of such features, and be classified for example as:

- Poorly preserved
- Eroded
- Partially buried
- Subdued

- Well preserved
- Pristine

An example of a geological map where the geomorphological features are present but distinguished by the ‘objective’ geological units is provided in Figure 4.1.

Figure 4.1: Geological Map of Greg crater (Mars) (Tsibulskaia, et al., 2020)



Tectonic structures deserve specific considerations through structural maps aimed at unravelling the deformation history of specific areas or regions. In this case the faults need to be characterized in order to distinguish the extensional, compressional or strike-slip behaviour. In some cases, structural features are classified according to their

morphological aspect being lobate scarps and wrinkle ridges expression of compressional environment and troughs of extensional effects. In other cases, faults are classified using rigorous structural terminology, being reverse faults and thrusts expression of compressional strain, normal faults and grabens of extensional strain field and strike slip faults of transcurrent kinematics. Attention should be paid on their cross-cutting relationships as well as to their hierarchy being possible the distinction between different fault sets and within each set between conjugates and main faults (e.g. Yin et al., 2012; Rossi et al. 2020). Linkages among fault segments such as bridge structures, restraining and releasing bends as well as fault termination geometries can give important info on fault kinematics (e.g. Massironi et al., 2015) whereas their cross-cutting/overlapping relationships with other features and specifically craters might be useful for quantitative assessment of the associated displacement and retrieval of regional stress fields (e.g. Galluzzi et al. 2015; 2019) as well as age determination of fault activity (e.g. Banks et al. 2015; Giacomini et al. 2015; 2020)

When stratified series can be recognized, in addition to faults also folds can be recognized and mapped according to their main typology (antiforms and synforms), symmetry (e.g. symmetric folds or asymmetric vergent folds) and relation with faults (e.g. fault propagation folds or fault bend folds) (e.g. Okubo, 2014; PLANMAP 2020b, c).

Hence the typical features recognizable on structural maps are: faults subdivided according to set pertinence, typology (normal, strike slip, reverse) and hierarchy (e.g. major and secondary); morphological features related to deformations (wrinkle ridges, lobate scarps, troughs); folds subdivided according to their typology and eventual symmetry.

The structural features are always mapped as linear shape files although in structural maps geological units can also be represented with the usual polygonal shape file. From structural maps and series of geological sections with different orientations 3D geometric models inferring the subsurface geological setting can be also reconstructed (PLANMAP 2020b, c).

5. Chronostratigraphic Maps

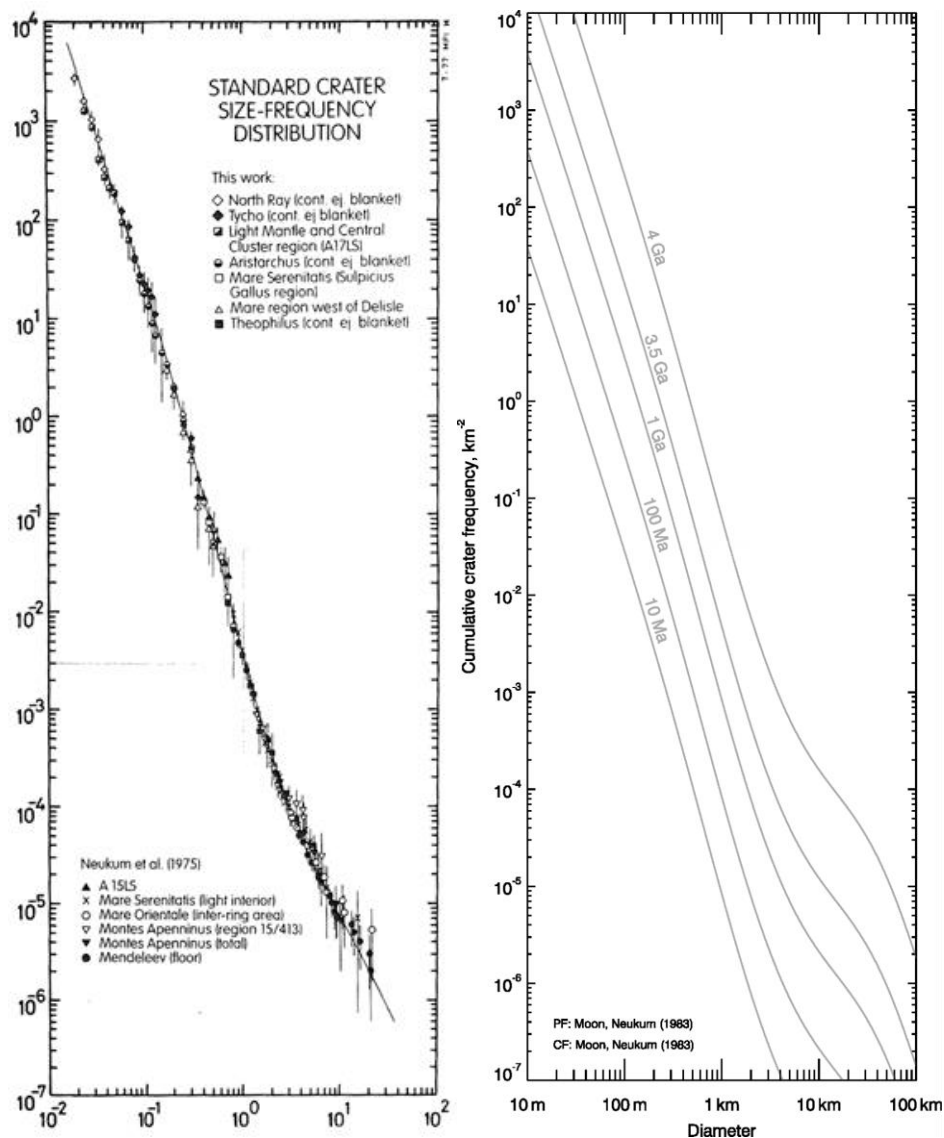
a. Science rationale

In chronostratigraphic maps, geological units are linked to stratigraphic ages (either relative or absolute) that fix the units into a stratigraphic context at regional or global scale. The ages in these maps relate to either the timing of rock formation or a modification event for the surface. These ages make units comparable over a planetary body and allow the definition of the evolution of an area or a planetary body over time.

Chronostratigraphies for planetary bodies other than Earth are not straightforward. On Earth, stratigraphy is based on the appearance and disappearance of index fossils or globally occurring lithostratigraphic layers. However, these criteria cannot be used on planetary bodies. Therefore, stratigraphies on planetary bodies often use large impact craters and basins that affected large parts of the planetary body as a marker horizons for their stratigraphy.

A chronostratigraphic map requires a geological or geomorphological map with homogenous units as a base. These units can then be sorted by their relative ages according to their geomorphological appearance (e.g. degradation state, density of craters) and superposition, with the general concept of younger units overlying, cutting, or overlapping older units. Additionally, the relative density of craters on different units can be used to determine relative ages, where units with a higher density of craters is older than a unit with a lower crater density. In this case, a crater production function (PF), that gives the size-frequency distribution of craters forming on the planetary body, can be used as a tool for better comparisons between the crater densities of different units (Fig. 5.1a; Neukum 1983; Neukum and Ivanov, 1994; Neukum, 2001; Marchi et al. 2009; Le Feuvre and Wieckzorek 2011). The PF can be used to determine the number of craters with diameters greater than or equal to a reference diameter, thus allowing the direct comparison of this relative age measure across diverse geological units. The crater frequency rises with increased exposure age of the surface unit, leading to a vertical shift in the position of the PF. This shift represents the relative ages of each unit (Fig. 5.1b).

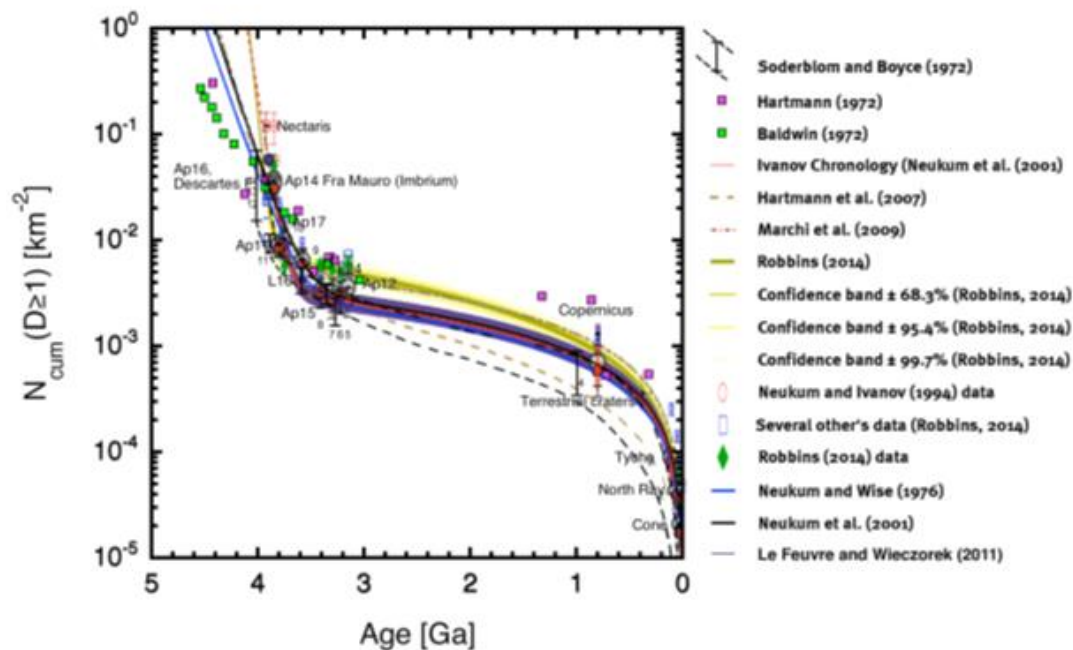
Figure 5.1. (a) The lunar standard crater size-frequency distribution or production function of König (1977) and Neukum and Ivanov (1994). (b) A vertical shift in the absolute position of the PF indicates surfaces with different ages.



An absolute stratigraphy of a region or globally needs to link CSFD measurements to absolute ages of samples. Radiometric dating gives the most reliable age for a geological surface. Sample return missions from the Moon have given us radiometric ages for several units on the lunar nearside (Neukum, 1983; Neukum and Ivanov, 1994; Stöffler and Ryder, 2001). These samples are biased in their small number and sampling location which in some cases cannot be unequivocally attributed to a single geological event. However, with lunar samples being the best indication of absolute ages for lunar geological units, independent CSFD measurements were performed on the geological units associated with the sample.

The chronology function calibrates the production function to radiometric ages giving absolute model ages for the studied unit. The chronology function uses a reference diameter and plots it against the radiometric age, given an absolute model age for a measured surface. In this scheme, it is possible to take CSFD measurements of any lunar surface to determine an absolute model age for it and thus determine its position in the global lunar stratigraphic context. Due to limited samples, different production function approaches and varying calculations, several chronology functions have been proposed (Fig 5.2).

Figure 5.2: Proposed lunar chronology functions (Hiesinger et al., 2020).

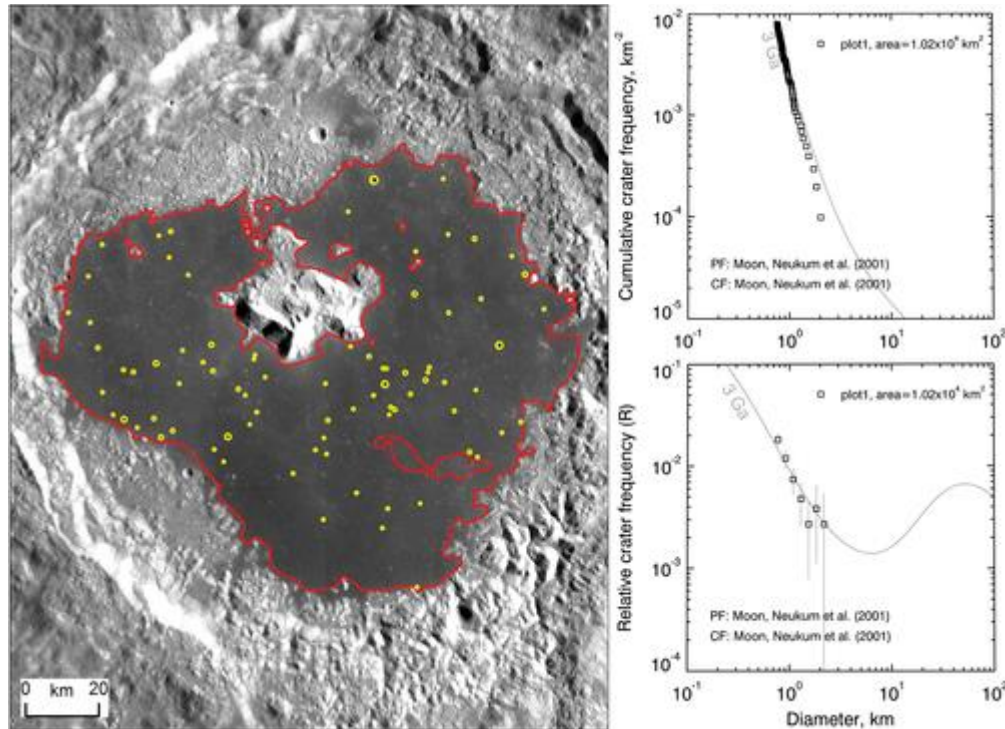


For other planetary bodies two major approaches to determine absolute model ages are being proposed: One Moon-derived and one asteroid-derived (e.g. Neukum et al., 2001; Wagner et al., 2006, Werner et al., 2011; Schmedemann et al., 2014, Fassett, 2016; Hiesinger et al., 2016). The Moon derived model scales the parameters of the lunar model and uses it as the basis for the chronology of that planetary body. The asteroid derived model takes an estimate of the asteroid population in the asteroid belt as a base and models the asteroid population in the early solar system to calculate an impactor rate for the planetary body.

b. Approaches

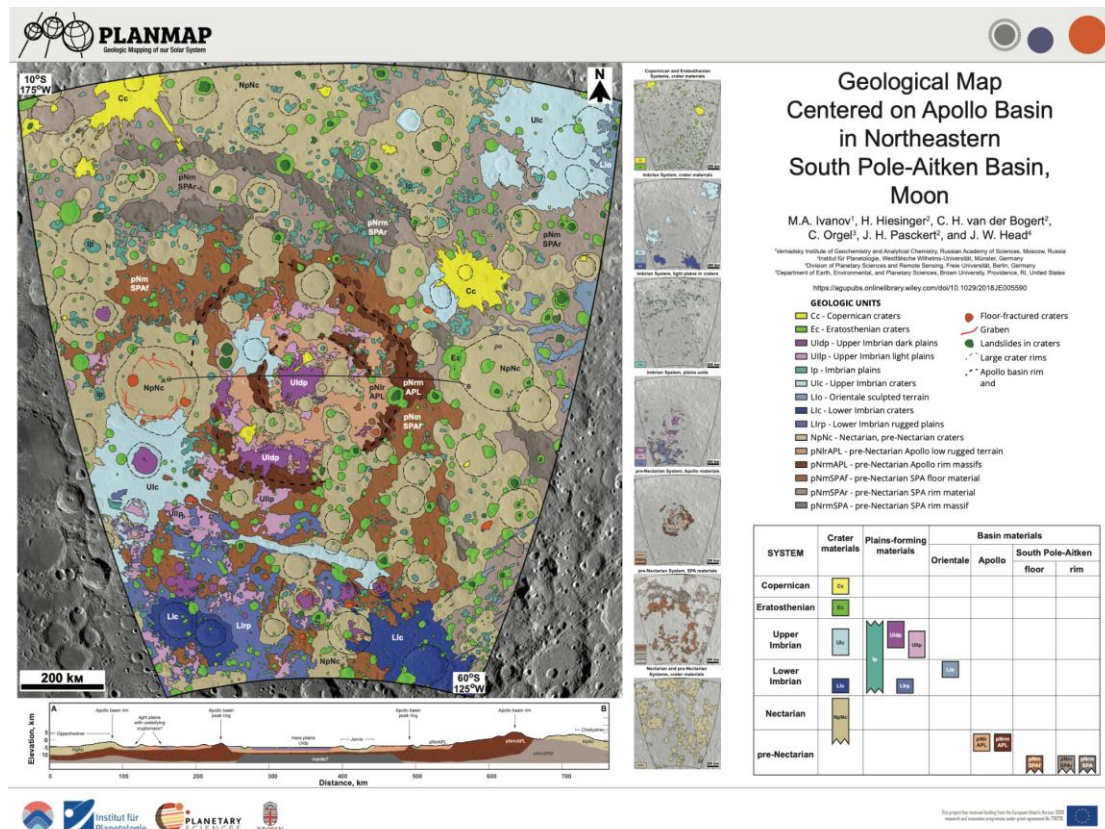
A chronostratigraphic map first needs a geomorphologic map with determined units. Within those units, homogenous areas can be used for CSFD measurements. In these areas secondary craters and other obstacles such as shadows, landfalls or other obscuring factors have to be excluded to work on a relatively clean and undisturbed surface. In ArgGIS the crater tool (Kneissl et al., 2011) is a helpful tool to measure areas and craters (Fig. 5.3). The CSFD measurement can then be plotted using crater stats (https://www.geo.fu-berlin.de/en/geol/fachrichtungen/planet/software/_content/software/index.html). The measurement can be calibrated with different production and chronology functions and then gets assigned an absolute model age. These ages set the different units into a set global chronology for the planetary body.

Figure 5.3: Example of crater size-frequency measurements ($D \geq 750\text{m}$) on Mare Tsiolkovsky. Count area in red, counted craters in yellow. Plotted as a cumulative and relative crater frequency plots. (Fassett, 2016).



In the final map a correlation chart gives an overview of geological units and their chronostratigraphic relation to each other (see chapter 1d, this deliverable). Within the chart the formation age of the different units is indicated and put into a regional or global context (Fig 5.4). The chronostratigraphic map tells the story of a region or planet over time, showing its evolution and history of events. In these maps periods of different activities such as volcanism get visible and units are grouped by their chronostratigraphic relations.

Figure 5.4: Chronostratigraphic map of the Apollo Basin region, Moon with unit correlation chart (Ivanov et al., 2018).



6. Landing site characterization

a. Science and engineering rationale

Characterization of landing sites for missions requires sets of maps that show a variety of data to provide information about the geological characteristics of the region, and also to aid in (1) defining landing site properties and conditions, (2) risk assessment and mitigation, (3) planning of mission operations, and (4) supporting entry, descent, and landing.

b. Approaches

In the scope of geological maps, a regional map (e.g. Figure 6.1; Scott and Carr, 1972) is typically augmented by a small-scale geomorphological or chronostratigraphic map (e.g. Figure 6.2; Lucchitta, 1972) of a landing site. The larger scale chronostratigraphic map provides regional to global context for interpreting the geological history of the landing site. These maps, paired with compositional and other information, are used to select specific landing sites and plan scientific investigations in the scope of sample collection, in situ measurements, and instrument placement (e.g. Kring and Durda, 2012). As new data sets are collected, the map products can be updated and new products produced (e.g., Figure 6.3; Iqbal et al., 2021). These evolved map products allow new and improved interpretation of other remote and in situ datasets, as well as returned samples (e.g. Iqbal et al. 2019, 2020).

Figure 6.1: Apollo 17 pre-mission map of the Taurus-Littrow region of the Moon with a scale of 1:250,000 (Scott and Carr, 1972).

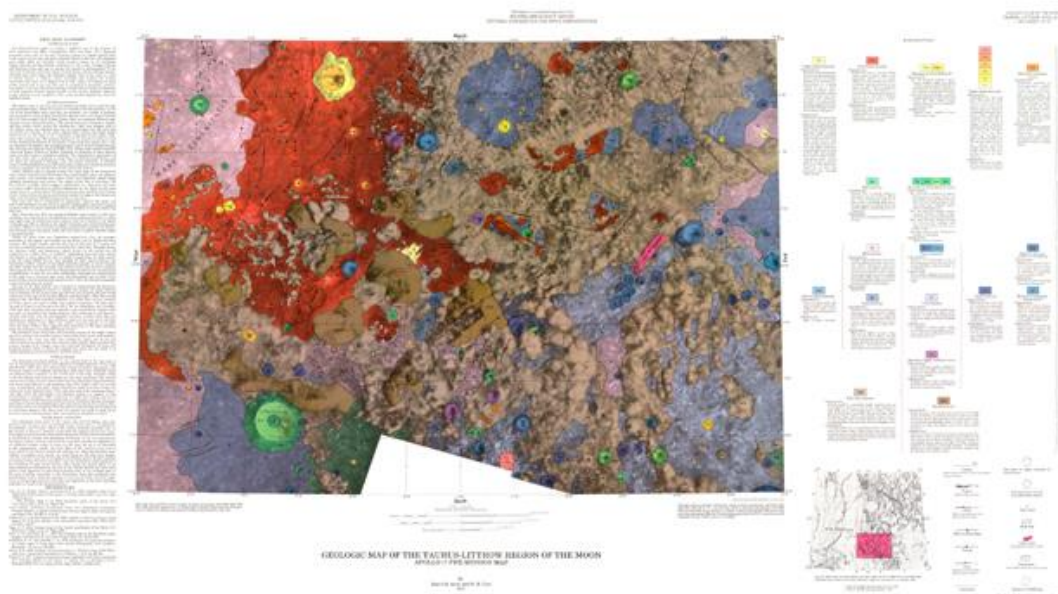


Figure 6.2: Apollo 17 pre-mission detail map of the Taurus-Littrow region of the Moon with a scale of 1:50,000 (Lucchitta, 1972).

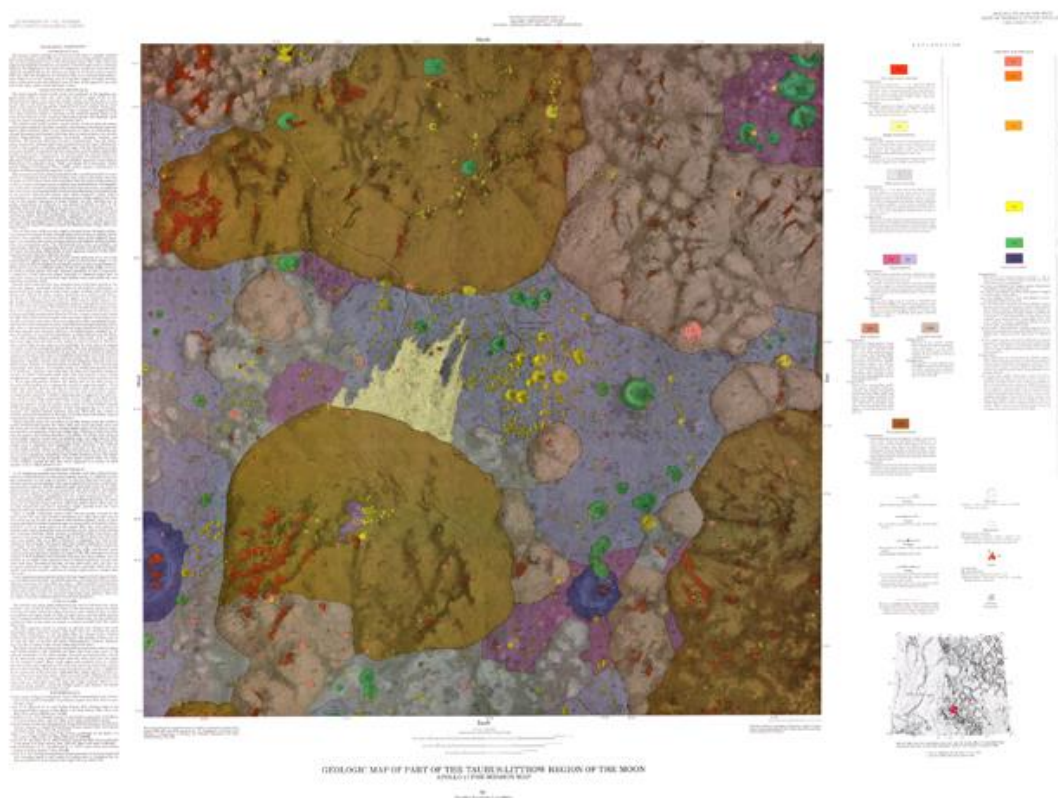
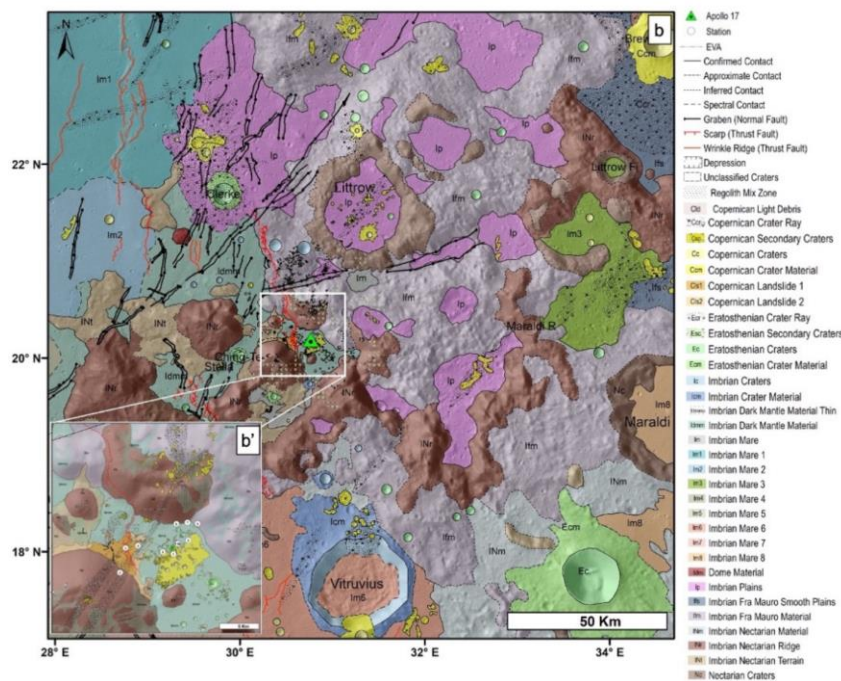


Figure 6.3: New geological maps with scales of 1:24,000 and 1:4,000 (inset) of the Apollo 17 landing site produced with modern lunar datasets (Iqbal et al., 2021).



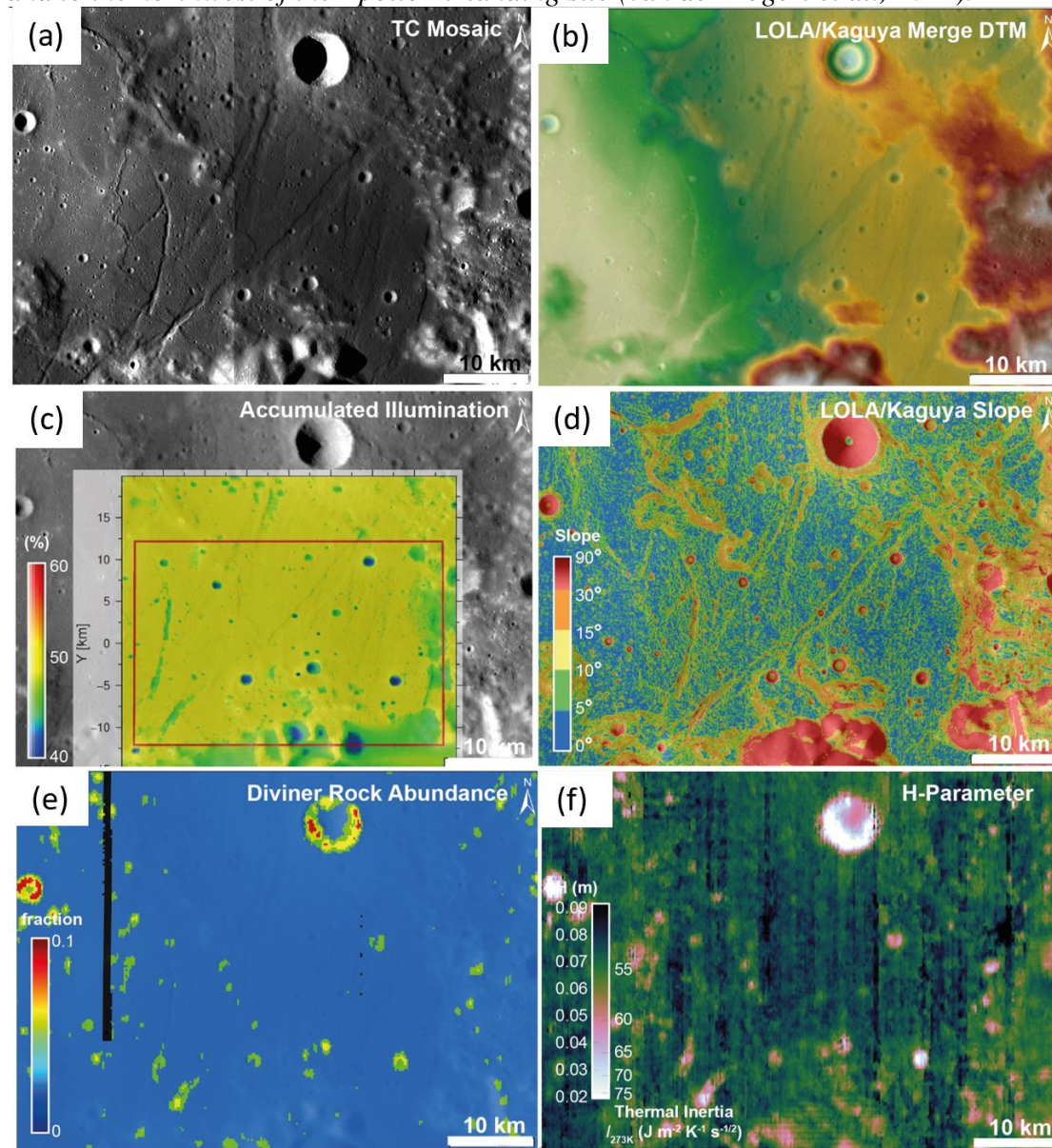
Beyond morphological and chronostratigraphic maps, additional map products for landing site characterization can be produced from digital terrain models (DTMs) to assess the topography, slopes, and illumination conditions (e.g., Barker et al., 2016; Gläser et al., 2014; Scholten et al., 2011). This information can be combined to provide spacecraft and instrument engineers with important constraints for design of landers and equipment, including development of power systems. On the other hand, where specific conditions are required by the hardware, the selection of landing sites can also be optimized for these engineering constraints (e.g. Figure 6.4a-d, van der Bogert et al., 2021)

Additional data sets also provide spatial information about surface temperatures and their variation over days and seasons. These data sets, combined with DTMs, can provide higher level data products showing thermophysical properties (e.g. Bauch et al., 2014; Pelivan, 2018; Williams et al., 2017). For example, the LRO Diviner instrument provides measurements that allow the derivation of rock abundance maps (Figure 6.4e, Bandfield et al., 2011) and H-parameter or thermal inertia maps (Figure 6.4f, Hayne et al., 2017). Both of these data sets are used to gain a more detailed understanding of regolith properties, applicable to both scientific and engineering goals. For example, knowledge of regolith properties in addition to slope maps allows assessment of the trafficability of the surface.

Boulder and crater maps, paired with slope maps, are used to select landing sites and traverses that minimize risk for landed assets, as well as rovers and astronauts (e.g. Garry et al., 2021). Such boulder mapping can be combined with geomorphological maps to provide detailed context for astronaut and rover mission operations (e.g. Pajola et al. 2016, Bernhardt et al., 2021). Indeed, by combining multiple sources of geospatial information, it is possible to plan detailed mission operations for proposed missions while considering both scientific goals and engineering constraints.

For entry, descent, and landing navigation, very accurate feature maps are required for automated landing systems, such as terrain relative navigation (TRN). For example, the Mars2020 mission used an orthorectified image mosaic generated from Mars Reconnaissance Orbiter Context Camera (CTX; Malin et al., 2007) images to provide a highly accurate navigational map for their autonomous hazard avoidance landing system (e.g., Fergason et al., 2020).

Figure 6.4: (a) Kaguya Terrain Camera (TC) image mosaic, compared with the (b) LOLA/Kaguya merge DTM, (c) accumulated illumination calculated from the DTM, (d) DTM-derived slopes, (e) Diviner rock abundance, and (f) H-parameter or thermal inertia for pyroclastic, mare, and highlands deposits in southeastern Mare Serenitatis and to the northwest of the Apollo 17 landing site (van der Bogert et al., 2021).



7. Resource maps for ISRU

a. Science, exploration, and commercial rationale

Resources that can be used in situ on the Moon, asteroids, or other planets would provide a sustainable path for both exploration and science activities, obviating the need to bring all essential materials from the Earth, in addition to potentially supporting a commercial planetary resources industry. Thus, space agencies have recently supported the development and testing of in situ resource utilization (ISRU) capabilities ranging from the extraction of oxygen to the construction of infrastructure from regolith (e.g., ESA, 2019; ISEGC, 2021). A major current focus is the investigation, characterization, and mapping of deposits of volatiles and regolith materials suitable for oxygen extraction. This initial phase of investigation has been termed prospecting (Taylor and Martel, 2003), partly because of the parallels that can be drawn with terrestrial resource prospecting. Global remote sensing maps are used to determine regions of potential interest, where local groundtruthing and characterization will be necessary for further refining the potential and characteristics of diverse resources (e.g., Sanders and Larson, 2012).

b. Approaches

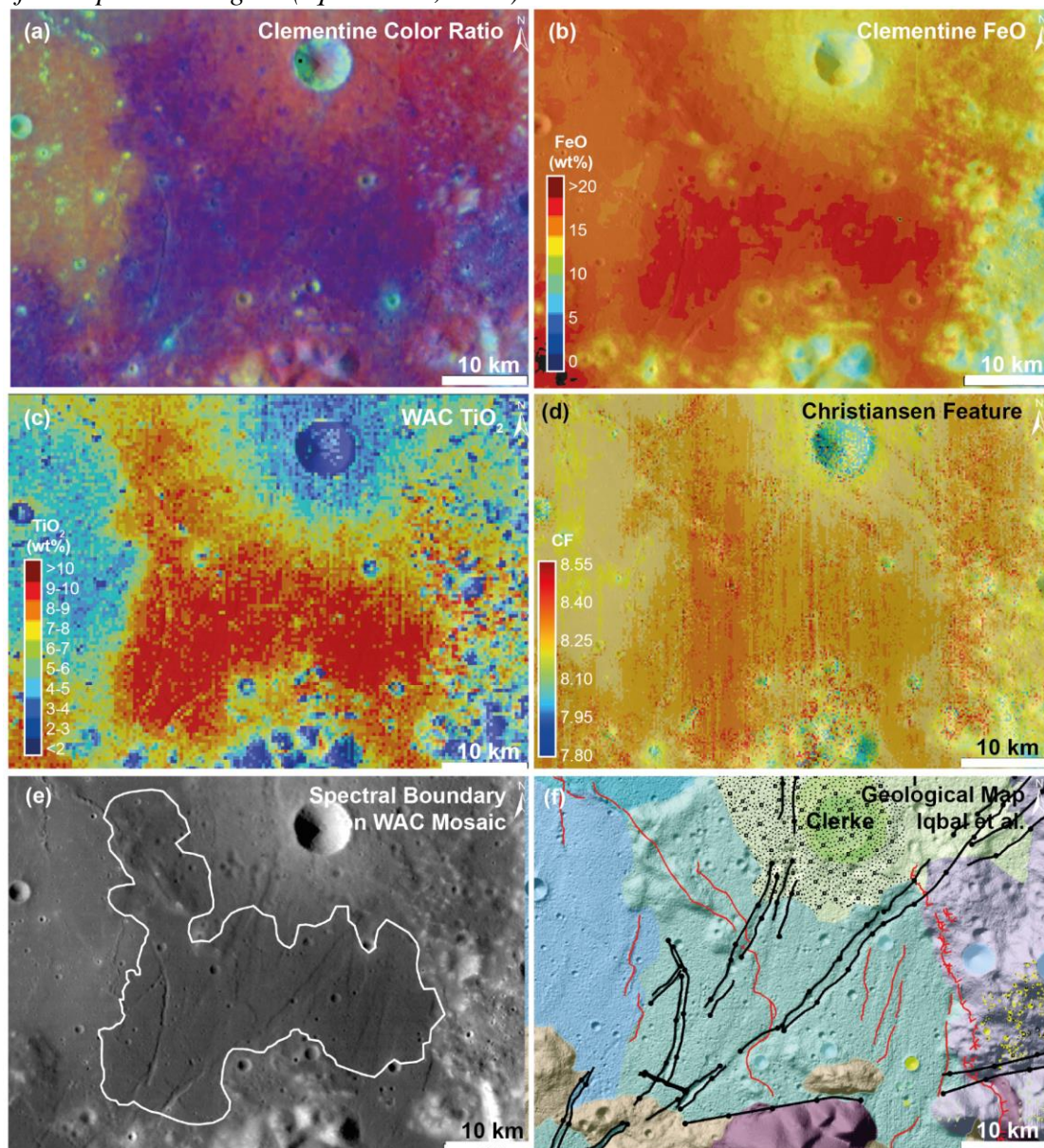
A first step in the production of planetary resource maps is to use the available compositional remote sensing data to define the surficial extent of potential resource deposits. For example, datasets showing high Ti and high Fe concentrations in mafic lunar pyroclastic deposits can be used to select locations where high ilmenite content is expected (Figure 7.1, van der Bogert et al., 2021). Oxygen can be extracted from both ilmenite and iron-rich volcanic glasses via hydrogen and methane reduction techniques, as well as a newly developed Fray-Farthing-Chen electrodeoxidation technique (e.g. Schwandt et al, 2012; Lomax et al., 2020; Sargent et al., 2020; Schlüter and Cowley, 2020; and references therein). Indeed, van der Bogert et al. (2021) examined potential landing sites for ESA's planned ISRU demonstration missions - for both locations that require additional groundtruthing of the resource characteristics and for a location where a small-scale ISRU oxygen extraction demo plant could be tested.

Alternately, recent investigations of a range of remote sensing data, combined with evidence for volatiles excavated during the LCROSS impact into the lunar south polar Cabeus crater (Colaprete et al., 2010), have allowed the mapping of potential volatiles sinks in the lunar polar regions (e.g. Li et al., 2018; Qiao et al., 2019). These studies either serve as the basis for volatiles prospecting missions or further support their development and completion. For example, ESA's PROSPECT will be launched on Roscosmos's Luna 27 mission to the lunar south pole, and aims to characterize lunar polar volatiles (Sefton-Nash et al., 2020). NASA's VIPER mission will rove the south polar region to characterize the distribution, extent, and nature of lunar volatiles (NASA, 2020).

The characterization of materials suitable for oxygen extraction or for mining of volatiles requires the collection of groundtruth to improve the interpretation of the remote sensing datasets that can be fed into improvements of first generation resource maps. As local and regional operations are established, for example on the Moon with

a south polar outpost, astronaut and robot geologists can make more detailed resource maps.

Figure 7.1: Multispectral remote sensing datasets can be combined to allow the mapping of units and locations with compositional characteristics optimized for specific ISRU techniques. For example, (a) the Clementine color ratio (Pieters et al., 1994; McEwen et al., 1994), (b) Clementine FeO (Lucey et al., 2000), (c) WAC TiO₂ (Sato et al., 2017), (d) LRO Diviner Christiansen feature (Greenhagen et al., 2010), and (e) LRO WAC albedo (Robinson et al., 2010) maps can be used to define a spectral unit boundary representing a high Ti, high Fe deposit suitable for a range of oxygen extraction techniques. (Same region as shown in Figure 6.4, northwest of the Apollo 17 landing site from van der Bogert et al., (2021). (f) Portion of the new geological map of the Apollo 17 region (Iqbal et al., 2021).



References

- Ansan, V., Loizeau, D., Mangold, N., Mouélic, L. S., Carter, J., Poulet, F., et al. (2011). Stratigraphy, mineralogy, and origin of layered deposits inside Terby crater, Mars. *Icarus*, 211(1), 273–304. <https://doi.org/10.1016/j.icarus.2010.09.011>
- Ayoub, F., Avouac, J.-P., Newman, C. E., Richardson, M. I., Lucas, A., Leprince, S., & Bridges, N. T. (2014). Threshold for sand mobility on Mars calibrated from seasonal variations of sand flux. *Nature Communications*, 5(1), 5096. <https://doi.org/10.1038/ncomms6096>
- Baker, V.R.a, Boothroyd, J.C.b, Carr, M.H.c, et al. (1983). Channels and valleys on Mars. *Geological Society of America Bulletin*, 94(9), 1035.
- Baker, V., Strom, R., Gulick, V. et al. Ancient oceans, ice sheets and the hydrological cycle on Mars. *Nature* 352, 589–594 (1991). <https://doi.org/10.1038/352589a0>
- Baker, V. R., Carr, M. H., Gulick, V. C., Williams, C. R., & Marley, M. S. (1992). Channels and valley networks. *Mars*, 493–522.
- Baker, V. R., Hamilton, C. W., Burr, D. M., Gulick, V. C., Komatsu, G., Luo, W., et al. (2015). Fluvial geomorphology on Earth-like planetary surfaces: A review. *Geomorphology*, 245, 149–182. <https://doi.org/10.1016/j.geomorph.2015.05.002>
- Bandfield J. L., R. R. Ghent, A. R. Vasavada, D. Paige, S. J. Lawrence, and M. S. Robinson (2011) Lunar surface rock abundance and regolith fines temperatures derived from LRO Diviner radiometer data, *Journal of Geophysical Research* 116, E00H02–18, 10.1029/2011JE003866.
- Banks, M. E., Z. Xiao, T. R. Watters, R. G. Strom, S. E. Braden, C. R. Chapman, S. C. Solomon, C. Klimczak, and P. K. Byrne (2015), Duration of activity on lobate-scarp thrust faults on Mercury, *J. Geophys. Res. Planets*, 120, 1751–1762, doi:10.1002/2015JE004828.
- Banham, S. G., Gupta, S., Rubin, D. M., Watkins, J. A., Sumner, D. Y., Edgett, K. S., et al. (2018). Ancient Martian aeolian processes and palaeomorphology reconstructed from the Stimson formation on the lower slope of Aeolis Mons, Gale crater, Mars. *Sedimentology*, 65(4), 993–1042. <https://doi.org/10.1111/sed.12469>
- Barker M. K., Mazarico E., Neumann G. A., Zuber M. T., Haruyama J., and Smith D. E., (2016) A new lunar digital elevation model from the Lunar Orbiter Laser Altimeter and SELENE Terrain Camera, *Icarus* 273, 346–355.
- Barrett, A. M., Balme, M. R., Patel, M. R., & Hagermann, A. (2018). The distribution of putative periglacial landforms on the martian northern plains. *Icarus*, 314, 133–148. <https://doi.org/10.1016/j.icarus.2018.05.032>
- Bauch, K. E., H. Hiesinger, J. Helbert, M. S. Robinson, and F. Scholten (2014) Estimation of lunar surface temperatures and thermophysical properties: test of a

thermal model in preparation of the MERTIS experiment onboard BepiColombo, Planetary and Space Science, 101, 27-36, 10.1016/j.pss.2014.06.004.

Bernhardt, H., Hiesinger, H., Reiss, D., Ivanov, M., & Erkeling, G. (2013). Putative eskers and new insights into glacio-fluvial depositional settings in southern Argyre Planitia, Mars. Planetary and Space Science, 85, 261–278. <https://doi.org/10.1016/j.pss.2013.06.022>

Bernhardt H. and M. S. Robinson, 2021, Preliminary geomorphic map (1:10,000) of Artemis III AOI 001 & 004 on the Shackleton-De Gerlache Ridge, Lunar and Planetary Science Conference 52, #1264, <https://www.hou.usra.edu/meetings/lpsc2021/pdf/1264.pdf>.

Bland, M. T., Becker, T. L., Edmundson, K. L., Roatsch, T., Archinal, B. A., Takir, D., Patterson, G. W., et al. (2018). A new Enceladus global control network, image mosaic, and updated pointing kernels from Cassini's 13-year mission. Earth and Space Science, 5(10), 604–621. <https://agupubs.onlinelibrary.wiley.com/doi/full/10.1029/2018EA000399>

Bridges, N. T., Sullivan, R., Newman, C. E., Navarro, S., Beek, J., Ewing, R. C., et al. (2017). Martian aeolian activity at the Bagnold Dunes, Gale Crater: The view from the surface and orbit. Journal of Geophysical Research: Planets, 122(10), 2077–2110. <https://doi.org/10.1002/2017je005263>

Buczkowski D.L., Barnouin-Jha O.S., Prockter L.M., (2008) 433 Eros lineaments: Global mapping and analysis. Icarus 193 (2008) 39–52

Butcher, F. E. G., Balme, M. R., Conway, S. J., Gallagher, C., Arnold, N. S., Storrar, R. D., et al. (2021). Sinuous ridges in Chukhung crater, Tempe Terra, Mars: Implications for fluvial, glacial, and glaciofluvial activity. Icarus, 357, 114131. <https://doi.org/10.1016/j.icarus.2020.114131>

Byrne P.K., Klimczak C., Sengör A.M.C., Solomon S.C., Watters T.R., Hauck S.A. (2014). Mercury's global contraction much greater than earlier estimates. Nature Geoscience. DOI: 10.1038/NGEO2097.

Cardinale, M., Komatsu, G., Silvestro, S., & Tirsch, D. (2012). The influence of local topography for wind direction on Mars: two examples of dune fields in crater basins. Earth Surface Processes and Landforms, 37(13), 1437–1443. <https://doi.org/10.1002/esp.3289>

Carr, M. H. (1996). Water on Mars. Oxford University Press/OUP USA.

Carr, M. H., & Head III, J. W. (2003). Oceans on Mars: An assessment of the observational evidence and possible fate. *Journal of Geophysical Research: Planets*, 108(E5).

Catuneanu, O. (2006). *Principles of Sequence Stratigraphy*. Elsevier, 375 pages.

Chapman, M., Neukum, G., Dumke, A., Michael, G., van Gasselt, S., Kneissl, T., Zuschneid, W., Hauber, E., Ansan, V., Mangold, N., & Masson, P. (2010), Noachian–Hesperian geologic history of the Echus Chasma and Kasei Valles system on Mars: New data and interpretations, *Earth Planet Sc Lett*, 294(3-4), 256–271, doi:10.1016/j.epsl.2009.11.032.

Clifford, S. M., & Parker, T. J. (2001). The evolution of the Martian hydrosphere: Implications for the fate of a primordial ocean and the current state of the northern plains. *Icarus*, 154(1), 40-79.

Colaprete, A., Schultz, P., Heldmann, J., Wooden, D., Shirley, M., Ennico, K., Hermalyn, B., Marshall, W., Ricco, A., Elphic, R.C., Goldstein, D., Summy, D., Bart, G.D., Asphaug, E., Korycansky, D., Landis, D., Sollitt, L., 2010. Detection of water in the LCROSS ejecta plume. *Science* 330, 463-468.

Collins, G.C., Patterson, G.W., Head, J.W., Pappalardo, R.T., Prockter, L.M., Lucchitta, B.K., and Kay, J.P., 2013, Global geologic map of Ganymede: U.S. Crow-willard, E. N., & Pappalardo, R. T. (2015). Structural mapping of Enceladus and implications for formation of tectonized regions. *Journal of Geophysical Research: Planets*, 928–950. <https://doi.org/10.1002/2015JE004818>.

Clark, C. S., & Clark, P. E. (2020). Progress 2020-B: Constant-Scale Natural Boundary Mapping to Depict Material Transport on Comet 67P/C-G. 2138.

Craddock, R. A., and Howard, A. D., (2002). The case for rainfall on a warm, wet early Mars, *J. Geophys. Res.*, 107(E11), 5111, doi:10.1029/2001JE001505, 2002.

Crosta, G. B., Frattini, P., Valbuzzi, E., & Blasio, F. V. D. (2018). Introducing a New Inventory of Large Martian Landslides. *Earth and Space Science*, 5(4), 89–119. <https://doi.org/10.1002/2017ea000324>

Di Achille, G., Marinangeli, L., Ori, G. G., Hauber, E., Gwinner, K., Reiss, D., and Neukum, G. (2006), Geological evolution of the Tyras Vallis paleolacustrine system, Mars, *J. Geophys. Res.*, 111, E04003, doi:10.1029/2005JE002561.

Di Pietro, I., Ori, G. G., Pondrelli, M., and Salese, F., 2018, Geology of Aeolis Dorsa alluvial sedimentary basin, Mars: *Journal of Maps*, v. 14, no. 2, p. 212-218.

Dickson, J. L., Head, J. W., & Marchant, D. R. (2008). Late Amazonian glaciation at the dichotomy boundary on Mars: Evidence for glacial thickness maxima and multiple glacial phases. *Geology*, 36(5), 411–414. <https://doi.org/10.1130/g24382a.1>

Erkeling, Hiesinger, Reiss, Hielscher, and Ivanov (2011), The stratigraphy of the Amenthes region, Mars: Time limits for the formation of fluvial, volcanic and tectonic landforms, *Icarus*, 215(1), 128–152, doi:10.1016/j.icarus.2011.06.041.

European Space Agency (2019) Space Resources Strategy, <https://exploration.esa.int/s/WyP6RXw>

Fassett, C.I.: 2016. Analysis of impact crater populations and the geochronology of planetary surfaces in the inner solar system, *JGR Planets*, 121, 10.

<https://doi.org/10.1002/2016JE005094>

Ferguson, R. L., T. M. Hare, D. P. Mayer, D. M. Galuszka, B. L. Redding, E. D. Smith, J. R. Shinaman, Y. Cheng, and R. E. Otero, 2020, Mars 2020 terrain relative navigation flight product generation: Digital terrain model and orthorectified image mosaics, Lunar and Planetary Science Conference 51, #2020.

Figueredo, P. H., Chuang, F. C., Rathbun, J., Kirk, R. L., & Greeley, R. (2002). Geology and origin of Europa's "Mitten" feature (Murias Chaos). *Journal of Geophysical Research E: Planets*, 107(5), 1–15. <https://doi.org/10.1029/2001je001591>

Figueredo, P. H., & Greeley, R. (2004). Resurfacing history of Europa from pole-to-pole geological mapping. *Icarus*, 167(2), 287–312. <https://doi.org/10.1016/j.icarus.2003.09.016>

Gallagher, C., & Balme, M. (2015). Eskers in a complete, wet-based glacial system in the Phlegra Montes region, Mars. *Earth and Planetary Science Letters*, 431, 96–109. <https://doi.org/10.1016/j.epsl.2015.09.023>

Galluzzi V., Di Achille G., Ferranti L., Popa C., Palumbo P. (2015) Faulted craters as indicators for thrust motions on Mercury. In: Platz, T., Massironi, M., Byrne, P. K. & Hiesinger, H. (eds) *Volcanism and Tectonism Across the Inner Solar System*. Geological Society, London, Special Publications, 401, 313-325.

Galluzzi, V., Ferranti, L., Massironi, M., Giacomini, L., Guzzetta, L., Palumbo, P., 2019, Structural Analysis of the Victoria Quadrangle Fault Systems on Mercury: Timing, Geometries, Kinematics, and Relationship with the High-Mg Regio: *Journal of Geophysical Research: Planets*, v.124, Issue 10, p. 2543-2562, DOI: 10.1029/2019JE005953.

Garry, W. B., Williams, D. A., Dapremont, A. M., and Shean, D. E. (2018). The 1:1,000,000 geologic map of Arsia Mons, Mars. *Planetary Geologic Mappers Meeting 2018*, abs.#7028.

Garry W. B., N. E. Petro, D. P. Moriarty, M. K. Barker, 2021, The distribution and geologic context of boulders and outcrops along the connecting ridge lunar south pole exploration site. NESF-ELS Joint Meeting 2021, https://dl.airtable.com/.attachments/8a9c26cd9472965c6de456ca1aa014ba/14595f34/Garry_NESF_2021_LunarSPboulders_v3.pdf

Geological Survey Scientific Investigations Map 3237, pamphlet 4 p., 1 sheet, scale 1:15,000,000, <http://dx.doi.org/10.3133/sim3237>

Giacomini, L., M. Massironi, M. R. El-Maarry, et al. 2016 Geologic Mapping of the Comet 67P/Churyumov–Gerasimenko's Northern Hemisphere. *Monthly Notices of the Royal Astronomical Society* 462(Suppl 1): S352–S367.

Giacomini L., Massironi M., Marchi S., Fassett C.I., Di Achille G., Cremonese G. (2015). Age dating of an extensive thrust system on Mercury: implications for the planet's thermal evolution In: Platz, T., Massironi, M., Byrne, P. K. & Hiesinger, H. (eds) *Volcanism and Tectonism Across the Inner Solar System*. Geological Society, London, Special Publications, 401, 291-311.

Giacomini, L., Massironi, M., El-Maarry, M. R., Penasa, L., Pajola, M., Thomas, N., Lowry, S. C., Barbieri, C., Cremonese, G., Ferri, F., Naletto, G., Bertini, I., La Forgia, F., Lazzarin, M., Marzari, F., Sierks, H., Lamy, P. L., Rodrigo, R., Rickman, H., ... Vincent, J.-B. (2016). Geologic mapping of the Comet 67P/Churyumov–Gerasimenko's Northern hemisphere. *Monthly Notices of the Royal Astronomical Society*, 462(Suppl 1), S352–S367. <https://doi.org/10.1093/mnras/stw2848>

Giacomini L., Massironi M., Galluzzi V., Ferrari S., Palumbo P., 2020. Dating long thrust systems on Mercury: New clues on the thermal evolution of the planet. *Geoscience Frontiers* Volume 11, Issue 3, Pages 855-870.

Gläser, P., F. Scholten, D. De Rosa, R. M. Figuera, J. Oberst, E. Mazarico, G. A. Neumann, and M. S. Robinson, 2014, Illumination conditions at the lunar south pole using high resolution digital terrain models from LOLA, *Icarus* 243, 78-90.

Glamoclija, M., L. Marinangeli, and G. Komatsu (2011), Harmakhis Vallis Source Region, Mars: Insights into the recent geothermal history based on geological mapping, *Planet Space Sci*, 59(11-12), 1179–1194, doi:10.1016/j.pss.2010.09.017.

Greeley, R., Heiner, S., Klemaszewski, J.E., 2001. Geology of Lofn Crater, Callisto. *J. Geophys. Res.* 106, 3261–3273. <https://doi.org/10.1029/2000JE001262>

Greenhagen B. T., P. G. Lucey, M. B. Wyatt, T. D. Glotch, C. C. Allen, J. A. Arnold, J. L. Bandfield, N. E. Bowles, K. L. Donaldson Hanna, P. O. Hayne, E. Song, I. R. Thomas, and D. A. Paige (2010) Global silicate mineralogy of the Moon from the Diviner lunar radiometer, *Science* 329, 1507-1509, 10.1126/science.1192196.

Grieger, B., & Vincent, J.-B. (2018). A closed self-organizing map of Chury. *EPSC2018-298*.

Groenleer, J. M., & Kattenhorn, S. A. (2008). Cycloid crack sequences on Europa: Relationship to stress history and constraints on growth mechanics based on cusp angles. *Icarus*, 193(1), 158–181. <https://doi.org/10.1016/j.icarus.2007.08.032>

Grotzinger, J. P., Arvidson, R. E., Bell, J. F., Calvin, W., Clark, B. C., Fike, D. A., et al. (2005). Stratigraphy and sedimentology of a dry to wet eolian depositional system, Burns formation, Meridiani Planum, Mars. *Earth and Planetary Science Letters*, 240(1), 11–72. <https://doi.org/10.1016/j.epsl.2005.09.039>

Hargitai H. I., V. C. Gulick & N. H. Glines (2018) The geology of the Navua Valles region of Mars, *Journal of Maps*, 14:2, 504-508, DOI: 10.1080/17445647.2018.1496858

Hayne P. O., J. L. Bandfield, M. A. Siegler, A. R. Vasavada, R. R. Ghent, J.-P. Williams, B. T. Greenhagen, O. Aharonson, C. M. Elder, P. G. Lucey, and D. A. Paige (2017) Global regolith thermophysical properties of the Moon from the Diviner Lunar Radiometer Experiment, *Journal of Geophysical Research* 122, 2371-2400, 10.1002/2017JE005387.

Hayward, R.K., Mullins, K.F., Fenton, L.K., Hare, T.M., Titus, T.N., Bourke, M.C., Colaprete, A., and Christensen, P.R., 2007 Mars Global Digital Dune Database: MC2 - MC29: U.S. Geological Survey Open-File Report 2007-1158. [http://pubs.usgs.gov/of/2007/1158/].

Head, J. W., & Marchant, D. R. (2003). Cold-based mountain glaciers on Mars: Western Arsia Mons. *Geology*, 31(7), 641–644. [https://doi.org/10.1130/0091-7613\(2003\)031<0641:cmgomw>2.0.co;2](https://doi.org/10.1130/0091-7613(2003)031<0641:cmgomw>2.0.co;2)

Head, J., Neukum, G., Jaumann, R. et al. Tropical to mid-latitude snow and ice accumulation, flow and glaciation on Mars. *Nature* 434, 346–351 (2005). <https://doi.org/10.1038/nature03359>

Hernández, M. Á. de P., & Carrillo, J. D. C. (2012). Geomorphological map of the lower NW flank of the Hecates Tholus volcano, Mars (scale 1:100,000). *Journal of Maps*, 8(3), 208–214. <https://doi.org/10.1080/17445647.2012.703902>

Hobbs, S. W., Paull, D. J., & Bourke, M. C. (2010). Aeolian processes and dune morphology in Gale Crater. *Icarus*, 210(1), 102–115. <https://doi.org/10.1016/j.icarus.2010.06.006>

Howard, A. D. et al. Pluto: Pits and mantles on uplands north and east of Sputnik Planitia. *Icarus* 293, 218–230 (2017).

Hiesinger, H., Marchi, S., Schmedemann, N., Schenk, P., Pasckert, J.H., Neesemann, A., O'Brian, D.P., Kneissl, T., Ermakov, A.I., Fu, R.R., Bland, M.T., Nathues, A., Williams, D.A., Jaumann, R., Castillo-Rogez, J.C., Ruesch, O., Schmidt, B., Park, R.S., Preusker, F., Buczowski, D.L., Russell, C.T., and Raymond, C.A.: 2016. Cratering on Ceres: Implications for its crust and evolution. *Science*, 353, 6306
DOI: 10.1126/science.aaf4759

International Space Exploration Coordination Group (2021) In situ resource utilization gap assessment report, <https://www.globalspaceexploration.org/wordpress/wp-content/uploads/2021/04/ISECG-ISRU-Technology-Gap-Assessment-Report-Apr-2021.pdf>

Iqbal W., Hiesinger H., and van der Bogert C. H., 2019, Geological mapping and chronology of lunar landing sites: Apollo 11, *Icarus*, 333, 528-547, [10.1016/j.icarus.2019.06.020](https://doi.org/10.1016/j.icarus.2019.06.020).

Iqbal W. Hiesinger H., and van der Bogert C. H., 2020, Geological mapping and chronology of lunar landing sites: Apollo 12, Icarus, 352, 113991, [10.1016/j.icarus.2020.113991](https://doi.org/10.1016/j.icarus.2020.113991).

Iqbal W., Hiesinger H., van der Bogert C. H., and Head J. W., 2021, Comprehensive geological mapping of Apollo 15 and Apollo 17 landing sites and their implications, Planetary Geologic Mappers Meeting, Lunar and Planetary Institute Contribution No. 2610, 7047.

International Subcommittee on Stratigraphic Classification (ISSC), 1999. International Stratigraphic Guide - An abridged edition (Michael A. Murphy and Amos Salvador, eds.): Episodes, v. 22, no. 4, pp. 255-271.

Kirk, R. L., Barrett, J. M., & Soderblom, L. A. (2003, February). Photoclinometry made simple. In Proceedings of the ISPRS Commission IV Symposium (Vol. 34, p. 4).

Kneissl, T, van Gasselt, S., and Neukum, G.: 2011. Map-projection-independent crater size-frequency determination in GIS environments - New software tool for ArcGIS, Planetary and Space Science, 59, 1243-1254, DOI: 10.1016/j.pss.2010.03.015

Kring, D. A. and D. D. Durda, 2012, A global lunar landing site study to provide the scientific context for exploration of the Moon, Lunar and Planetary Institute Contribution No. 1694, 688 pp., <https://www.lpi.usra.edu/exploration/CLSE-landing-site-study/>.

Kukkonen, S. and V.-P. Kostama (2018), Mapping and dating based evolution studies of the Niger Vallis outflow channel, Mars, Planet Space Sci, 153, 54–71, doi:10.1016/j.pss.2017.12.012.

Lapotre, M., Ewing, R., Weitz, C., Lewis, K., Lamb, M., Ehlmann, B., & Rubin, D. (2018). Morphologic Diversity of Martian Ripples: Implications for Large-Ripple Formation. Geophysical Research Letters, 45(19), 10,229-10,239. <https://doi.org/10.1029/2018GL079029>

Lee, Jui-Chi, Matteo Massironi, Wing-Huen Ip, et al. 2016 Geomorphological Mapping of Comet 67P/Churyumov–Gerasimenko’s Southern Hemisphere. Monthly Notices of the Royal Astronomical Society 462(Suppl_1): S573–S592.

Le Feuvre, M. and Wiecorek, M.A: 2011, Nonuniform cratering of the Moon and a revised crater chronology of the inner Solar System, Icarus, 214, 1-20. <https://doi.org/10.1016/j.icarus.2011.03.010>

Li, S. et al., 2018. Direct evidence of surface exposed water ice in the lunar polar regions. PNAS 115, 8907-8912.

Lomax B. A., M. Conti, N. Khan, N. S. Bennett, A. Y. Ganin, and M. D. Symes (2020) Proving the viability of an electrochemical process for the simultaneous extraction of oxygen and production of metal alloys from lunar regolith, *Planetary and Space Science* 180, 104748.

Lucchitta, B. K., 1972, Geologic map of part of the Taurus-Littrow region of the Moon, US Geological Survey, Geologic Atlas of the Moon, I-800-2, https://www.lpi.usra.edu/resources/mapcatalog/usgs/I800_2/.

Lucey, P. G., D. T. Blewett, and B. L. Jolliff (2000) Lunar iron and titanium abundance algorithms based on final processing of Clementine ultraviolet-visible images, *J. Geophys. Res.*, 105(E8), 20297–20305, 10.1029/1999JE001117.

Malin, M., and K. Edgett (2003), Evidence for Persistent Flow and Aqueous Sedimentation on Early Mars, *Science*, 302(5652), 1931–1934, doi:10.1126/science.1090544.

Malin, M.C., Bell, J.F., III, Cantor, B.A., Caplinger, M.A., Calvin, W.M., Clancy, R.T., Edgett, K.S., Edwards, L., Haberle, R.M., and James, P.B., 2007, Context Camera investigation on board the Mars Reconnaissance Orbiter: *Journal of Geophysical Research*, v. 112, E05S04, doi: 10.1029/2006JE002808.

Marchi S, Mottola S, Cremonese G, Massironi M., Martellato E (2009). A new chronology for Moon and Mercury. *THE ASTRONOMICAL JOURNAL*, 137; 4936-4948.

Martin, E. S., Patthoff, D. A., Bland, M. T., Watters, T. R., Collins, G. C., & Becker, T. (2018, June). Building a Geologic Map of Neptune's Moon Triton. In *Planetary Geologic Mappers Annual Meeting* (Vol. 2066, p. 7026).

Massironi, M., Di Achille, G. Rothery D. A., Galluzzi V., Giacomini L., Ferrari S., Zusi M., Cremonese G., Palumbo P. (2015). Lateral ramps and strike-slip kinematics on Mercury. In: Platz, T., Massironi, M., Byrne, P.K. & Hiesinger, H. (eds) *Volcanism and Tectonism Across the Inner Solar System*. Geological Society, London, Special Publications, 401, 269-290.

Massironi M.; Marchi S.; Pajola M.; Snodgrass C.; Thomas N.; Tubiana C.; Baptiste J. V.; Cremonese G.; Da Deppo V.; Ferri F.; Magrin S.; Sierks H.; Barbieri C.; Lamy P.; Rickman H.; Rodrigo R.; Koschny D.; OSIRIS Team (2012). Geological map and stratigraphy of asteroid 21 Lutetia *PLANETARY AND SPACE SCIENCE*, 66, 125-136.

Martin, E. S. et al. Pit chains on Enceladus signal the recent tectonic dissection of the ancient cratered terrains. *Icarus* 294, 209–217 (2017).

McEwen, A.S., Eliason, E.M., Bergstrom, J.W., Bridges, N.T., Hansen, C.J., Delamere, W.A., Grant, J.A., Gulick, V.C., Herkenhoff, K.E., Keszthelyi, L., Kirk, R.L., Mellon, M.T., Squyres, S.W., Thomas, N., and Weitz, C.M., 2007, Mars Reconnaissance Orbiter's High Resolution Imaging Science Experiment (HiRISE): *Journal of Geophysical Research*, v. 112, E05S02, doi: 10.1029/2005JE002605.

McEwen A. S., M. S. Robinson, E. M. Eliason, P. G. Lucey, T. C. Duxbury, and P. D. Spudis (1994) Clementine observations of the Aristarchus region of the Moon, *Science* 266, 1858-1862, 10.1126/science.266.5192.1858.

Moore, J., and A. Howard (2005), Large alluvial fans on Mars, *J Geophys Res Planets* 1991 2012, 110(E4), doi:10.1029/2004je002352.

NASA (2020) VIPER Mission Overview, <https://www.nasa.gov/viper/overview>.

Neukum, G.:1983, Meteoritenbombardement und Datierung Planetarer Oberflächen, Habilitation Dissertation for Faculty Membership, Univ. of Munich, 186 pp.

Neukum, G., and Ivanov, B.A.:1994, 'Crater Size Distribution and Impact Probabilities on Earth from Lunar, Terrestrial-planet, and Asteroid Cratering Data', in T. Gehrels (ed.), *Hazards due to Comets and Asteroids*, Univ. Arizona Press, Tucson, pp. 359-416.

Neukum, G., Ivanov, B.A., and Hartmann, W.K.: 2001, Cratering Records in the Inner Solar System in Relation to the Lunar Reference System, *Space Science Reviews*, 96, 55-86.

Neukum, G., Jaumann, R., and the HRSC Co-Investigator and Experiment Team, 2004, HRSC: The High Resolution Stereo Camera of Mars Express, in Wilson, A., ed., *Mars Express: The Scientific Payload: European Space Agency Special Publication SP-1240*, p. 17–35.

Okubo C.H.,(2014). Bedrock Geologic and Structural Map through the Western Candor Colles Region of Mars. USGS Scientific Investigations Map 3309

Pacifici, A. (2008), Geomorphological map of Ares Vallis, Mars ASI Planetary Map Series – Map n° 1, *Boll.Soc.Geol.It.*, 127, 75–92.

Pajola, M., Lucchetti, A., Semenzato, A., Poggiali, G., Munaretto, G., Galluzzi, V., Marzo, G.A., Cremonese, G., Brucato, J.R., Palumbo, P., Massironi, M., (2021). Lermontov crater on Mercury: Geology, morphology and spectral properties of the coexisting hollows and pyroclastic deposits. *Planetary and Space Science*, Volume 195, Article number 105136. DOI: 10.1016/j.pss.2020.105136

Pajola M., Rossato S. , Carter J. , Baratti E. , Pozzobon R. , Erculiani M.S, Coradini M., McBride K., (2016). Eridania Basin: An ancient paleolake floor as the next landing site for the Mars 2020 rover. *Icarus* 275, 163–182.

Pappalardo, R.T., Collins, G.C., Head, J.W., and 6 others, 2004, Geology of Ganymede, in: *Jupiter* (Bagenal, F., Dowling, T., McKinnon, W., eds.), Cambridge Univ. Press, p. 363-396.

Pappalardo, R. T., Vance, S., Bagenal, F., Bills, B. G., Blaney, D. L., Blankenship, D. D., et al. (2013). Science potential from a Europa Lander. *Astrobiology*, 13(8), 740–773. <https://doi.org/10.1089/ast.2013.1003>

Parker, T. J., Gorsline, D. S., Saunders, R. S., Pieri, D. C., and Schneeberger, D. M. (1993), Coastal geomorphology of the Martian northern plains, *J. Geophys. Res.*, 98(E6), 11061– 11078, doi:10.1029/93JE00618.

Parker, T. J., Saunders, R. S., & Schneeberger, D. M. (1989). Transitional morphology in west Deuteronilus Mensae, Mars: Implications for modification of the lowland/upland boundary. *Icarus*, 82(1), 111-145.

Patterson, G.W., Collins, G.C., Head, J.W., and 4 others, 2010, Global geological mapping of Ganymede: *Icarus*, v. 207, p. 845-867.

Pelivan I., 2018, Thermophysical modelling for high-resolution digital terrain models, *Monthly Notices of the Royal Astronomical Society* 478, 386-398.

Pieters C. M., M. I. Staid, E. M. Fischer, S. Tompkins, and G. He (1994) A sharper view of impact craters from Clementine data, *Science* 266, 1844-1848, 10.1126/science.266.5192.1844.

PLANMAP (2020a). D.2.4 Update of the Mapping Standards. Document and Spectral data integration into geomorphic maps. Open Access deliverable from H2020-776276 PLANMAP project.

https://wiki.planmap.eu/display/public/Deliverables?preview=/8193472/30083898/776276_planmap_D2.4.pdf

PLANMAP (2020b). D6.1 3D geomodels based on multiple datasets of Mars (implicit or explicit modelling). Open Access deliverable from H2020-776276 PLANMAP project.

https://wiki.planmap.eu/display/public/Deliverables?preview=/8193472/29622308/776276-planmap_D6.1.pdf

PLANMAP(2020c). D6.3 D geo -models based on multiple advanced datasets of Mercury (explicit modelling). Open Access deliverable from H2020-776276 PLANMAP project.

https://wiki.planmap.eu/display/public/Deliverables?preview=/8193472/30083908/776276_planmap_D6.3.pdf

Platz T., Byrne P.K., Massironi M., Hiesinger H., (2015). Volcanism and tectonism across the inner solar system: an overview. In: Platz, T., Massironi, M., Byrne, P. K. & Hiesinger, H. (eds) *Volcanism and Tectonism Across the Inner Solar System*. Geological Society, London, Special Publications, 401, 1-56.

Pondrelli, Rossi, L. Deit, Schmidt, Pozzobon, Hauber, and Salese (2019), Groundwater Control and Process Variability on the Equatorial Layered Deposits of Kotido Crater, Mars, *Journal of Geophysical Research: Planets*, doi:10.1029/2018JE005656.

Pondrelli, M., Rossi, A.P., Marinangeli, L., Hauber, E., Gwinner., K., Baliva A., Di Lorenzo, S., (2008). Morphofacies analysis and depositional architecture of the Eberswalde crater, Mars. *ICARUS*, doi:10.1016/j.icarus.2008.05.018.

Preusker, F., Scholten, F., Matz, K.-D., Roatsch, T., Willner, K., Hviid, S. F., Knollenberg, J., Jorda, L., Gutiérrez, P. J., Kürt, E., Mottola, S., A'Hearn, M. F., Thomas, N., Sierks, H., Barbieri, C., Lamy, P., Rodrigo, R., Koschny, D., Rickman, H., ... Vincent, J.-B. (2015). Shape model, reference system definition, and cartographic mapping standards for comet 67P/Churyumov-Gerasimenko – Stereo-photogrammetric analysis of Rosetta/OSIRIS image data. *Astronomy & Astrophysics*, 583, A33. <https://doi.org/10.1051/0004-6361/201526349>

Qiao L., Z. Ling, J. W. Head, M. A. Ivanov, and B. Liu (2019) Analyses of Lunar Orbiter Laser Altimeter 1,064 nm albedo in permanently shadowed regions of polar crater flat floors: Implications for surface water ice occurrence and future in situ exploration, *Earth and Space Science* 6, 467–488.

Ramsdale, J. D., Balme, M. R., Gallagher, C., Conway, S. J., Smith, I. B., Hauber, E., et al. (2019). Grid Mapping the Northern Plains of Mars: Geomorphological, Radar, and Water-Equivalent Hydrogen Results From Arcadia Plantia. *Journal of Geophysical Research: Planets*, 124(2), 504–527. <https://doi.org/10.1029/2018je005663>

Rapin, W., Dromart, G., Rubin, D., Deit, L. L., Mangold, N., Edgar, L. A., et al. (2021). Alternating wet and dry depositional environments recorded in the stratigraphy of Mount Sharp at Gale crater, Mars. *Geology*, 49(7), 842–846. <https://doi.org/10.1130/g48519.1>

Roatsch, T., Kersten, E., Matz, K.-D., Preusker, F., Scholten, F., Jaumann, R., Raymond, C. A., & Russell, C. T. (2016). High-resolution Ceres High Altitude Mapping Orbit Atlas derived from Dawn Framing Camera images. *Planetary and Space Sciences*, 125, 103–107. <https://doi.org/10.1016/j.pss.2016.05.011>

Robbins, S. J., Beyer, R. A., Spencer, J. R., Grundy, W. M., White, O. L., Singer, K. N., et al. (2019). Geologic Landforms and Chronostratigraphic History of Charon as Revealed by a Hemispheric Geologic Map. *Journal of Geophysical Research: Planets*, 124(1), 155–174. <https://doi.org/10.1029/2018JE005684>

Rodriguez, A. J., Kargel, J. S., Baker, V. R., Gulick, V. C., Berman, D. C., Fairén, A. G., et al. (2015). Martian outflow channels: How did their source aquifers form, and why did they drain so rapidly? *Scientific Reports*, 5(1), 13404. <https://doi.org/10.1038/srep13404>

Rossi, A. P., Gasselt, S. V., Pondrelli, M., Dohm, J., Hauber, E., Dumke, A., et al. (2011). Evolution of periglacial landforms in the ancient mountain range of the Thaumasia Highlands, Mars. *Geological Society, London, Special Publications*, 356(1), 69–85. <https://doi.org/10.1144/sp356.5>

Rossi, A. P., and van Gasselt, S. editors (2018) *Planetary Geology*, 441 p., ISBN: 978-3-319-65177-4, ISSN: 2366-0082, DOI: 10.1007/978-3-319-65179-8, *Astronomy and Planetary Sciences series*

Rossi, C., Cianfarra, P., Salvini, F., 2020. Structural geology of Ganymede regional groove systems (60°N–60°S). *Journal of Maps* 16, 6–16. <https://doi.org/10.1080/17445647.2019.1685605>

Salamunićcar, G., Lončarić, S., & Mazarico, E. (2012). LU60645GT and MA132843GT catalogues of Lunar and Martian impact craters developed using a Crater Shape-based interpolation crater detection algorithm for topography data. *Planetary and Space Science*, 60(1), 236-247. <http://doi.org/10.1016/j.pss.2011.09.003>

Sanders G. B. and W. E. Larson (2012) Progress made in lunar in-situ resource utilization under NASA's Exploration Technology and Development Program, *Journal of Aerospace Engineering* 26, [10.1061/9780784412190.050](https://doi.org/10.1061/9780784412190.050).

Sargent H. M., F. A. J. Abernathy, S. J. Barber, I. P. Wright, M. Anand, S. Sheridan, and A. Morse (2020) Hydrogen reduction of ilmenite: Towards an in situ resource utilization demonstration on the surface of the Moon, *Planetary and Space Science* 180, 104751.

Sato H., M. S. Robinson, S. J. Lawrence, B. W. Denevi, H. Hapke, B. L. Jolliff, and H. Hiesinger (2017) Lunar mare TiO₂ abundances estimated from UV/Vis reflectance, *Icarus* 296, 216-238, doi:10.1016/j.icarus.2017.06.013.

Schenk, P.M., 1995. The geology of Callisto. *Journal of Geophysical Research* 100, 23–40.

Schenk, P. M., & Pappalardo, R. T. (2004). Topographic variations in chaos on Europa: Implications for diapiric formation. *Geophysical Research Letters*, 31(16), 1–5. <https://doi.org/10.1029/2004GL019978>

Schenk, P., Matsuyama, I. & Nimmo, F. A Very Young Age for True Polar Wander on Europa From Related Fracturing. *Geophys. Res. Lett.* 47, 0–3 (2020).

Schlüter L. and A. Cowley (2020) Review of techniques for in-situ oxygen extraction on the Moon, *Planetary and Space Science* 181, 104753.

Schmedemann, N., Kneissl, T., Ivanov, B.A., Michael, G.G., Wagner, R.J., Neukum, G., Ruesch, O., Hiesinger, H., Krohn, K., Roatsch, T., Preusker, F., Sierks, H., Jaumann, R., Reddy, V., Nathues, A., Walter, S.H.G., Neeesemann, A., Raymond, C.A., and Russell, C.T.:2014. The cratering record, chronology and surfaces ages of (4) Vesta in comparism to smaller asteroids and the ages of HED meteorites.

Scholten F., J. Oberst, K.-D. Matz, T. Roatsch, M. Wählisch, E. J. Speyerer, and M. S. Robinson (2012) GLD100 – the near-global lunar 100 meter raster DTM from LROC WAC stereo image data, *Journal of Geophysical Research* 117, E00H17, [10.1029/2011JE003926](https://doi.org/10.1029/2011JE003926).

Schwandt C., J. A. Hamilton, D. J. Fray, and I. A. Crawford (2012) The production of oxygen and metal from lunar regolith, *Planetary and Space Science* 74, 49-56, 10.1016/j.pss.2012.06.011.

Scott D. H. and Carr M. H., 1972, Geologic map of the Taurus-Littrow region of the Moon, US Geological Survey, Geologic Atlas of the Moon, I-800-1, https://www.lpi.usra.edu/resources/mapcatalog/usgs/I800_1/.

Sefton-Nash E., R. Fisackerly, R. Trautner, S. J. Barber, P. Reiss, D. Marin, D. Heather, B. Houdoe, the PROSPECT Science Team and Industrial Consortium (2020) The ESA PROSPECT payload for Luna 27: Development status, Lunar and Planetary Science Conference 51, 2367.

Semenzato, A.; Massironi, M.; Ferrari, S.; Galluzzi, V.; Rothery, D. A.; Pegg, D. L.; Pozzobon, R.; Marchi, S., 2020. An integrated geologic map of the rembrandt basin, on Mercury, as a starting point for stratigraphic analysis. REMOTE SENSING, Volume 12, Issue 19, DOI: 10.3390/rs12193213

Skinner, J.A. Jr., Huff, A.E., Fortezzo, C.M., Gaither, T., Hare, T.M., Hunter, M.A., Buban, H., 2019, Planetary geologic mapping—program status and future needs: U.S. Geological Survey Open-File Report 2019–1012, 40 p., <https://doi.org/10.3133/ofr20191012>

Silvestro, S., Achille, G. D., & Ori, G. G. (2010). Dune morphology, sand transport pathways and possible source areas in east Thaumasia Region (Mars). *Geomorphology*, 121(1–2), 84–97. <https://doi.org/10.1016/j.geomorph.2009.07.019>

Silvestro, S., Vaz, D. A., Ewing, R. C., Rossi, A. P., Fenton, L. K., Michaels, T. I., et al. (2013). Pervasive aeolian activity along rover Curiosity's traverse in Gale Crater, Mars. *Geology*, 41(4), 483–486. <https://doi.org/10.1130/g34162.1>

Silvestro, S., Pacifici, A., Salese, F., Vaz, D. A., Neesemann, A., Tirsch, D., et al. (2021). Periodic Bedrock Ridges at the ExoMars 2022 landing site: Evidence for a changing wind regime. *Geophysical Research Letters*, 48, e2020GL091651. <https://doi.org/10.1029/2020GL091651>

Simioni E., Pajola M., Massironi M., Cremonese G. (2015). Phobos grooves and impact craters: A stereographic analysis. *ICARUS*, vol. 256, p. 90-100, ISSN: 0019-1035, doi: 10.1016/j.icarus.2015.04.009

Smith, I. B., Putzig, N. E., Holt, J. W., & Phillips, R. J. (2016). An ice age recorded in the polar deposits of Mars. *Science*, 352(6289), 1075–1078. <https://doi.org/10.1126/science.aad6968>

Soare R. J. , Conway S. J. , Gallagher C. , Dohm J. M. and Reiss D. (2018). Geological Society, London, Special Publications, 467, 211-231, <https://doi.org/10.1144/SP467.7>

Stern, S. A., Bagenal, F., Ennico, K., Gladstone, G. R., Grundy, W. M., McKinnon, W. B., et al. (2015). The pluto system: Initial results from its exploration by New Horizons. *Science*, 350(6258). <https://doi.org/10.1126/science.aad1815>

Stöffler, D., and Ryder, G. (2001). Stratigraphy and Isotope Ages of Lunar Geologic Units: Chronological Standard for the Inner Solar System', *Space Sci. Rev.*, 96, 9-54. DOI: [10.1023/A:1011937020193](https://doi.org/10.1023/A:1011937020193)

Stooke, P., & Pajola, M. (2019). Mapping Irregular Bodies. In H. Hargitai (Ed.), *Planetary Cartography and GIS* (pp. 191–203). Springer International Publishing. https://doi.org/10.1007/978-3-319-62849-3_8

Taylor G. J. and L. M. V. Martel (2003) Lunar prospecting, *Advances in Space Research* 31, 2403-2412.

Tanaka, K. L., Skinner, J. A., & Hare, T. M. (2005). Geologic map of the northern plains of Mars.

Tanaka, K. L., Skinner, J. A., Hare, T. M., Joyal, T., & Wenker, A. (2003). Resurfacing history of the northern plains of Mars based on geologic mapping of Mars Global Surveyor data. *Journal of Geophysical Research: Planets*, 108(E4).

Thomas, R., B. Hynek, M. Osterloo, and K. Kierein-Young (2017), Widespread exposure of Noachian phyllosilicates in the Margaritifer region of Mars: Implications for paleohydrology and astrobiological detection, *Journal of Geophysical Research: Planets*, 122(3), 483–500, doi:10.1002/2016je005183.

Tsibulskaya, V., Hepburn, A. J., Hubbard, B., & Holt, T. (2020). Surficial geology and geomorphology of Greg crater, Promethei Terra, Mars. *Journal of Maps*, 16(2), 524–533. <https://doi.org/10.1080/17445647.2020.1785343>

van der Bogert C. H., H. Hiesinger, I. Pretto, F. Venditti, A. Lewang, L. Richter, D. Binns, and P. Gläser, (2021). Science-rich sites for in situ resource utilization characterization and end-to-end demonstration missions, *Planetary Science Journal* 2, 84, <https://doi.org/10.3847/PSJ/abedbb>.

van Gasselt, S., Hauber, E., & Neukum, G. (2007). Cold-climate modification of Martian landscapes: A case study of a spatulate debris landform in the Hellas Montes Region, Mars. *Journal of Geophysical Research: Planets* (1991–2012), 112(E9). <https://doi.org/10.1029/2006je002842>

S. Van Gasselt, E. Hauber, A.-P. Rossi, A. Dumke, R. Orosei and G. Neukum
Geological Society, London, Special Publications, 356, 43-67, 1 January 2011, <https://doi.org/10.1144/SP356.4>

Vaz, D. A., & Silvestro, S. (2014). Mapping and characterization of small-scale aeolian structures on Mars: An example from the MSL landing site in Gale Crater. *Icarus*, 230, 151–161. <https://doi.org/10.1016/j.icarus.2013.08.007>

Werner, S.C. and Tanaka, K.L.: 2011, Redefinition of the crater-density and absolute-age boundaries for the chronostratigraphic system of Mars. *Icarus*, 215, 603-607.

<https://doi.org/10.1016/j.icarus.2011.07.024>

White, O. L. et al. Washboard and fluted terrains on Pluto as evidence for ancient glaciation. *Nat. Astron.* 3, 62–68 (2019).

Williams J.-P., D. A. Paige, B. T. Greenhagen, and E. Sefton-Nash (2017) The global surface temperatures of the Moon as measured by the Diviner lunar radiometer experiment, *Icarus* 283, 300-325, 10.1016/j.icarus.2016.08.012.

Williams D.A., Denevi B.W., Mittlefehldt D.W. et al. (2014). The geology of the Marcia quadrangle of asteroid Vesta: Assessing the effects of large, young craters. *Icarus* 244, 74–88

Wilson, L., Ghatan, G. J., Head, J. W., & Mitchell, K. L. (2004). Mars outflow channels: A reappraisal of the estimation of water flow velocities from water depths, regional slopes, and channel floor properties. *Journal of Geophysical Research*, 109(E9), E09003 1-10. <https://doi.org/10.1029/2004je002281>

Yin A. (2012). Structural analysis of the Valles Marineris fault zone: Possible evidence for large-scale strike-slip faulting on Mars. *Lithosphere* 4;286-330, doi: 10.1130/L192.1

Zimbelman, J. R., & Griffin, L. J. (2010). HiRISE images of yardangs and sinuous ridges in the lower member of the Medusae Fossae Formation, Mars. *Icarus*, 205(1), 198–210. <https://doi.org/10.1016/j.icarus.2009.04.003>

Zubarev, A., Nadezhdina, I., Brusnikin, E., Giese, B., Oberst, J., 2017. A search for Ganymede stereo images and 3D mapping opportunities. *Planetary and Space Science* 146, 40–54. <https://doi.org/10.1016/j.pss.2017.07.021>